Programa de Doctorado en Optometría y Ciencias de la Visión (RD 1393/2007)

Light vergence detection in monocular and monochromatic accommodation

Doctorando:

Antonio Jesús Del Águila Carrasco

Directores:

Iván Marín Franch

Norberto López Gil

Robert Montés Micó

Burjassot, Mayo de 2017

Light vergence detection in monocular and monochromatic accommodation

Memoria presentada por

Antonio Jesús Del Águila Carrasco

para optar al grado de

DOCTOR en OPTOMETRÍA Y CIENCIAS DE LA VISIÓN

The project that led to the writing of this thesis has received funding from the European Research Council, Starting Grant ERC-2012-StG-309416. The author of this thesis has been supported by a research scholarship grant Atracció de Talent (UV-INV-PREDOC14-179135) from the Universidad de Valencia.

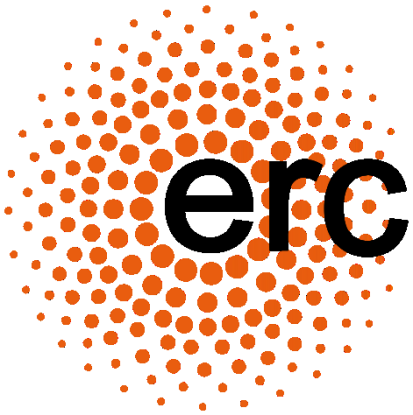

VNIVERSITAT DE VALÈNCIA

El Dr. Iván Marín Franch, Investigador Senior de la Universidad de Valencia, el Prof. Norberto López Gil, Catedrático de la Universidad de Murcia, y el Prof. Robert Montés Micó, Catedrático de la Universidad de Valencia

CERTIFICAN que la presente memoria "Light vergence detection in monocular and monochromatic accommodation", resume el trabajo de investigación realizado, bajo su dirección, por D. Antonio Jesús Del Águila Carrasco y constituye su Tesis para optar al Grado de Doctor en Optometría y Ciencias de la Visión.

Y para que así conste, y en cumplimiento de la legislación vigente, firma el presente certificado en Valencia, a mayo de dos mil diecisiete.

Fdo. Iván Marín Franch Fdo. Norberto López Gil Fdo. Robert Montés Micó

DECLARATION

No portion of the work referred to in the thesis has been submitted in support of an application for another degree or qualification of this or any other university or other institution of learning.

To Alejo and Rosi

“And many strokes, though with a little axe,

hew down and fell the hardest-timber’d oak.”

Henry VI, Part 3. William Shakespeare

“Life's barely long enough to get good at one thing.

So be careful what you get good at.”

Rust Cohle

“Good is not enough. Good does not change the world.”

Dr. John Thackery

“Bang.”

Spike Spiegel

Contents

Acknowledgements

I am very thankful to my supervisors. To Dr. Iván Marín-Franch for his dedication, guidance and support. Also for "encouraging" me to learn Matlab programming a few years ago, for helping me to improve my exposition skills, and for all the beers, pizzas and TV series that have led to this thesis (eventually). To Prof. Norberto López-Gil for sharing with me some of his vast knowledge in optics and vision, and for granting me the opportunity to work in his lab at Universidad de Murcia for several months, where we worked hard and had some fun. To Prof. Robert Montés-Micó for his support and advice, and for giving me the opportunity to work in this research group and in this challenging project.

I express my gratitude also to Dr. Philip B. Kruger, for his outstanding ideas and the many fruitful discussions we had about this work. And to the rest of the members of the SACCO team, Dr. José Juan Esteve-Taboada and Paula Bernal-Molina, for the hours shared making this project become a reality. Thanks also to Xavier Levecq for his invaluable help developing the algorithm that allowed us to complete this project and save what was left of our sanity.

Many thanks to Prof. D. Robert Iskander for granting me the opportunity to be in his lab for several months at Wroclaw University of Technology, and for the fascinating scientific discussions we had during those months.

Thanks also to all the people in the Optometry Research Group at Universidad de Valencia, in the CIVIUM at Universidad de Murcia, and the people that I have shared time with from the ITN Networks AGEYE and EDEN. It has been fun!

I don't want to miss the opportunity to also thank my friends Urbano, Javi, Curro, Poyato, and Migue for the moral support, even if it was by Skype. A special mention to Shiki for being so kind as to be my chauffeur in many occasions.

Last, but not least, thanks a lot to my mother, who has always supported me, and to *Elenaki mou*, for her continuous support, her love, and for bearing stoically with me during this tough period.

List of important definitions

Vergence of a point (V) or a target (TV): Inverse of the distance from a point or a target to the subject. By default, the subject's corneal vertex is assumed the as plane of reference (see Figure d1). Units of vergence are usually diopters (D) and throughout this thesis, a sign criteria is assumed in which vergence is negative for objects in front of the corneal plane (i.e. real target) and positive for objects placed behind the corneal plane (i.e. virtual target).

Refractive state (RS): Vergence of the retinal conjugate in the object space. Retina here is assumed as the photoreceptor plane at the center of the fovea.

Far point (FP): Refractive state of the non-accommodated eye (see Figure d1).

Refraction (Rx): Vergence of the far point.

Accommodative demand (AD): Dioptric difference between the refraction and the target vergence (AD = Rx−TV).

Accommodation or accommodative response (AR): Dioptric difference between the refraction and the refractive state (AR = Rx−RS).

Accommodative error (AE): Dioptric difference between accommodative demand and accommodative response (AE = AD−AR = RS−TV).

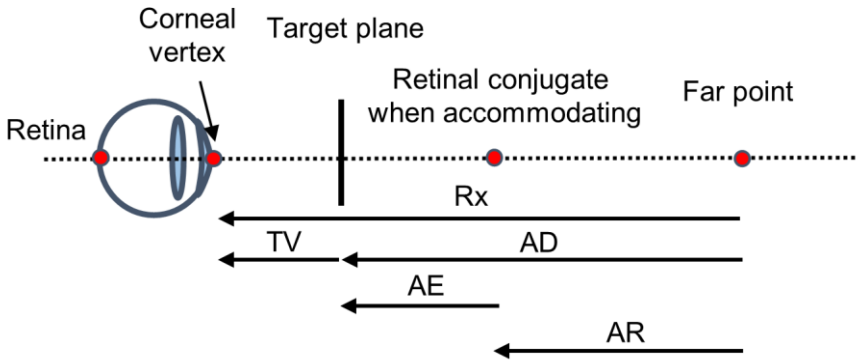

Figure d1. Illustration of important concepts. The far point is the retinal conjugate of the eye when it is not accommodating. All the distances showed in this figure are given in diopters.

Accommodative lag: Positive accommodative error (see Figure d2).

Accommodative lead: Negative accommodative error (see Figure d2).

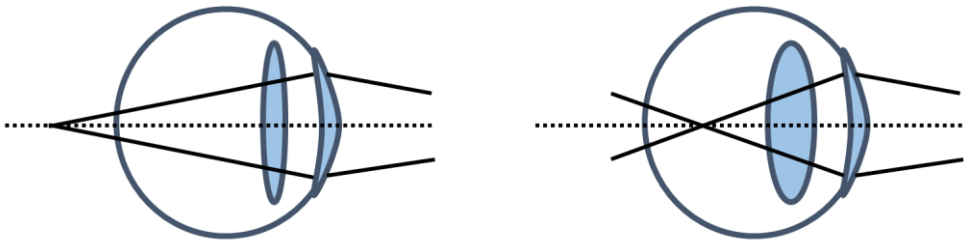

Figure d2. The eye in the left is under-accommodating and as a consequence presents accommodative lag (hyperopic defocus). The eye in the right is over-accommodating, and as consequence presents accommodative lead (myopic defocus).

Longitudinal chromatic aberration: Effect in which different colors fail to focus to the same point, as a consequence of the change in refractive index depending on the wavelength of the light. The eye presents greater power for short-wavelength than for long-wavelength light. This disparity in the focus of the different wavelengths creates differences in the retinal images depending on whether the target is focused in front of or behind the retina (see Figure d3).

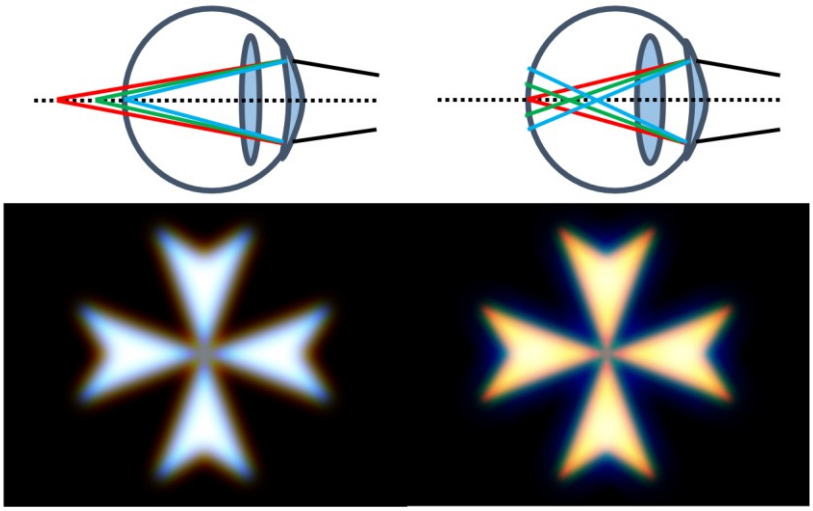

Figure d3. Effect of longitudinal chromatic aberration. Left column shows a negative defocus corresponding to an image focused behind the retina. Right column shows a positive defocus corresponding to an image focused in front of the retina. Upper row shows how the different wavelengths are focused depending on the sign of defocus. Lower row shows retinal images simulations of a polychromatic white Maltese cross. Note the different color generated around the white cross depending on the sign of defocus. Simulations were performed for a 4-mm pupil and assuming that 550 nm was the wavelength focused on the retina. The Maltese cross subtends 1.95°. When the paper is put at approximately 1 m away from the eye of the reader, the crosses subtend 1.95°.

Point spread function (PSF): Image of a distant point source through an optical system.

Even-order aberrations: aberrations defined only by Zernike polynomials having an even radial order (see Section 2.1.2 for further information). These aberrations (except spherical defocus) produce different retinal images when the target is focused in front of (myopic defocus) or behind (hyperopic defocus) the retina (see Figure d4). Examples of these aberrations are astigmatism and spherical aberration.

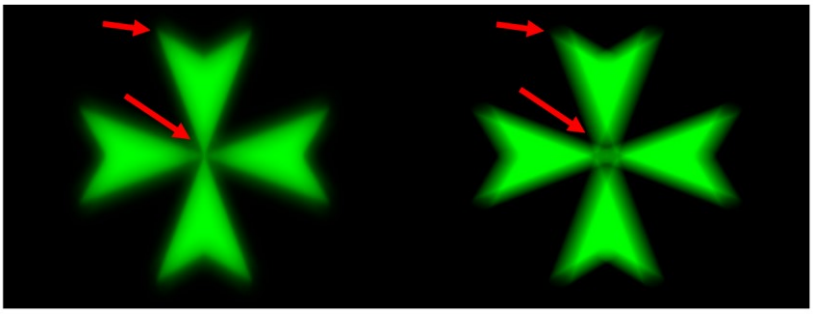

Figure d4. Effect of a monochromatic even-order aberration on the retinal image of a Maltese cross, in this case −0.1 μm of spherical aberration for a 4-mm pupil. Red arrows point out differences in the two images depending on the sign of defocus. The Maltese cross subtends 1.95°. When the paper is put at approximately 1 m away from the eye of the reader, the crosses subtend 1.95°.

Odd-order aberrations: aberrations defined by Zernike polynomials having an odd radial order. These aberrations produce the exact same image whether the target is focused in front of (myopic defocus) or behind (hyperopic defocus) the retina (see Figure d5). Example of these aberrations are coma and trefoil.

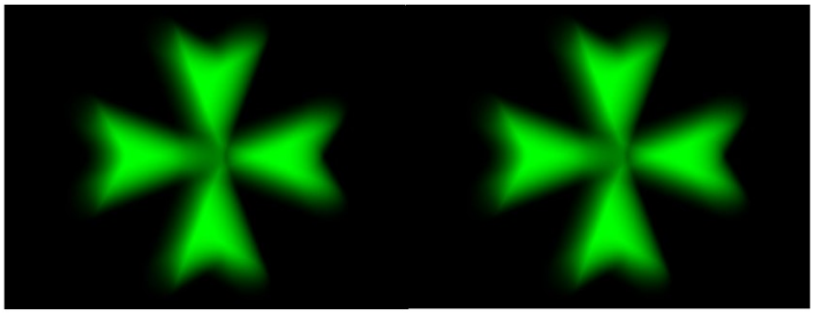

Figure d5. Effect of a monochromatic odd-order aberration on retinal image, in this case 0.1 μm of horizontal coma for a 4-mm pupil. Other details as in Figure d4.

Higher-order aberrations (HOAs): aberrations defined by Zernike polynomials having a radial order greater than 2. These aberrations correspond to those that cannot be compensated by using prisms or spherocylindrical lenses.

Unsigned cues: monocular optical cues that do not provide information about the direction in which the eye has to accommodate. For example, spherical defocus and odd-order aberrations are unsigned cues for accommodation (see Figure d5).

Signed cues: monocular optical cues that provide information about the direction in which the eye has to accommodate. Even-order aberrations or longitudinal chromatic aberration are signed cues (see Figure d3 and Figure d4).

Optical blur: it is the blur in the retinal image of the target as a consequence of inaccurate focus on the retina. This type of blur is produced in the presence of an accommodative error and optical aberrations.

Target blur: it is blur in the target itself created by a convolution between the original target and the PSF of a wavefront with a certain value of defocus or other aberrations. Even if the eye is focusing the target accurately on the retina, it will appear blurred to the eye since the target itself is blur (see Figure d4 and Figure d5 for examples of blurred targets). Thus, it is not caused by changes in target vergence.

Closed-loop accommodation: Accommodation condition where there is a feedback mechanism to focus the object accurately on the retina. This is the natural accommodation condition. For instance, let a subject be perfectly accommodating to a target at 2 D and there is a sudden change in accommodative demand from 2 to 3 D (retinal image blurred by 1 D). If the eye started changing its dioptric power by relaxing accommodation (wrong direction), the accommodative error would increase and the subject would know it because the retinal image will get even blurrier. The accommodative feedback system will indicate the right direction to accommodate and the accommodative error will decrease, improving the quality of the retinal image.

Open-loop accommodation: Accommodation condition with lack of feedback to improve the quality of the retinal image. It can be achieved under three artificial scenarios: by paralyzing accommodation; by inserting a very small artificial pupil in a plane conjugated to the eye's pupil, thus increasing largely depth of focus due to the narrowness of the pencil of rays coming from the pupil, so the target is seen clearly by the eye whatever its response is. Alternatively, it can be achieved by

providing always a fixed level of defocus on the retina, regardless the refractive state of the eye.

Resumen

El ojo proyecta información desde el mundo tridimensional a la retina, la cual es una superficie bidimensional. Por este motivo, teóricamente sólo objetos que se encuentren en el plano conjugado a la retina pueden ser enfocados de forma correcta y, por tanto, objetos que se encuentren por delante o por detrás del plano conjugado, serán percibidos como imágenes borrosas. Por suerte, la acomodación ocular permite al ojo joven ver objetos situados a diferentes distancias de forma nítida. Este sistema de autoenfoque se consigue gracias al cambio de potencia dióptrica experimentado por el ojo como consecuencia del cambio en la morfología del cristalino.

Debido a la alta frecuencia temporal de las ondas electromagnéticas del espectro visible, el ojo solo es capaz de detectar la intensidad de dichas ondas, perdiéndose inicialmente la información referente a la composición espectral y la distancia del objeto en el que la luz se refleja para posteriormente alcanzar la retina. El sistema visual, sin embargo, usa estrategias para tratar de recuperar la información perdida. Por ejemplo, existen tres tipos distintos de conos que responden de manera diferente a la luz con una distribución espectral concreta, permitiendo al cerebro interpretar la información referente al color de los objetos. Por otra parte, para recuperar la información sobre la distancia de la fuente de luz, el sistema visual compara la disparidad entre dos imágenes que provienen de dos ojos distintos, interpretando profundidad. Se sabe que esta información es usada para acomodar. Es bien sabido que somos capaces de acomodar en condiciones monoculares. Para ello el sistema visual aprende a detectar distancias a partir de la distancia aparente, tamaño cambiante, interposición de objetos, etc. Todos estos factores son conocidos como pistas monoculares de la percepción de la profundidad y son usados por el sistema visual para acomodar correctamente.

Sin embargo, aun cuando estas pistas monoculares son eliminadas, la mayoría de los ojos siguen siendo capaces de acomodar de forma correcta. Esto es debido a que existen otras pistas, conocidas como pistas ópticas, que proveen información al sistema visual para saber hacia qué sentido y cuánto debe acomodar. Las pistas ópticas se basan en la imagen formada en la retina. Estas pistas pueden ser impares (o *unsigned*), si dan información acerca de la magnitud y sentido de la

acomodación, o pares (*signed*), si solo dan información acerca de la magnitud. Por ejemplo, la borrosidad provocada por el desenfoque es una pista de tipo *unsigned* que puede activar el sistema acomodativo. Además, existen otras pistas ópticas que están basadas en que la imagen retiniana es diferente si se forman delante (desenfoque miópico) o detrás de la retina (desenfoque hipermetrópico), con lo cual son pistas de tipo *signed*. Entre este tipo de pistas se encuentra la aberración cromática longitudinal, las aberraciones monocromáticas de orden par (excepto el desenfoque), el efecto Stiles-Crawford y las pupilas con forma irregular. Todas ellas generan imágenes diferentes de un objeto si éste es enfocado delante o detrás de la retina.

A pesar de ser una pista importante, ha sido demostrado que muchos ojos no necesitan la aberración cromática para acomodar. Actualmente, existen tres teorías que intentan explicar el funcionamiento del mecanismo acomodativo. La primera de estas teorías se basa en las diferencias que existen en la imagen retiniana si la formación de la imagen del objeto se realiza delante o detrás de la retina. Las imperfecciones que existen en los ojos, como aberraciones y pupilas irregulares constituyen las pistas ópticas que hacen que las imágenes de objetos enfocados delante o detrás de la retina sean diferentes. Esta teoría supone que existe algún mecanismo en el cual la imagen retiniana es analizada, extrayendo de dicho análisis la información referente a la magnitud y al sentido de la acomodación. La segunda teoría postula que la acomodación se basa en un mecanismo de ensayo y error hasta encontrar la borrosidad mínima y, por tanto, el máximo contraste posible en la imagen retiniana. La tercera y última de estas teorías está basada en que el sistema visual humano es capaz de detectar directamente cambios en la vergencia de la luz y que es capaz de extraer la información referente a la magnitud y el sentido de la acomodación dependiendo si los rayos de luz que llegan a la retina son convergentes o divergentes. La teoría más ampliamente aceptada es la del mecanismo de ensayo y error, y esta se ve reforzada por la existencia de microfluctuaciones en la acomodación, las cuales podrían ayudar al sistema visual a escoger el sentido en el cual acomodar de forma correcta.

En 1951, Fincham demostró que un alto porcentaje de sujetos era capaz de acomodar sin la pista proporcionada por la aberración cromática. Fincham propuso la hipótesis de que el ojo detectaba la vergencia de la luz directamente para saber hacia qué sentido y cuánto debía acomodar. Según él, eran pequeños movimientos oculares, que asociados con el efecto Stiles-Crawford, permitían al sistema visual

saber hacia dónde y cuánto acomodar. Sin embargo, futuros experimentos acerca del posible papel del efecto Stiles-Crawford en la acomodación refutaron dicha hipótesis. En 1956, Heath concluyó que la acomodación era una respuesta a los gradientes de contraste de la imagen. En su experimento, cuando el objeto era emborronado, la respuesta acomodativa era menos intensa, llegando a ser nula cuando el emborronamiento era muy grande. Según Heath, si el ojo fuese sensible a la vergencia de la luz, éste debería acomodar aunque el objeto esté muy emborronado. En 1959, Campbell y Westheimer volvieron a poner en evidencia el importante papel jugado por la aberración cromática longitudinal, junto con algunas aberraciones monocromáticas como la aberración esférica y el astigmatismo. En 1977, Phillips y Stark demostraron en su experimento que la borrosidad producida por el desenfoque era suficiente para guiar la acomodación. Este experimento, junto con el de Heath, hicieron pasar a un segundo plano la teoría de la detección de la vergencia de Fincham y promovieron un mecanismo de ensayo y error para la acomodación. No fue hasta 1993 cuando las ideas de Fincham fueron recuperadas por Kruger y otros, en un experimento parecido al realizado en 1951, pero esta vez grabando la respuesta acomodativa dinámica a un estímulo sinusoidal. Por otro lado, el reciente desarrollo y aumento del uso de sistemas de óptica adaptativa, ha permitido comprobar si las aberraciones monocromáticas de orden par tienen algún efecto en la respuesta acomodativa. Aunque existe cierta controversia, la mayor parte de los estudios recientes parecen demostrar que estas aberraciones no ejercen efecto alguno sobre la acomodación dinámica.

En esta Tesis analizamos las diferentes teorías sobre el funcionamiento de la acomodación. El objetivo principal de la misma ha sido testear si la acomodación está guiada por los cambios en la vergencia de la luz, por las diferencias existentes en la imagen retiniana debida a las imperfecciones oculares, o si está guiada por un mecanismo de ensayo y error que minimice la borrosidad de la imagen retiniana y, por tanto, maximice su contraste.

Para este propósito, se ha desarrollado y montado un sistema personalizado de óptica adaptativa. Este sistema es capaz de medir y corregir aberraciones a alta velocidad. Está formado por un sensor de frente de onda Hartmann-Shack, que es el encargado de medir las aberraciones de la luz que le llega; un espejo deformable con 52 actuadores, el cual puede manipular las aberraciones mediante el cambio local de la forma de su superficie; un sistema Badal motorizado que permite el cambio de la

vergencia de la luz sin que se produzcan cambios en el tamaño aparente del objeto; un *microdisplay* junto con un filtro interferencial para así disponer de un objeto cuasi monocromático con una longitud de onda de 550 ± 5 nm; una cámara infrarroja, cuya función es la monitorización de la pupila de los sujetos, permitiendo así una alineación y centrado adecuados con respecto al sistema; un láser He-Ne utilizado para calibrar el sistema; y un diodo infrarrojo superluminiscente usado para tomar medidas a los sujetos. El funcionamiento de este sistema óptico se ha controlado a través de Matlab, mediante el uso de *software* personalizado basado en funciones y librerías proporcionadas por el fabricante (Imagine Eyes, Francia).

Para testear las diferentes teorías, primero se seleccionaron los participantes que eran capaces de acomodar monocularmente a cambios de vergencia de la luz sinusoidales entre 1 y 3 dioptrías (D) de demanda acomodativa y a una frecuencia temporal de 0,2 Hz. Una función sinusoidal con la misma frecuencia temporal que la demanda acomodativa se ajustó a la respuesta obtenida en cada caso. De este ajuste, se extrajeron la amplitud (variación máxima de la sinusoidal) y la fase temporal (diferencia temporal entre la demanda acomodativa y la respuesta) de la respuesta. El cociente entre la amplitud de la respuesta y la amplitud de la demanda es lo que se conoce como ganancia. La ganancia, junto con la fase temporal fueron los parámetros elegidos para caracterizar las respuestas acomodativas a demandas sinusoidales. Como umbral para conocer si un sujeto acomodaba o no de forma adecuada a la demanda sinusoidal, se seleccionó una ganancia de mayor o igual a 0,2. Este umbral está justificado debido a que valores menores de 0,2 pueden ser consecuencia de ruido en la medida o pequeñas fluctuaciones que ocurren frecuentemente, aunque no se siga de forma correcta el movimiento sinusoidal. En este experimento preliminar, las pistas monoculares de profundidad se eliminaron mediante el uso de un sistema Badal y las pistas proporcionadas por la aberración cromática se eliminaron usando un objeto monocromático. El experimento preliminar consistió en 6 pruebas de 25 segundos cada una a cada sujeto, y era necesario puesto que los experimentos principales evaluaban la acomodación en condiciones tanto o más estrictas que en este experimento. De entre los 16 sujetos a los que se les realizaron estas pruebas preliminares, sólo 9 fueron capaces de acomodar correctamente en condiciones monoculares y monocromáticas. Estos 9 sujetos presentaron ganancias medias de entre 0,26 y 0,78, y fases temporales de entre 0,22 y 0,58 segundos.

Con el sistema experimental previamente descrito se realizaron tres experimentos sobre estos 9 sujetos que se detallan a continuación.

Experimento I: Para testear la teoría de que el ojo extrae hacia dónde ha de acomodar y cuánto de las diferencias existentes en la imagen retiniana como consecuencia de las imperfecciones, se realizó un experimento en el cual se midió la respuesta acomodativa dinámica monocular a un objeto monocromático, usando un sistema Badal. En este caso, se eliminó el *feedback* de la acomodación usando una pupila artificial de pequeño diámetro, la cual incrementó en gran medida la profundidad de campo de los sujetos, eliminando así la posibilidad de detectar cambios en la vergencia de la luz. Se reprodujeron en un *microdisplay* varios vídeos simulando la borrosidad producida por una variación sinusoidal en el desenfoque entre −1 y +1 D, mientras se midió la respuesta acomodativa a una frecuencia de 20 Hz usando un aberrómetro Hartmann-Shack. Además, la respuesta acomodativa también se midió con vídeos simulando el mismo cambio sinusoidal en la borrosidad, junto con la borrosidad producida por una cantidad fija de astigmatismo, de aberración esférica y de las aberraciones de cada sujeto. Se realizaron 6 pruebas con una duración de 25 segundos cada una por condición y sujeto, haciendo un total de 24 pruebas por sujeto. Siete de los nueve sujetos mostraron una respuesta acomodativa prácticamente plana, con ganancias medias menores a 0,1, mientras que los dos restantes mostraron una mayor actividad, con ganancias medias entre 0,23 y 0,46, pero tampoco fueron capaces de seguir la variación sinusoidal de la borrosidad. Los resultados de este experimento indican que el ojo no acomoda según la primera teoría; esto es, el sistema visual no usa las diferencias en la imagen retiniana causadas por las imperfecciones del ojo para acomodar. De estos resultados se puede concluir también que el ojo debe usar o bien la vergencia de la luz, o bien el *feedback* de la propia acomodación, o ambos a la vez.

Experimento II: Para comprobar si el ojo usa los cambios en vergencia de la luz para acomodar de forma correcta, se realizó un experimento en el que las aberraciones de los sujetos, excepto el desenfoque, fueron corregidas a 20 Hz mediante un sistema de óptica adaptativa. En este experimento se introdujeron dos condiciones diferentes: una en la que el espejo deformable proveía un nivel de desenfoque en la retina que variaba sinusoidalmente entre −1 y +1 D, y otra en la que el espejo deformable siempre proveía un desenfoque de cero en la retina, pero el objeto en el *microdisplay* era emborronado sinusoidalmente de la misma forma que

en la condición anterior, pero artificialmente. Los sujetos veían el objeto monocularmente a través del sistema Badal y de una pupila artificial circular de 4 mm, con lo que todas las pistas binoculares y monoculares fueron eliminadas. Los sujetos solo disponían de la información de los cambios en la vergencia de la luz y de la borrosidad (primera condición) o sólo cambios en la borrosidad (segunda condición). En este experimento tampoco existía información procedente del *feedback* de la acomodación, puesto que el espejo deformable siempre proveía un nivel fijo de desenfoque (sinusoidal en la primera condición y siempre cero en la segunda), abriendo por tanto el lazo acomodativo. Se realizaron 6 pruebas con una duración de 25 segundos cada una por condición a cada sujeto, lo que hizo un total de 24 pruebas por sujeto. Ocho de los nueve sujetos fueron capaces de acomodar de forma satisfactoria cuando el espejo proporcionaba cambios sinusoidales de la vergencia de la luz, mostrando una ganancia media (±2 errores estándar de la media) de 0,50 ± 0,19; mientras que ninguno fue capaz de acomodar cuando el espejo proporcionaba un desenfoque nulo en retina y el objeto era directamente emborronado sinusoidalmente, obteniendo una ganancia media de 0,07 ± 0,02. Estos resultados demostraron que el ojo usa los cambios que se producen en la vergencia de la luz para acomodar de forma correcta, mientras que el ojo no es capaz de seguir los cambios producidos en la borrosidad del objeto cuando no existe *feedback* de la acomodación, tal y como se demostró también en el experimento anterior.

Experimento III: Para testear si la acomodación sigue un mecanismo de ensayo y error que minimiza la borrosidad y por ende maximiza el contraste de la imagen retiniana, o bien se basa en la detección de forma directa los cambios que se producen en la vergencia de la luz, se realizó un experimento con las dos mismas condiciones que en el experimento anterior, pero esta vez el ojo sí que disponía de *feedback* de la acomodación, es decir, el lazo acomodativo era cerrado. En la primera condición, el *feedback* provenía de la acomodación en sí, ya que el espejo deformable no proveía un nivel fijo de desenfoque en la retina, sino que lo dejaba intacto; mientras que, en la segunda condición, el *feedback* se consiguió de manera artificial como se describe a continuación. Dependiendo de la respuesta del ojo, el objeto se emborronaba o se aclaraba. Por ejemplo, si el objeto experimentaba un cambio en borrosidad correspondiente al aumento de la demanda acomodativa en 1 D, y el ojo respondía acomodando 0,6 D en el sentido correcto, el objeto disminuía su borrosidad hasta coincidir con una borrosidad equivalente a 0,4 D, que se corresponde con el error acomodativo en este caso. Si el ojo continuaba acomodando hasta alcanzar 1 D,

el objeto se aclaraba consecuentemente. Estas dos condiciones se testearon en 3 sub-experimentos diferentes, dependiendo del tipo de cambio que se producía en el estímulo: en el primer sub-experimento, el estímulo permanecía fijo a una demanda acomodativa de 2 D durante 50 segundos; en el segundo sub-experimento, el estímulo presentaba variaciones bruscas en forma de escalón de 1 D de amplitud. El estímulo siempre estaba centrado en 2 D de demanda acomodativa, saltando de forma aleatoria en el tiempo o bien a 3 D o a 1 D. Luego volvía a saltar a 2 D de demanda acomodativa, y así sucesivamente, durante 50 segundos. En el tercer sub-experimento, la demanda acomodativa cambiaba de forma sinusoidal entre 1 y 3 D a cuatro frecuencias diferentes: 0,05, 0,10, 0,20 y 0,40 Hz. Para cada frecuencia, la duración de las pruebas era diferente: 40 segundos para 0,05 Hz, 30 segundos para 0,10 Hz, y 25 segundos para 0,20 y 0,40 Hz. La variación en cuanto a la duración de las pruebas se debió a un intento de compensación entre el número de ciclos de la sinusoidal y la propia duración. Se le realizaron 6 pruebas a cada sujeto por sub-experimento y condición, elevándose a un total de 72 pruebas por sujeto. En el primer sub-experimento, en el que el estímulo era estacionario, se evaluó el error acomodativo de los sujetos en las dos condiciones. En este caso, no hubo diferencias entre el error acomodativo medio de cada sujeto entre condiciones, excepto para uno de los nueve sujetos. El error cuadrático medio (RMS) del error acomodativo resultó ser consistentemente mayor en la condición en la que no había cambios en la vergencia de la luz, sólo en la borrosidad del objeto, indicando que había más fluctuaciones que cuando sí había cambios en la vergencia de la luz. Esto pudo ser debido a que era algo más complicado para los sujetos mantener el nivel de acomodación adecuado cuando cambios en la vergencia de la luz no estaban presentes. En el caso del estímulo variando de forma brusca en escalones, la respuesta acomodativa era más errática, más lenta y de menor magnitud cuando no había cambios en la vergencia de la luz. La diferencia media de ganancias entre ambas condiciones fue de 0,41 ± 0,20. En esta condición, los sujetos respondían en el sentido erróneo en mayor proporción que cuando sí existían cambios reales en la vergencia de la luz. Con respecto al estímulo que variaba de forma sinusoidal, los sujetos acomodaron mucho mejor cuando había cambios en la vergencia de la luz. A partir de 0,20 Hz de frecuencia temporal, las respuestas acomodativas empeoraban en ambas condiciones, pero de forma más brusca cuando los cambios eran solo en la borrosidad del objeto. Para 0,40 Hz, solo algunos sujetos eran capaces de acomodar satisfactoriamente, y solo en la condición en la que había cambios en la vergencia de

la luz. Las diferencias de ganancias medias fueron de 0,36 ± 0,16, 0,43 ± 0,15, 0,44 ± 0,12, and 0,19 ± 0,20 para las frecuencias temporales de 0,05, 0,10, 0,20 y 0,40 Hz, respectivamente. A la luz de estos resultados, se concluyó que lo más probable es que la acomodación esté guiada tanto por la detección de cambios en la vergencia de la luz, como por un mecanismo de ensayo y error, aunque la acomodación funciona bastante mejor cuando cambios en la vergencia de la luz están presentes.

La corrección de aberraciones e inducción del desenfoque necesario por parte del sistema de óptica adaptativa era esencial para los experimentos II y III. La corrección de aberraciones de forma óptima es importante para eliminar las pistas que estas aberraciones proporcionan. La inducción de la cantidad de desenfoque necesaria es importante para eliminar el *feedback* de la acomodación y, por tanto, para evitar que el ojo pueda obtener información para acomodar de forma correcta de este *feedback*. Por este motivo, se evaluó cuidadosamente el comportamiento del sistema en dichos experimentos. La corrección de aberraciones fue óptima en todos los casos, con valores de RMS de astigmatismo y aberraciones de alto orden casi siempre por debajo de 0,1 micras. La inducción del desenfoque requerido en cada experimento se evaluó calculando el error cometido en el desenfoque. El error medio era siempre menor de 0,01 D, presentando una desviación absoluta de la mediana máxima de 0,09 D. Dado que la inducción del desenfoque se realizaba a 20 Hz, es muy posible que cambios tan pequeños en el desenfoque y tan cortos en el tiempo no influyan en la respuesta acomodativa de los sujetos.

Por tanto, la conclusión general de esta Tesis es que los cambios en la vergencia de la luz juegan un papel fundamental en el mecanismo de la acomodación humana; posiblemente más fundamental que el mecanismo de ensayo y error, el cual era el más aceptado por la comunidad científica. Sin embargo, la generalización de estos resultados es compleja, dado que todos los experimentos realizados fueron bajo condiciones muy restrictivas. En cualquier caso, parece razonable especular que para objetos policromáticos, algunos de estos sujetos también usarían cambios en la vergencia de la luz para extraer diferencias de desenfoque entre conos sensibles a longitudes de onda corta, media y larga, respectivamente.

Aunque no es el objetivo de esta Tesis, sería interesante conocer cómo detecta el ojo los cambios de vergencia. Como indican los resultados obtenidos en esta Tesis, la vergencia de la luz es esencial para que el ojo sea capaz de acomodar de forma correcta. Pero, ¿cómo puede el ojo detectar cambios en la vergencia de la luz si sólo

detecta intensidades? Parece lógico por tanto pensar en la existencia de un mecanismo que produzca un cambio en la distribución de intensidades en la retina en función del signo del desenfoque. Recientemente se han descrito dos modelos teóricos que intentan explicar la manera en la que el sistema visual es capaz de detectar cambios en la vergencia de la luz. El primero de estos modelos se basa en que los conos podrían actuar como antenas y serían capaces de diferenciar entre luz convergente y divergente gracias a la dispersión y reflexiones internas que se producirían en estos fotorreceptores. El segundo modelo se basa en las diferencias en la imagen retiniana que se produce dependiendo de si la luz converge o diverge como consecuencia de los vasos sanguíneos que se encuentran en la retina. Dado que en esta Tesis la acomodación ha sido evaluada de forma dinámica, podría existir la posibilidad de que el movimiento del objeto aporta información del signo del desenfoque, como ocurre en retinoscopía. Este campo presenta posibilidades de futuros estudios a realizar que explicarían el mecanismo de detección de la vergencia por parte del sistema visual humano.

Los resultados obtenidos en esta tesis y muchos de los trabajos realizados en los dos últimos siglos nos permiten afirmar que la acomodación está guiada por la conjunción de una serie de pistas o mecanismos que se basan en pistas binoculares y monoculares, aberración cromática, vergencia de la luz y quizás el mecanismo de ensayo y error, todos ellos actuando en conjunto.

Además de la implicación de estos resultados en el conocimiento de aspectos fundamentales del proceso acomodativo, éstos podrían tener consecuencias en el conocimiento del proceso de emetropización con potenciales implicaciones clínicas. Este proceso es el crecimiento coordinado de todos los elementos ópticos del ojo de tal forma que la imagen de un objeto lejano sea enfocada en retina. Si este proceso de emetropización falla, puede desencadenar en miopía, que es un problema de salud pública que, presente en gran magnitud, puede llegar a provocar ceguera. La acomodación y el proceso de emetropización podrían compartir un lazo o bucle de *feedback* similar para enfocar la imagen de un objeto en retina. Lógicamente, los ajustes oculares necesarios para la emetropización van a un ritmo mucho más lento que en la acomodación.

En las últimas décadas, la prevalencia de la miopía ha aumentado considerablemente en países desarrollados. Este hecho parece estar ligado con el

gran aumento en el uso de la visión cercana (*smartphones*, videoconsolas, lectura…) por parte de gente joven, cuyos ojos aún se encuentran en período de crecimiento. Por tanto, parece razonable pensar que el uso aumento en el uso de la visión cercana está relacionado con el aumento de la prevalencia de la miopía. Además, estudios realizados en distintos animales han mostrado que el ojo de los vertebrados compensa la vergencia positiva o negativa con cambios en su longitud axial. Por estos motivos, el comprender cómo funciona el mecanismo de acomodación puede ayudar a desarrollar tratamientos efectivos para el control de la miopía.

Abstract

Ocular accommodation is the autofocus mechanism of the healthy young eye that allows objects at different distances to be seen clearly. Even in the absence of binocular, monocular, and chromatic cues, most eyes continue to be able to accommodate. How? The fundamental mechanism driving accommodation under these stringent conditions is still unclear. There are three main theories. The first theory is that the visual system is able to use the small differences in retinal images formed when the object is focused behind or in front of the retina. These differences are due to imperfections that exist in the optics of all eyes, such as monochromatic aberrations and irregularly shaped pupils. The second, and most widely accepted theory is that accommodation works as a trial-and-error system, with the goal to minimize retinal image blur, and thus maximize retinal contrast. The third theory is that the eye is able to extract the necessary information to accommodate in the right direction directly from light vergence.

The aim of this thesis was to put the aforementioned theories to the test. Three experiments were devised that required the use of a custom-built adaptive optics system. Accommodation was recorded with a Shack-Hartmann wavefront sensor, while participants viewed a monochromatic Maltese cross monocularly through a Badal optical system and while their aberrations were being corrected with the adaptive-optics system.

This thesis presents evidence against the first theory (in agreement with previous works) and in support of the second and third theory. Even though the human eye can accommodate using a trial-and-error function to minimize blur and maximize contrast, it is considerably more precise when light vergence is present. Thus, the results obtained here support the less accepted theory that the human eye is able to detect and use light vergence to accommodate.

1. Introduction

1.1. Ocular Accommodation

The first stage in human vision is the formation of an image on the retina from an object located at a certain distance from the eye. Image formation on the retina is possible thanks to the optical system of the human eye, whose dioptric power depends on the cornea and the crystalline lens. Since the eye projects information from the three-dimensional world onto a two-dimensional surface (retina), only objects that are located at a certain distance can be theoretically imaged sharply. In other words, only the conjugated plane of the fovea can be focused on the retina. Therefore, objects that are closer or further away from that point appear as blurred images. Nonetheless, besides the fact that retinal images are not perfect due to the presence of aberrations, the eye presents a certain tolerance to images that are out of focus. This tolerance is known as depth of focus (Campbell, 1957; Ogle & Schwartz, 1959; Atchison et al. 1997), and it allows clear images to be seen even if the target is slightly displaced from the conjugated plane. Fortunately, the dioptric power of the healthy and young human eye varies for objects that are outside the range of the depth of focus by changing the shape of the crystalline lens (see Figure 1.1) to form sharp images on the retina. The variation in dioptric power is known as accommodation (Young & Brocklesby, 1793) and it was first described in 1619 (Scheiner 1619).

Accommodation is generally unconscious (Kaufman, 1992) and it can be regarded as the autofocus system of the eye. This autofocus system is relatively fast (Mordi & Ciuffreda, 2004) and, despite the well-known existence of errors in accommodation (Heath, 1956; Tucker & Charman, 1975; López-Gil et al. 2013), whether it is lag (under-accommodation) or lead (over-accommodation), it is precise enough for the healthy young eye to perform daily tasks. But how does the visual system know when to accommodate and by how much?

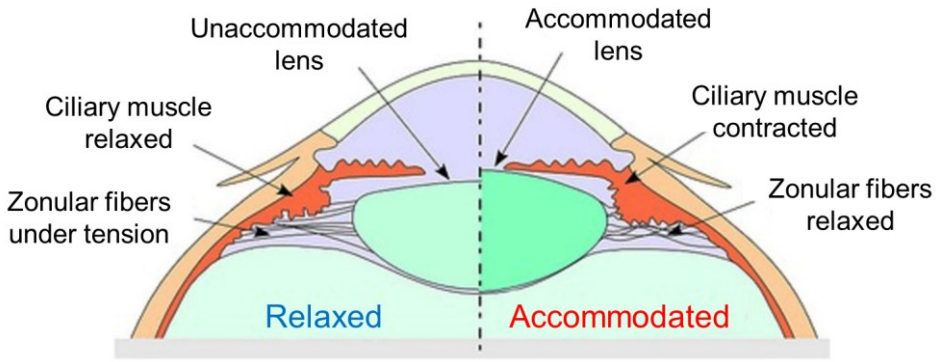

Figure 1.1. Illustration of a human eye. The right half of the figure shows the eye relaxed or not accommodating, whereas the left half of the figure shows the eye while accommodating. Note the differences in the crystalline lens shape between the two halves. Figure adapted from Petrash (2013).

1.1.1. Binocular cues for accommodation

Electromagnetic waves in the visible spectrum correspond to an electromagnetic field that changes extremely fast in time (between 1.25×10^{-15} and 2.50×10^{-15} s). The retina is able to detect only the square of the amplitude of the electromagnetic wave, which is the intensity (Hecht, 1987). Thus, the spectral distribution of light reflected by objects and reaching the retina, as well as its distance, is lost. Nevertheless, the visual system has different strategies to recover partially the information lost. For instance, the visual system has three different types of cone photoreceptors that respond differently to light with certain spectral distribution, allowing the brain to interpret the reflectance properties of objects as perceived color (von Helmholtz, 1866). For recovering information about the distance to the source of light, or depth information, the visual system has a different strategy: comparing disparity from signals coming from the two separate eyes. This strategy is analogous to the one used by the auditory system, in which the distance from the source of the sound waves is inferred by computing the time lag between the signals arriving to each ear. From the disparity between the two signals, or images, the visual system is able to interpret depth (Wheatstone, 1838; Qian, 1997). This depth information is used for accommodation (Wheatstone, 1838; Fincham, 1951). Information that can be used by the visual system to know how much and where to accommodate (accommodation or disaccommodation) is commonly referred to as cues for accommodation. Cues can be signed or unsigned, depending on whether

they provide information about the sign of the defocus or not (see Definitions). Are binocular cues necessary to accommodate or are monocular cues sufficient?

1.1.2. Monocular cues for accommodation

Most eyes are able to accommodate correctly under monocular conditions because the visual system is able to extract depth information from monocular cues. Some of these monocular cues are apparent distance (Ittelson & Ames, 1950; Takeda et al. 1990); changing size (Kruger & Pola 1986; Kruger & Pola 1987); and interposition of objects (Takeda et al., 1990).

1.1.3. Optical cues for accommodation

Even if all these binocular and monocular cues are suppressed, the majority of eyes can still accommodate correctly. They do so with the aid of information that can be extracted from the image formed on the retina and are consequence of the optics of the eye. This information is referred to as optical cues throughout this thesis. An out-of-focus retinal image of a perfect eye without astigmatism and HOAs can trigger accommodation (Phillips & Stark, 1977). But there are other signed optical cues that are based on the fact that images formed at the retina differ if they are focused in front (myopic defocus) or behind the retina (hyperopic defocus). Examples of signed optical cues are chromatic aberration (see Figure d3) (Kruger & Pola 1986; Flitcroft 1990; Kruger et al. 1993; Kruger et al. 1995), and even-order monochromatic aberrations (see Figure d4), which generate different images for different signs of defocus (Wilson et al. 2002; López-Gil et al. 2007). Also, irregularly shaped pupils (Wyatt, 1995; López-Gil et al. 2007), and the Stiles-Crawford effect (Kruger et al. 2001; Kruger et al. 2004; Stark et al. 2009), can lead to different retinal images of the object depending upon if they are formed in front of or behind the retina (López-Gil et al. 2007).

1.1.4. Accommodation theories

Previous works have shown that longitudinal chromatic aberration helps the eye to accommodate (Fincham, 1951; Campbell & Westheimer, 1959; Kruger et al. 1993). However, the eye is also able to accommodate even in monochromatic viewing

conditions (Fincham, 1951; Kruger et al. 1993, 1995; Chin et al. 2009a, 2009b). There are three main theories that try to explain how the accommodative process works.

1.1.4.1. Shape of blur in the retinal image

Imperfections in the optics of the eye, such as astigmatism and HOAs, or irregularly shaped pupils (see Section 1.1.3) lead to the formation of different retinal images when the object is focused in front of or behind the retina. This theory is based on the fact that there is some kind of image processing that analyses the shape of the retinal image in order to extract the sign of defocus. The eye then would use this information to accommodate in the right direction.

1.1.4.2. Trial-and-error system

Another theory states that human accommodation is achieved by a trial and error so that retinal contrast is maximized. This theory has been the most widely accepted since the 1950s (Heath 1956; Troelstra et al. 1964; Stark & Takahashi 1965; Smithline 1974; Phillips & Stark 1977; Day et al. 2009; Metlapally et al. 2016), and it is supported by the existence of microfluctuations in accommodation (Charman & Heron 1988; Charman & Heron 2015) that appear even when the eye is accommodating to a steady-state target. These small-magnitude fluctuations could help the accommodative system to determine the correct direction of accommodation. For an out-of-focus target, a fluctuation toward one direction would improve the retinal image contrast and decrease its blurriness, whereas a fluctuation in the opposite direction would deteriorate the retinal image contrast and increase its blurriness.

1.1.4.3. Detection of light vergence

A less-accepted theory was proposed by Fincham (1951). He hypothesized that there must be a more direct way to extract the sign and magnitude of defocus than by trial and error. He speculated that the human visual system detects light vergence, that is, whether light rays reach the retina diverging or converging. According to his theory, the sign and magnitude of defocus is extracted by the visual system from light vergence at the retina. He proposed that this information was extracted with the help of the Stiles-Crawford effect and using small and rapid ocular movements to scan the scene. Nonetheless, a later work found that the visual system seems to not use the average Stiles-Crawford effect for accommodating (Kruger et al. 2001).

1.2. Previous work

1.2.1. Classic accommodation experiments

1.2.1.1. Fincham's 1951 experiment

One of the first studies of the effect of the monocular optical cues on accommodation dates back to 1951, when Hartridge suggested to Fincham that the necessary information for accommodating in the right direction had to be extracted from longitudinal chromatic aberration. Fincham performed an experiment where he tested this theory (Fincham, 1951). In one of his experiments, he stimulated the accommodation of young subjects by using spherical lenses in monocular conditions. When the target was illuminated by white light, all the participants were able to accommodate and disaccommodate correctly without any problem. When the target was illuminated by monochromatic light, however, he found that approximately 60% of the subjects found it difficult to accommodate and disaccommodate, or they were just not able to do it. Fincham also used special lenses that neutralized the longitudinal chromatic aberration, obtaining the same result as with monochromatic light. The refractive index for short wavelengths (which appear blue on a black background) is greater than for longer wavelengths (which appear red on a black background). Consequently, shorter-wavelength light focuses before longer-wavelength light. Therefore, the retinal image of a target illuminated by white light would appear surrounded by a blue edge or fringe when there is a myopic defocus and by a red fringe when there is a hyperopic defocus (see Figure d3).

Since around 40% of the participants were still able to accommodate under monocular conditions and monochromatic light, Fincham postulated that these subjects were using spherical aberration as the cue to accommodate. In another experiment, Fincham neutralized the effect of the spherical aberration by the use of an annular pupil and then proceeded to repeat the experiment on those subjects who could accommodate when the target was illuminated with monochromatic light. Subjects accommodated with the annular pupil as well as without it, which led Fincham to speculate that in absence of chromatic aberration, the visual system was extracting the necessary information for accommodating correctly from light vergence. He concluded that the eye is able to determine whether the light rays coming from an object are divergent or convergent at the retina, and then it adjusts its dioptric power consequently.

1.2.1.2. Heath's 1956 experiment

The theory that the visual system extracts the information to accommodate from light vergence faded into the background when Heath (1956) concluded that accommodation must be a response to the contrast gradients in the image, since blurring the target reduced the accommodative reflex and removed it entirely when the amount of blur was too much. He performed an experiment in which he tested accommodation when the object was progressively blurred using glass diffusing screens. According to Heath, if the eye was sensitive to light vergence, it should accommodate even when the image was greatly blurred. However, the results showed that the accommodative response decreased when the optical blur of the object increased.

1.2.1.3. Campbell and Westheimer's 1959 experiment

A few years later, Campbell & Westheimer (1959) confirmed the role of chromatic aberration in accommodation. They showed images defocused randomly in both directions to subjects under cycloplegia and then asked them to bring the images into focus by moving the object by turning a knob. First, they used an object illuminated with white light; in this condition the subjects could bring the object into focus after just a few initial trials to familiarise themselves with the experiment. After this, subjects were deprived of spherical aberration. In this condition, none of the subjects were able to respond correctly all the time. Interestingly, after introducing a cylindrical lens and after some training, subjects were able to respond correctly again, indicating that astigmatism was a cue used by the subjects to know which direction to move the object to see it clearly. This experiment was important to corroborate Fincham's findings on chromatic aberration and, at the same time, it gave importance to the potential cues provided by spherical aberration for accommodation. Nevertheless, it should be noted that this experiment did not follow real accommodation conditions, since subjects were allowed to familiarise with the experiment and learn the shape of the targets for a positive or negative defocus.

1.2.1.4. Phillips and Stark's 1977 experiment

Phillips and Stark (1977) demonstrated that blur alone could trigger accommodation. In their experiment, the loop in target blur was closed by constantly measuring the response of the eye, and then modifying accordingly the blurriness of the target without changing the vergence of the light reaching the retina. For example, if the target was blurred the equivalent of 1 D of defocus and the eye

accommodated that exact amount in the right direction, the target was cleared. However, if the eye continued accommodating, the target was blurred consequently. Since under these conditions, there were no signed cues, the only way in which the eye could accommodate was by trial and error, or how Phillips and Stark referred to it, the eye was constantly "hunting", searching for the correct accommodation. The recorded responses were at times in the wrong direction, and then changed rapidly towards the correct direction. Phillips and Stark used a sophisticated system to perform an outstanding work for that time, however, their main conclusion that blur alone drives accommodation, seems too far fetched from their measurement in a single subject who, in addition usually responded in the wrong direction to a sudden change in target vergence (see Figure 1.2).

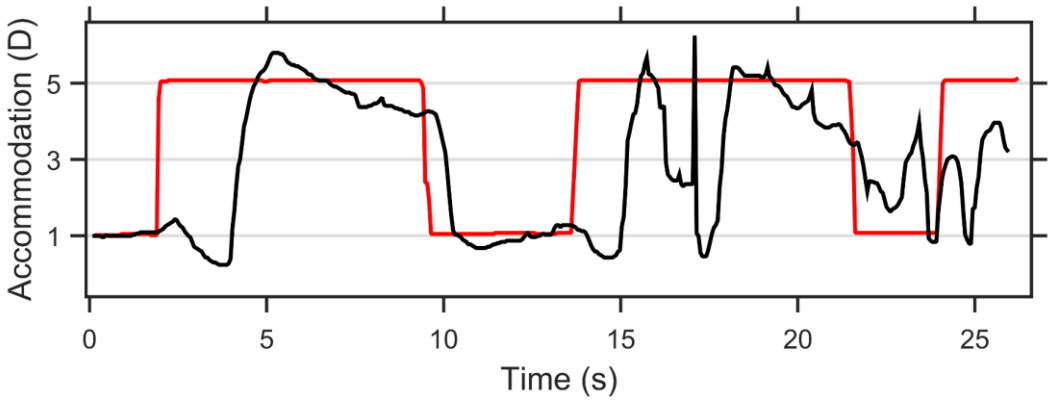

Figure 1.2. Accommodation driven by closed-loop target blur. Red solid line shows the change in target blur, whereas black solid curve shows the accommodative response of a subject. Note the wrong initial direction of accommodation in the first part of the trial and the erratic nature of the response in the second part of the trial. Figure reprinted from Phillips and Stark (1977).

1.2.2. Fincham revisited

It was not until the late 1980's and the beginning of the 1990's, when Fincham's ideas were revived by Kruger and collaborators (1993). They carried out a series of experiments similar to those performed by Fincham in 1951, but recording the dynamic accommodative response to a sinusoidally changing stimulus. They used a polychromatic and monochromatic targets, and neutralized the chromatic aberration using a special lens. Moreover, they introduced a new condition that reversed the effect of longitudinal chromatic aberration. The accommodative response of the subjects decreased when longitudinal chromatic aberration was

neutralized, but not as much as when monochromatic light was used. This result was in disagreement with Fincham's findings since in his experiment neutralizing chromatic aberration and using monochromatic light yielded the same results. There was no clear explanation for this result, but Kruger hypothesized that could be caused by the residual longitudinal chromatic aberration that the lens could not neutralize, or that perhaps it was caused by the spectral characteristics of the white light used. When the longitudinal chromatic aberration was reversed, the responses were clearly affected, sometimes they were absent and sometimes even in counter-phase. The authors concluded that there are two systems involved in accommodation: an achromatic one, which is slow and relatively inefficient, and a chromatic one, that when supplements the activity of the achromatic system, the accommodative response is more precise and effective.

The importance of chromatic aberration was highlighted again in experiments in which the eye was able to accommodate to polychromatic simulations of sinusoidal target blur under open-loop accommodation (Kruger et al. 1995), whereas when the simulated target blur was monochromatic, no eye could accommodate correctly (Kruger et al. 1997).

1.2.3. Contemporary experiments with adaptive optics

The development and implementation of adaptive optics (AO) in vision (Roorda, 2011; Marcos et al. 2017) allowed investigators to test whether monochromatic aberrations, such as spherical aberration and astigmatism, were helping the eye to better accommodate. Using AO technology, some or all aberrations of the eye can be corrected or induced in real time. By correcting particular monochromatic aberrations and evaluating the accommodative response, it is possible to assess the effect of these aberrations on accommodation. Recent studies manipulating the eye's natural aberrations suggest that the eye does not use monochromatic aberrations for accommodation (Chen et al. 2006; Chin et al. 2009a, 2009b), since no significant differences were found between the response with natural aberrations present, or corrected. In the latest experiment (Bernal-Molina et al. 2017), the accommodative response of 2 out of 8 subjects seemed to increase slightly when astigmatism was present while the rest of monochromatic aberrations were corrected.

1.3. Motivation and aim

The overarching aim of this thesis is to test the different theories on human monocular and monochromatic accommodation. In particular, whether accommodation is driven by changes in light vergence, by the differences in shape of retinal blur due to imperfections of the eye, or if accommodation is driven by trial and error to minimize retinal blur and maximize contrast. The long accepted theory has been that accommodation is driven by a trial-and-error strategy; however, the accommodation response of the eye to variations in vergence over time seems too fast to be explained just by the use of such a simple trial-and-error strategy, which relies on the relatively "sluggish" frequency characteristics of microfluctuations of accommodation (Charman & Heron 2015).

1.4. Structure of the thesis

In the remainder of this thesis, the system that was built to carry out all the experiments is described in detail in Chapter 2. Chapter 3 describes a preliminary experiment that was carried out to select adequate participants for the rest of the experiments. These participants had to be able to accommodate under certain stringent conditions (open-loop accommodation in monocular and monochromatic target blur) that were common in the three main experiments. After this, the three main experiments to study the role of light vergence in accommodation are described in detail. First, Chapter 4 describes an experiment to evaluate if differences in images formed in front of or behind the retina, as consequence of monochromatic aberrations, were enough to drive accommodation when the rest of the cues were not available to the eye is presented in Chapter 4. Chapter 5 describes an experiment to study if light vergence or blur alone can drive accommodation. Chapter 6 describes a series of experiments to test the two main hypotheses about human accommodation described before (accommodation driven by light vergence vs. accommodation driven by a trial-and-error strategy). Finally, Chapter 7 presents the overall conclusions of this thesis and future work.

2. Optical system characterization

In this Chapter, the basics for correction of aberrations with AO are described. Then, the custom-made AO system that was used to perform the experiments mentioned in Section 1.4 is fully described and characterized. The AO system has already been used in (Papadatou et al. 2016; Jaskulski et al. 2016; Del Águila-Carrasco et al. 2017; Marín-Franch et al. 2017).

2.1. Adaptive optics

Adaptive optics was first developed and used in astronomy (Babcock, 1953; Roddier, 1999) to try and remove distortions in the images obtained with telescopes. It was not until 1997, when AO was first applied in the human eye (Liang et al. 1997). Since then, AO has rapidly increased its popularity in vision: from retinal imaging in the living eye (Miller, 2000; Morris et al. 2015; King et al., 2017) to applications regarding visual optics (Chen et al. 2006; Benard et al. 2011; Papadatou et al. 2016).

The primary goal of AO in vision is to correct the aberrations of the eye, so that a perfect image is formed on the retina (Porter et al. 2006; Tyson, 2012). In other words, the aim is to bypass the optics of the eye and as a result avoid the degradation of the image produced by these very same optics. If there is a point object, the ideal scenario would be to obtain the same point imaged on the retina. This, however, is not possible because of diffraction that takes place when the light passes through the eye's pupil (Cowley, 1995).

In order to achieve this goal every AO system requires two basic elements: an instrument for measuring the aberrations of the eye, and an instrument for manipulating those aberrations (Porter et al. 2006; Roorda, 2011; Tyson, 2012; Marcos et al. 2017). The first key element is typically a Shack-Hartmann wavefront sensor (Thibos, 2000; Platt & Shack, 2001), which is essentially formed of a series of micro-lenses that focuses an incoming light beam to the CCD of a camera (see Figure 2.1). If the wavefront coming from the eye is perfect, the micro-lenses will project a regular pattern of spots in the camera sensor. However, if the wavefront coming from the eye is aberrated, the spots projected in the camera sensor will show an irregular pattern. The second key element is typically a deformable mirror, which is a

reflective surface which shape can be locally modified, thus changing the shape of the wavefront.

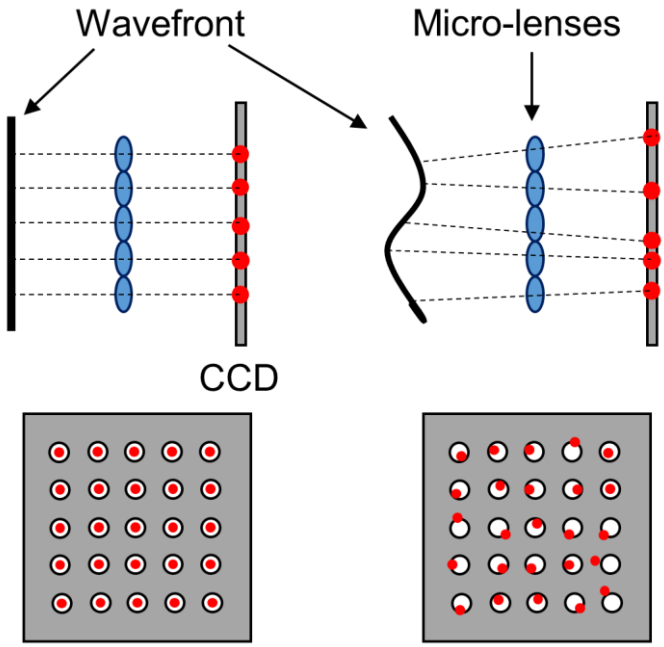

Figure 2.1. Flat wavefront (left) and aberrated wavefront (right) reaching a Shack-Hartmann sensor. In both conditions, the light passing through the micro-lenses forms light spots on the CCD (red dots). When the wavefront is flat, the light spots match the center of the micro-lenses (white circles), whereas when the wavefront is aberrated, the light spots present deviations with respect to the center of the micro-lenses. Wavefront slopes can be obtained from these deviations at every location.

2.1.1. Wavefront aberrations and Zernike polynomials.

A wavefront is a surface defined by points of rays that have the same phase (Whelan & Hodgson, 1989). When the wavefront is plane, it is called perfect wavefront, and it is not aberrated. However, when the shape of the wavefront is irregular, it is aberrated, as depicted in Figure 2.1.

All eyes are aberrated. There is a widely used standard for characterizing ocular aberrations (Thibos et al. 2002) with Zernike polynomials (Zernike, 1934). A comprehensive guide of Zernike polynomials can be found in Lakshminarayanan & Fleck (2011). Zernike polynomials are an infinite sequence of polynomials that are continuous and orthogonal over a unit circle. They are typically defined in polar coordinates. Any wavefront surface can be described perfectly by the sum of the infinite set of Zernike polynomials each multiplied by a coefficient. The infinite set of coefficients that multiply the polynomials are typically called Zernike coefficients.

Let r and θ be the polar coordinates defining a unit circle. And let n and m represent the radial order and the angular frequency of the polynomial. If C_n^m are the Zernike coefficents and and $Z_n^m(r,\theta)$ the Zernike polynomials over the unit circle, then,

$$W(r,\theta) = \sum_{n,m} C_n^m Z_n^m(r,\theta), \tag{2.1}$$

Figure 2.2 shows the surfaces described by each Zernike polynomial up to the sixth radial order in pyramid form.

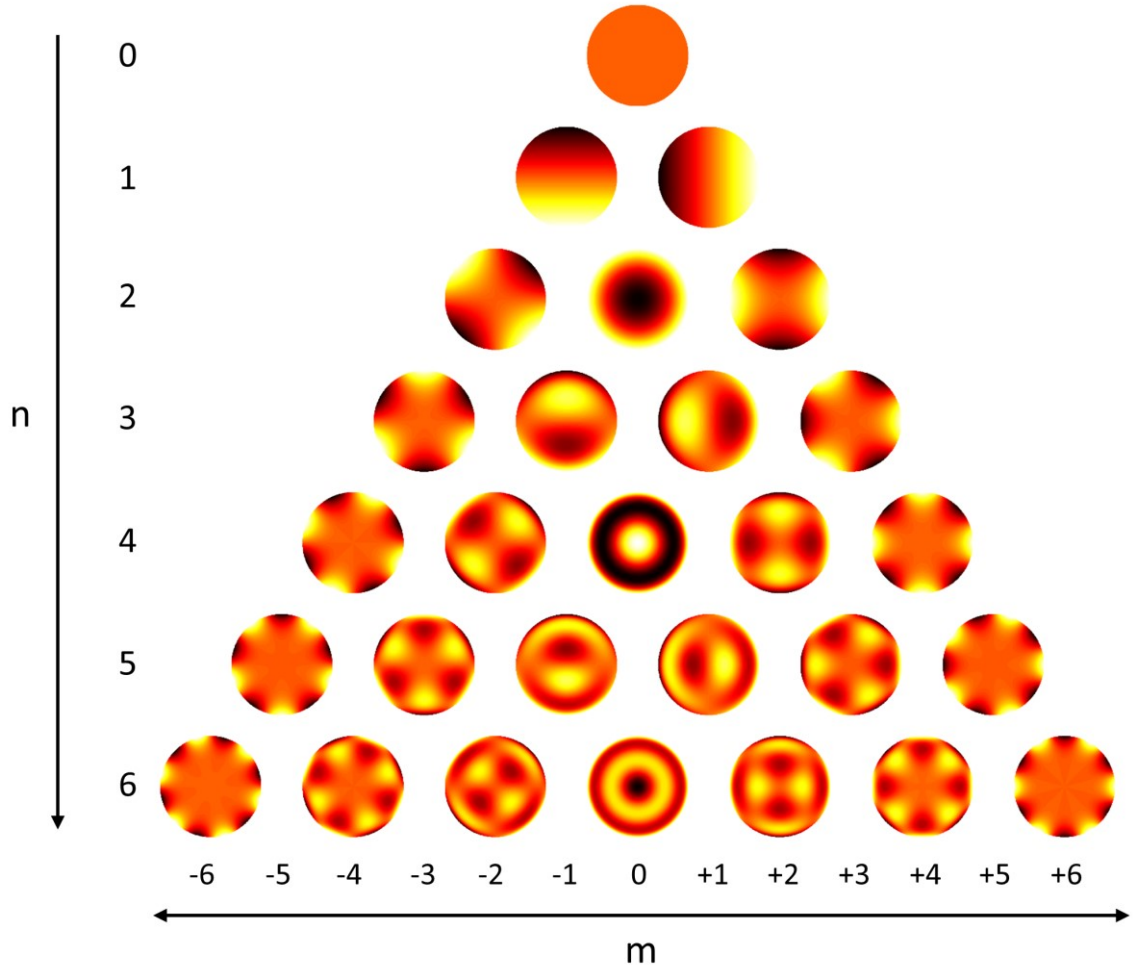

Figure 2.2. Maps defined by each Zernike polynomial up to and including sixth radial order. Each row corresponds to a different radial order (n), which increases towards the bottom. Different columns correspond to the angular frequency (m). In this representation all the coefficients were set to 1 µm. Dark colors indicate negative values, whereas light colors indicate positive values.

Zernike polynomials are commonly used to describe ocular aberrations because of the several advantages that they provide. Several Zernike modes or polynomials relate well to common aberrations used in clinical practice. For instance, second order Zernike polynomials correspond to refractive errors (spherical defocus and astigmatism). Another advantage that these polynomials present is the fact that the root mean square (RMS) of the wavefront deviation caused by a particular mode is equal to the value of that Zernike coefficient.

2.1.2. General characterization of an adaptive-optics system

A typical Shack-Hartmann aberrometer measures the wavefront of the incoming light by computing the wavefront slopes (Southwell, 1980; Platt & Shack, 2001), which can be calculated directly from the deviations of the centroids of the formed spots (see Figure 2.3) with respect to the center of each micro-lens (Thomas et al. 2006). Knowing the center and the radius of the circumference that contains the lit spots, one can calculate the wavefront from the slopes values by integration (Southwell, 1980; Lane & Tallon, 1992). And from the wavefront, Zernike coefficients can be obtained with an ordinary least square fitting, using the Zernike polynomials (Zernike, 1934; Mahajan, 2007). Zernike coefficients could also be obtained by performing an ordinary least square fitting of their derivatives (Zhao & Burge, 2007).

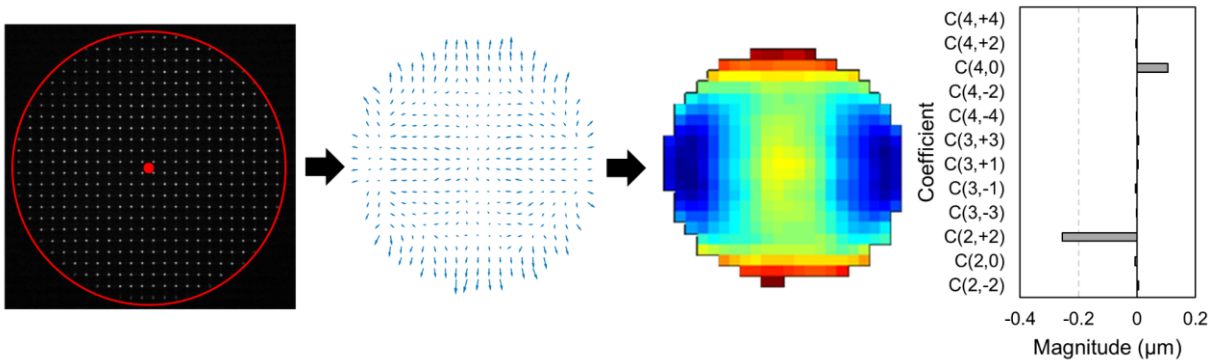

Figure 2.3. Example of the process followed for calculating Zernike coefficients. First, the Shack-Hartmann sensor takes a spots image, and the diameter and center (denoted by red circumference and dot) are determined. Slopes are calculated from the deviations of the centroids in the spots image, and are shown in a gradient plot, where the arrows indicate the deviations. From here, the wavefront is calculated by integration, and finally, Zernike coefficients are computed with ordinary least square fitting. In this example there was −0.25 µm of vertical astigmatism and 0.10 µm of spherical aberration for a pupil diameter of 5 mm.

Aberrations of the eye can be fully or partially corrected only after the effects of modifying the deformable mirror on the Shack-Hartmann aberrometer are properly characterized. Typically, an AO system is characterized by measuring the effect that changes in the shape of the deformable mirror surface has on the wavefront as measured by the Shack-Hartmann aberrometer (Tyson, 2012). This translates into the relationship between the measured slopes s and the voltage values of each of the mirror actuators a. Assuming linearity, this relationship can be described through an interaction matrix M_{I}, thus,

$$s = M_{\mathrm{I}} a, \tag{2.2}$$

where s is a column vector with a length of twice the total number of micro-lenses, containing first the horizontal slopes and then the vertical slopes in an vector array. The relationship between the voltage of an actuator and mirror deflection, or deformation, is typically nonlinear, since actuators movement is spatially coupled with adjacent actuators (Zou & Burns, 2009).

The interaction matrix M_{I} is generally obtained following a procedure known as *push and pull* (Kasper et al. 2004; Tyson, 2012). This operation involves the application of voltages of, e.g., −0.2 and 0.2 V to each actuator individually to obtain a total of $2k$ slope vectors (two values of voltages times k actuators). If l is the number of micro-lenses in the Shack-Hartmann sensor, the slopes are arranged so that $s_{-0.2}$ is a $2l \times k$ matrix that contains $2l$ slopes values (vertical and horizontal) when the negative voltage was applied, and $s_{+0.2}$ contains $2l$ slopes values when the positive voltage was applied. Then, to obtain the change per unit of voltage increase, the following operation with the vectors obtained for each actuator was performed,

$$M_{\mathrm{I}} = \frac{s_{-0.2} - s_{+0.2}}{2 \cdot 0.2}. \tag{2.3}$$

After such operation, M_{I} has dimensions of $2l \times k$, which corresponds with twice the total number of micro-lenses times the number of actuators in the deformable mirror.

Since the goal is to correct or simulate particular aberrations, then it is essential to find an operation that allows for the calculation of the voltages that had to be input in each actuator in order to obtain the slopes of the desired aberrations. This is achieved by computing the Moore-Penrose pseudoinverse of M_{I}. To avoid

artifacts due to measurement errors, the interaction matrix M_{I} can be split into k eigenvalues with its k corresponding eigenvectors by means of single value decomposition. Small eigenvalues likely represent measurement errors, so their respective eigenvectors can be removed and then the inverse of M_{I} reconstructed. This new matrix, inverse of M_{I}, is called command matrix, M_{C}, and with it, the actuators' voltages can be calculated from the slopes, thus,

$$a = M_{\mathrm{C}} s, \tag{2.4}$$

In order to correct the aberrations of the system or of an eye, the following straightforward algorithm can be used:

1. Get wavefront slopes vector s and pupil center and radius from lit microlenses in the Shack-Hartmann wavefront sensor (see Figure 2.3).

2. Compute Zernike coefficients Z from s with the same pupil center and radius as in step 1.

3. Set to zero the Zernike coefficients in Z to be corrected to obtain the target Zernike coefficients Z_t.

4. Compute the target slopes s_t from the target Zernike coefficients Z_t.

5. Compute the differences between measured and target wavefront slopes, thus, $\Delta s = s - s_t$.

6. Compute changes in commands from slope differences, thus, $\Delta a = M_C \Delta s$.

7. Apply voltage changes to move each actuator of the deformable mirror.

For correcting the aberrations of the optical system, this algorithm is typically used iteratively (closed-loop) until the RMS of the aberrations measured is minimum. The actuators' voltage values for correcting the system's aberrations, a_0, were saved for applying them when required, avoiding the application of the closed-loop again. The algorithm described can be easily modified to induce particular values of any Zernike coefficient, such as Zernike defocus. For instance, to generate a sinusoidal profile, the relative change in spherical defocus in each AO closed-loop operation has to be calculated and added to the resulting set of target Zernike coefficients in Step 3.

2.1.3. Adaptive optics and accommodation

Recently, AO has been used to study accommodation, particularly for trying to elucidate whether monochromatic aberrations are used by the eye to accommodate (Fernández & Artal, 2005; Chen et al. 2006; Chin et al. 2009a; Bernal-Molina et al. 2017). With AO certain monochromatic aberrations can be corrected and others manipulated, while the subject's accommodative response is assessed with the wavefront sensor. Subjects' monochromatic aberrations can also be reversed in order to have a deeper understanding of their effect on accommodation (Chin et al. 2009b).

There are different ways to calculate accommodative response from the subjects' wavefront aberrations (Thibos et al. 2004; López-Gil et al. 2009; Tarrant et al. 2010). Throughout this thesis, the accommodative response was computed with the minimum-RMS refraction, which consists of finding the quadratic surface that best fits the wavefront in a least square sense (Thibos et al. 2004). The Shack-Hartmann sensor has access only to the accommodative error of the eye (AE), so the accommodative response (AR) is calculated from the accommodative demand (AD) and the accommodative error (see Figure d1), as follows

$$AR = AD - AE, \tag{2.5}$$

$$AE = -\frac{4\sqrt{3}C_2^0}{r^2} \tag{2.6}$$

where C_2^0 is the Zernike coefficient that corresponds to the spherical defocus in microns, and r is the pupil radius as measured by the wavefront sensor. Following the definitions given, eq. 2.6 represents the accommodative error, which is expressed in D when C_2^0 is expressed in microns and r in millimetres. Note that in eq. 2.6, Zernike coefficients follow the ANSI standard (Thibos et al. 2002), which means that a lead in accommodation is represented by a positive C_2^0, whereas a lag in accommodation is represented by a negative value.

The studies where monochromatic aberrations have been corrected in real time, while measuring the accommodative response of the subjects (Chin et al. 2009a; Hampson et al. 2010) have been performed with an extra wavefront sensing channel (Hampson et al. 2009), since it would be impossible to disentangle ocular aberrations from those induced by the mirror using a typical closed-loop AO algorithm (Marcos et al. 2017), such as the one described in the previous section.

When trying to correct some aberrations, while others are unmodified, that is, as measured by the sensor, the typical AO algorithm explained in Section 2.1.2 fails, and drifts in the aberrations left as measured by the sensor appear, as can be seen in Figure 2.4.

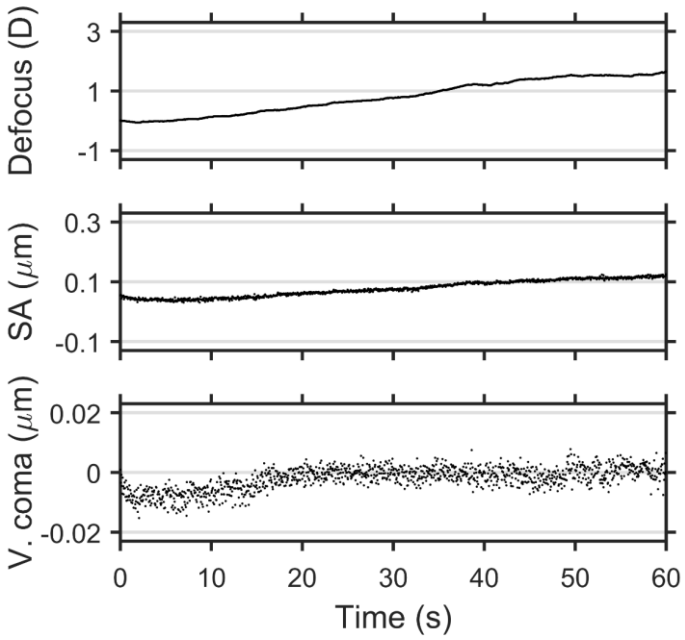

Figure 2.4. Upper panel shows the spherical defocus in Diopters, mid panel shows the spherical aberration in microns, and lower panel shows the vertical coma in microns during a period of 60 seconds. Odd-order aberrations were corrected using the algorithm described in subsection 2.1.2, while even-order aberrations were left as measured by the wavefront sensor. Drifts appear in both defocus and spherical aberration, which were supposed to remain constant.

2.2. Experimental set-up

The custom-made AO system that was built to carry out all the experiments described in this thesis is illustrated schematically in Figure 2.5. A photograph of the optical system arrangement can be seen in Figure 2.6. The AO system was controlled using custom-made software in MatLab (Mathworks, Inc., Natic, MA), based on the analysis and simulation software library and software development kits provided by the manufacturer (Imagine Eyes, France).

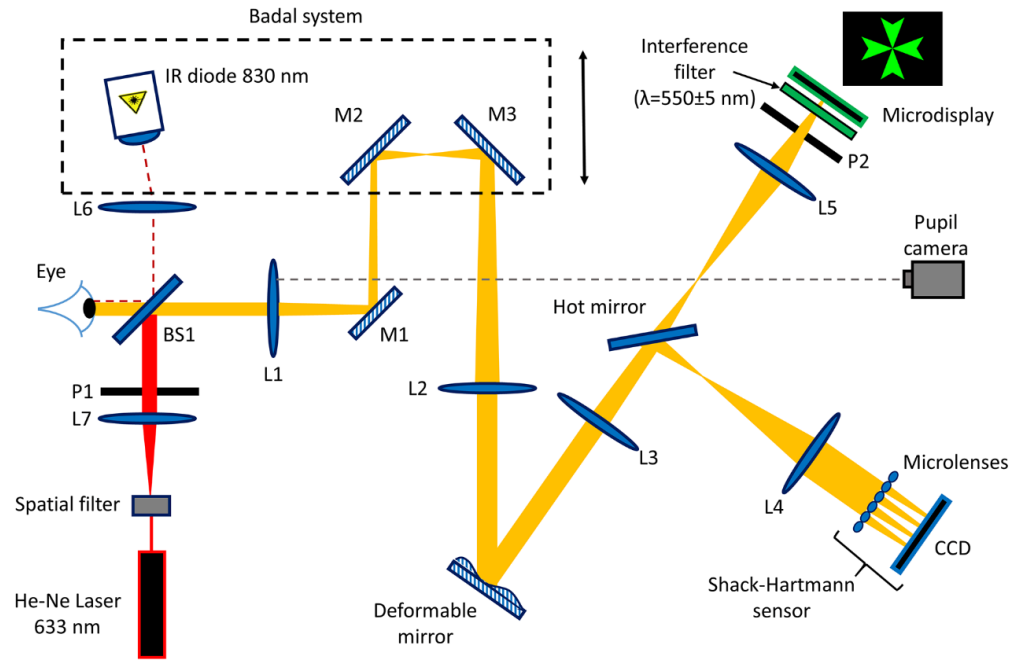

Figure 2.5. Schematic diagram of the AO system. Lenses L1, L2, L3, and L5 are achromatic doublets; lenses L4, L6 and L7 are singlets; M1, M2, and M3 are flat mirrors; P_1 is a variable iris; P2 is a pupil placeholder; and BS1 is a pellicle beam splitter. Reprinted from Del Águila-Carrasco et al. (2017).

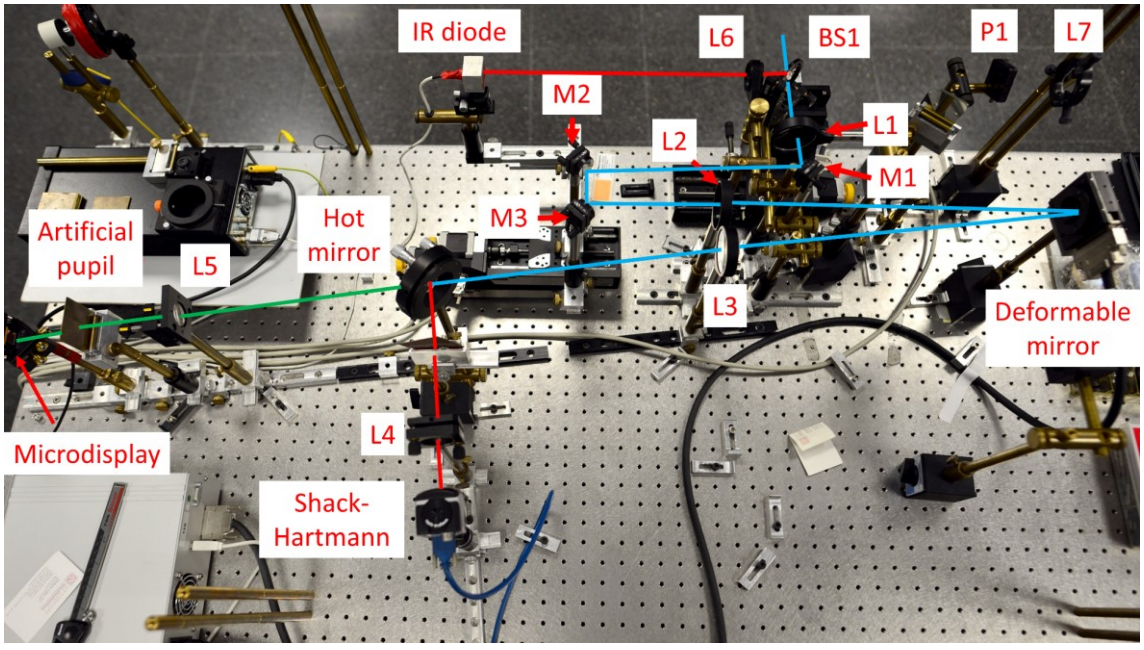

Figure 2.6. Photography of the AO system taken from above. The different elements in the picture are displayed. The He-Ne laser does not appear in the photograph. It is located outside the picture at the upper right part. The red line represents the path where there is only infrared light. The green line represents the path where there is only visible light coming from the microdisplay. The blue line represents the path where there are both type of lights. Photo credit: Matt Jaskulski.

2.2.1. Elements in the optical system

- *Wavefront aberration sensor:* The HASO 4 First (Imagine Eyes, France) was the Shack-Hartmann aberrometer employed (see left panel in Figure 2.7). It has an array of 40×32 micro-lenses and it is able to measure aberrations up to a frequency of 100 Hz. The working wavelength range is from 350 to 1100 nm.
- *Deformable mirror:* The Mirao 52e (Imagine Eyes, France) was the deformable mirror used for manipulating the aberrations (see middle panel in Figure *2.7*). This mirror consists of 52 actuators with an effective diameter of 15 mm. It works with a wide range of wavelengths and the input voltage to the actuators ranges from −1 to +1 V.
- *Microdisplay:* A green SVGA+ OLED Microdisplay of 800×600 pixels and 15-micron pixel pitch (eMagin, NY, USA) was chosen for presenting the stimulus (see right panel in Figure *2.7*). A narrowband (±5 nm) green interference filter with the peak transmission at 550 nm was placed in front of the microdisplay. The reason for choosing a green microdisplay, together with a narrowband interference filter was present a quasi-monochromatic stimulus, with peak emission as close as possible to the maximum sensitivity of the human eye (Schnapf et al. 1987). A luminancimeter (LS-110, Konica Minolta, Japan) was used to calibrate the microdisplay's luminance to the desired level.

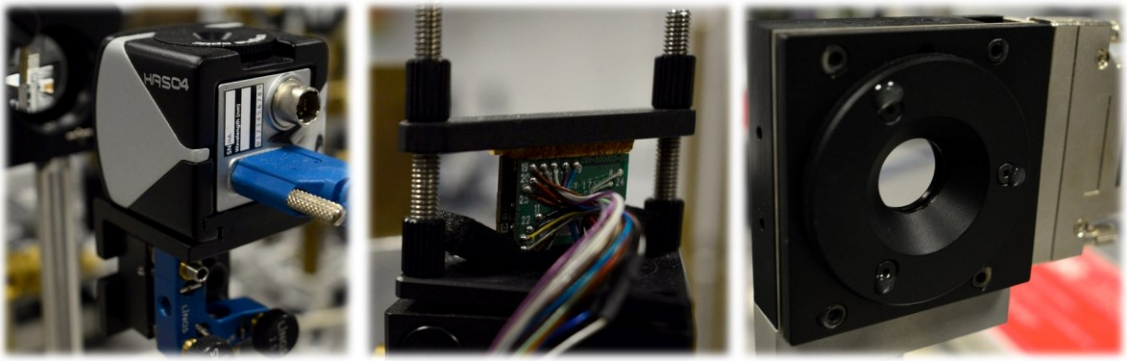

Figure 2.7. Details of the Shack-Hartmann wavefront sensor (left panel), back of the microdisplay (middle panel), and deformable mirror (right panel) used in the optical arrangement. Photo credit: Matt Jaskulski.

- *Badal optical system:* The Badal optical system consisted of a motorized stage (PLS-85, Micos, Germany), with three flat mirrors and a Badal lens (L1). This configuration allows for the modification in light vergence without changing the

apparent size or angle of the target, therefore removing monocular accommodation cues. The motor of the Badal was controlled by software developed in Matlab (Mathworks, Inc., Natic, MA).

- *Measurement infrared diode:* For measuring the eye's aberrations, an infrared superluminescent diode, with a wavelength of 830 nm was used. It had low intensity, approximately 102.5 μW, which was below the permitted limit for human eyes (Delori et al. 2007).
- *Laser He-Ne:* In order to calibrate the AO system and perform tests, a He-Ne laser with a wavelength of 633 nm was used.
- *Bite-plate:* In order to try and minimize the subjects' head movements a dental mould (bite-plate) was made for each subject using dentistry paste for impressions. The dental mould was mounted on a 3-D linear stage used for alignment between the subject's eye and the optical system, which can be seen in Figure 2.8.

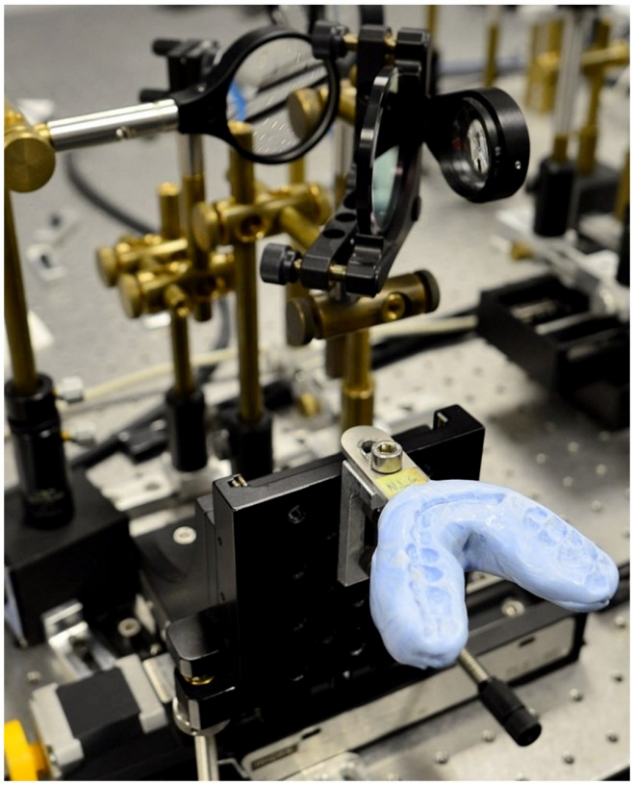

Figure 2.8. Detail of a subject's dental mould placed in the 3-D linear stage. Horizontal movements are controlled with a motor. Photo credit: Matt Jaskulski.

- *Pupil camera:* An infrared camera was utilized for aligning the subject with the AO system and monitoring the subjects' pupil in real time.

2.2.2. Optical paths

2.2.2.1. Calibration path

Figure 2.9 shows the optical path that was used for calibrating the optical system (alignment, calculation of interaction matrix, and correcting the aberrations of the AO system). The light beam coming from the He-Ne laser passed through a spatial filter to have a point source of light and then through the lens L7 to collimate it. After this, the beam passed through an artificial iris with variable aperture (P1) before reaching the beam-splitter BS1. The laser beam reflected in BS1 and it passed through the Badal optical system. First, it passed through the Badal lens L1 and before passing through the lens L2, the beam was reflected in mirrors M1, M2 and M3. After L2, the laser beam reached the deformable mirror and was reflected towards L3, to pass right afterwards through the hot mirror, where part of the laser beam was reflected to the Shack-Hartmann sensor, and the rest was transmitted towards the microdisplay. The part of interest for the calibration was the light going to the wavefront sensor, which passed through lens L4, before being registered by the CCD in the Shack-Hartmann. The beam reaching the microdisplay was used to align it with respect to the optical system.

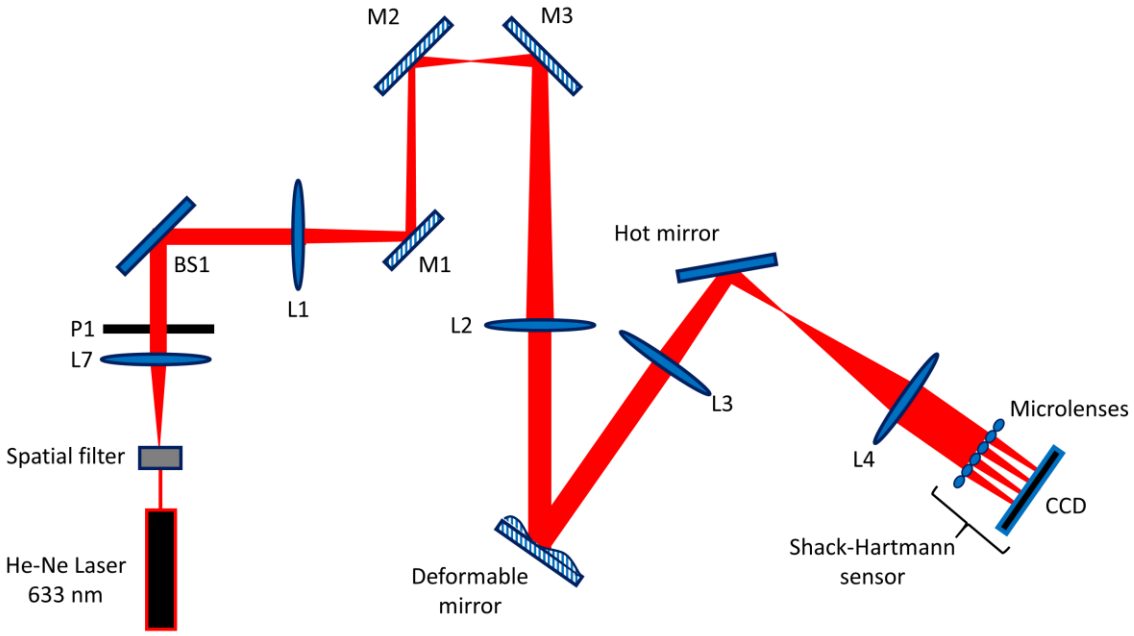

Figure 2.9. Path taken by the He-Ne laser that was used for calibrating the AO system highlighted in red.

For correcting the aberrations of the optical system, the algorithm described in Section 2.1.2 was used iteratively (closed-loop) until the RMS of the aberrations measured was lower than 0.02 µm for the maximum pupil diameter allowed by the AO system, approximately 8.5 mm.

2.2.2.2. Measurement path

The infrared beam emitted by the diode is collimated by L6 and is reflected by the beam splitter BS1, and then it enters the eye and forms a point on the retina. The reflection from the fovea then exits the eye. The relative position between the infrared beam of light and the eye plays an essential role in the efficacy of the correction of aberrations in the AO system. If, for example, the beam passes through the center of the eye to the retina, corneal reflections are very likely to appear in the image registered by the sensor. These reflections are an undesired artefact that can affect the measurement of aberrations. Reflections can be avoided by the use of polarized filters or by image processing. However, adding a polarized filter results in loss of light reaching the sensor, and the removal of corneal reflections through image processing is computationally demanding. Both solutions are bound to reduce the speed at which the AO system can manipulate wavefront aberrations. A typical solution that effectively prevents corneal reflections from distorting the images recorded by the wavefront sensor is to move the infrared beam slightly away from the center of the cornea. Then, the infrared beam can be aligned so that it falls on the fovea for an emmetropic eye. However, for accommodated or myopic eyes, there is a risk that the ray deviates outside the foveal isoplanatic patch, which presents a diameter from about 1° to 2° of visual angle according to the Maréchal criterion (Tarrant & Roorda, 2006; Bedggood et al. 2008). Then, there could be a mismatch between real foveal aberrations and the recorded ones when the refractive power due to myopia or accommodation is large. Luckily, there is a solution for those AO systems that include a motorized Badal that compensates the eye's ametropia and modifies light vergence of the target. For these systems, a simpler solution is to make the infrared beam pass through the optic path of the movable Badal system. The solution adopted here was to attach the infrared diode to the movable Badal system directly (Figure 2.10), having the advantage of a lower signal loss, as the infrared beam has to pass through one less beam splitter.

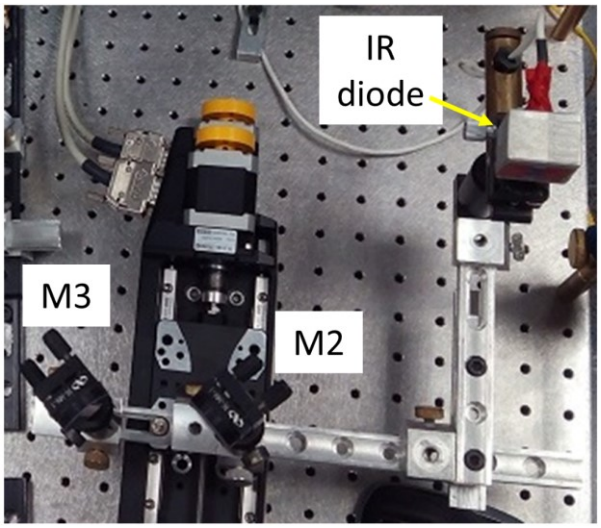

Figure 2.10. Detail of the infrared diode mounted on the same motorized stage as the Badal optical system. M2 and M3 are mirrors and are part of the Badal. Photo credit: Matt Jaskulski.

After exiting the eye, the infrared beam is transmitted through BS1 and passes through the Badal optical system. After this, it reaches the deformable mirror and it is reflected towards L3 and the hot mirror. Since the beam is infrared, it is reflected in the hot mirror towards L4 and, finally, reaches the Shack-Hartmann aberrometer. The aberrometer forms an image with a spot pattern that allows the calculation of slopes and hence the wavefront. A schematic showing the measurement path is shown in Figure 2.11.

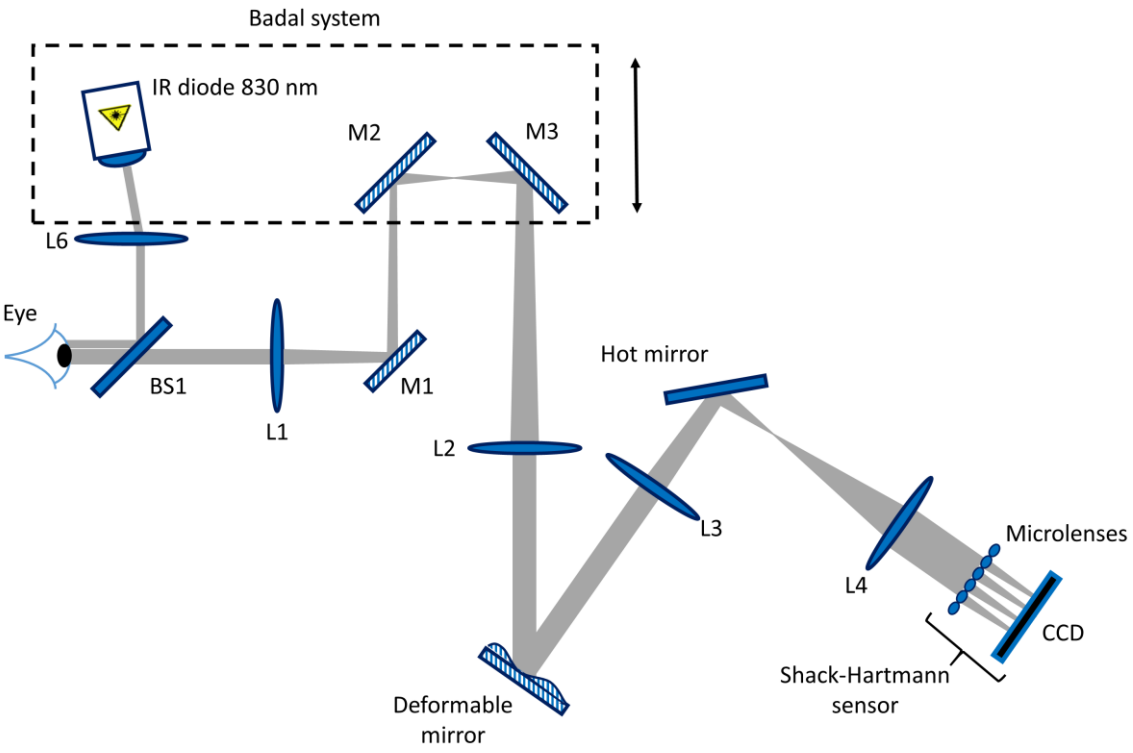

Figure 2.11. Measurements path highlighted in gray. The beam starts from the IR diode and finishes at the CCD of the Shack-Hartmann sensor.

2.2.2.3. Stimulus path

The stimulus shown in the microdisplay was a green Maltese cross with a luminance at the corneal plane of around 20 cd/m^2 on a dark background with less than 0.5 cd/m^2, subtending 1.95 degrees of visual angle. This angular size was not expected to limit the accommodation response, given the fact that stimuli subtending more than approximately 0.25° already evokes accommodation (Kruger et al. 2004). The Maltese cross is a widely used pattern as stimulus for accommodation experiments (Jacobson et al. 1958; Kruger & Pola, 1985; McLin & Schor, 1988; McLin et al. 1988), since it contains high-contrast edges in a variety of orientations and multiple spatial frequencies. The light beam coming from the microdisplay passed through the narrowband green interference filter, so the light was quasi-monochromatic (550±5 nm). Then, it passed through an artificial pupil (P2) before reaching the achromatic doublet L5. The hot mirror was used to prevent the visible light coming from the microdisplay from reaching the Shack-Hartmann sensor. After passing through the hot mirror, the light beam was reflected in the deformable mirror and then it passed through the Badal optical system. Finally, the light beam was transmitted through the beam splitter BS1 and reached the eye. Note that all

the lenses in this path are achromatic doublets, in order not to generate chromatic aberration. A schematic showing this path can be seen in Figure 2.12.

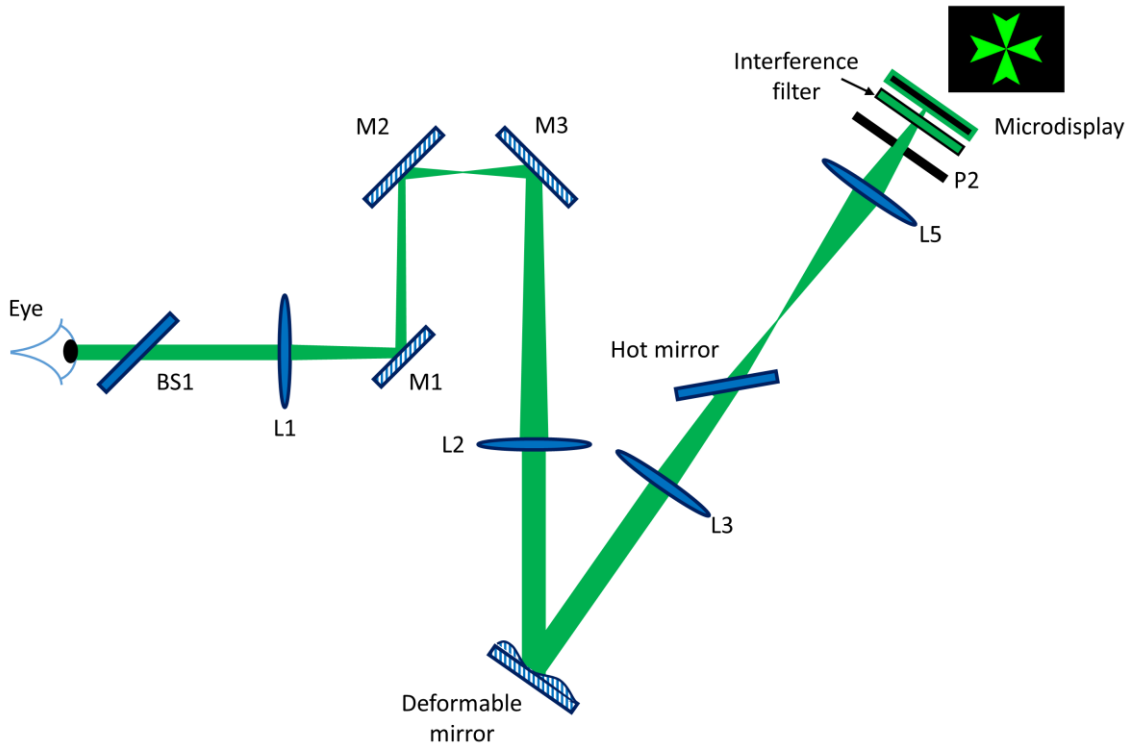

Figure 2.12. Stimulus path highlighted in green. The light comes from the microdisplay and finishes at the retina of the subject's eye.

The microdisplay was moved closer to L5 to adjust for the chromatic focus shift between the infrared light source (λ=830 nm) and the green stimulus (λ=550 nm). This displacement caused an approximate reduction of the apparent size of the image of 1.25% per diopter of vergence introduced by the Badal system. Nonetheless, the change in the apparent size was small and it was likely that it did not affect the measurements (Jaskulski et al. 2016).

2.2.3. Partial correction of aberrations

The main experiments described in the reminder of this thesis required the correction of certain monochromatic aberrations, while the spherical defocus was left as measured by the wavefront sensor. Although the algorithm described in Section 2.1.2 works fine when inducing fixed values of aberrations, it fails when some aberration term needs to be left as measured by the wavefront sensor. Drift artefacts in partial wavefront corrections seem to be a direct consequence of assuming linearity between the electronics that modify the deformable mirror and real optical

changes (see Section 2.1.2). Drifts are often non-linear and unpredictable and can occur for any Zernike coefficient left as measured by the wavefront sensor, not only defocus. They depend on measured pupil center and radius. They also depend critically on which aberrations are being corrected and which are left uncorrected, due to the intrinsic relationship between Zernike modes. For example, when leaving spherical aberration and spherical defocus as measured by the sensor, drifts appear in both Zernike modes (see Figure 2.4) because Zernike spherical aberration has a component of spherical defocus by definition.

The solution to the drift problem relies in disentangling the wavefront aberrations of the eye from those induced with the deformable mirror (Marcos et al. 2017). One way to solve this issue is to add an extra optical path to the system that can make direct measurements of the aberrations of the eye regardless the state of the mirror (Hampson et al. 2009; Marcos et al. 2017). The problem is the complexity added to the system and the signal loss that extra optical elements would add. Obviously, this would also be expensive, as it requires either an extra Shack-Hartmann sensor, or one which size allows for having two separate beams to reach it. Another possible solution is to characterize the AO system in a more complex way, by taking into account the existent nonlinearities, and the coupling of adjacent actuators. However, this characterization would be too complex and it would be impractical, due to the large number of different interaction matrices needed for all the possible pupil radii and centers.

Luckily, there is another solution for effectively controlling drift artefacts that is entirely based on software and it is moderately more complex, but computationally not much more inefficient than the standard algorithm described in Section 2.1.2. The key feature of this new algorithm is to calculate the undesired aberrations s_e that the mirror induces when those aberrations should be left unmodified, and then to recalculate the voltages that should be sent to the actuators. This algorithm shares the six first steps with the one described in Section 2.1.2. From there, the algorithm (Marín-Franch et al. 2017) is as follows:

7. Get current voltages applied to the actuators a_c.

8. Add these voltages to the commands changes calculated in Step 6 and subtract those for which the system's aberrations are corrected, $a = \Delta a + a_c - a_0$.

9. Calculate the wavefront slopes vector s_m that the mirror would induce from the actuators commands a calculated in the previous step, using $s_m = M_I a$.

10. Get the corresponding Zernike coefficients Z_m from the slopes s_m.

11. Calculate the error in Zernike coefficients Z_e committed in the standard closed loop that generates drifts by setting all Zernike coefficients to correct to zero in Z_m.

12. Get the error in the wavefront slopes vector s_e from the modified Zernike coefficients Z_e.

13. Get the relative commands changes from these slopes using $\Delta a_e = M_C s_e$.

14. Subtract the command changes Δa_e in actuators from those obtained in Step 6 to get the corrected commands changes, thus $\Delta a_c = \Delta a - \Delta a_e$.

15. Apply voltage changes Δa_c to move each actuator of the deformable mirror.

This algorithm also can be easily manipulated to induce a particular value of any aberration, such as generating a sinusoidal profile in the Zernike defocus, in the same way as for the standard algorithm. The effectiveness of the proposed algorithm can be seen in Figure 2.13. It is clear that with this algorithm, the defocus (upper panel), as well as the spherical aberration (middle panel), remain constant while the system is correcting all the other aberrations (see vertical coma in lower panel).

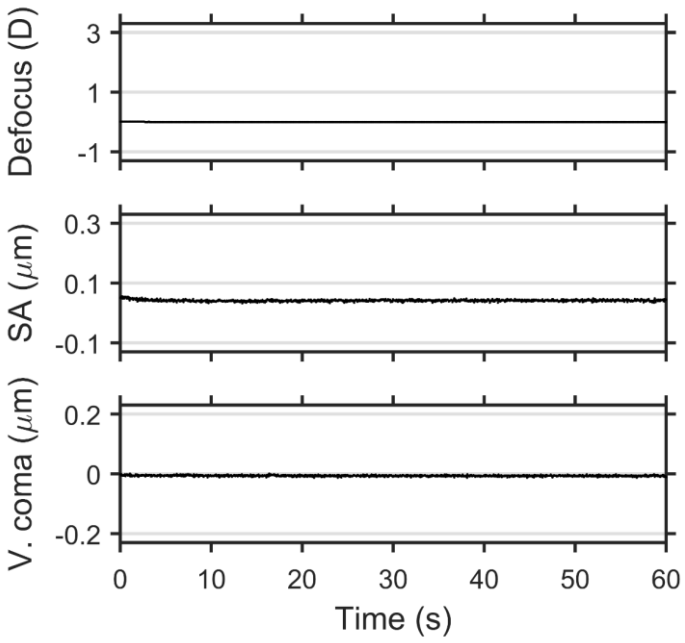

Figure 2.13. Zernike defocus in diopters (upper panel), spherical aberration in microns (middle panel), and vertical coma (lower panel) for a 4-mm pupil when the drift-control algorithm is applied. The closed-loop algorithm was intended to leave Zernike defocus, spherical, and all other even-order aberrations uncorrected, while correcting odd-order aberrations.

Figure 2.14 shows an example where the light vergence was intended to vary sinusoidally between −1 and +1 D of accommodative demand, at a frequency of 0.2 Hz, when both algorithms were applied during 60 seconds. In this and the previous examples, a phase plate with Zernike spherical aberration of +0.06 μm for a 4-mm pupil was introduced in the system and the measurements were taken with the He-Ne laser. Only odd-order aberrations were corrected, while even-order aberrations, which include spherical aberration, were left uncorrected. It can be seen how both spherical aberration and defocus start to drift towards greater values when the standard algorithm was applied, while the vertical coma is corrected. When the drift-control algorithm was applied, there were no drifts in defocus or spherical aberration. Note that the small sinusoidal experienced by the spherical aberration is a consequence of the sinusoidal change in the Zernike defocus.

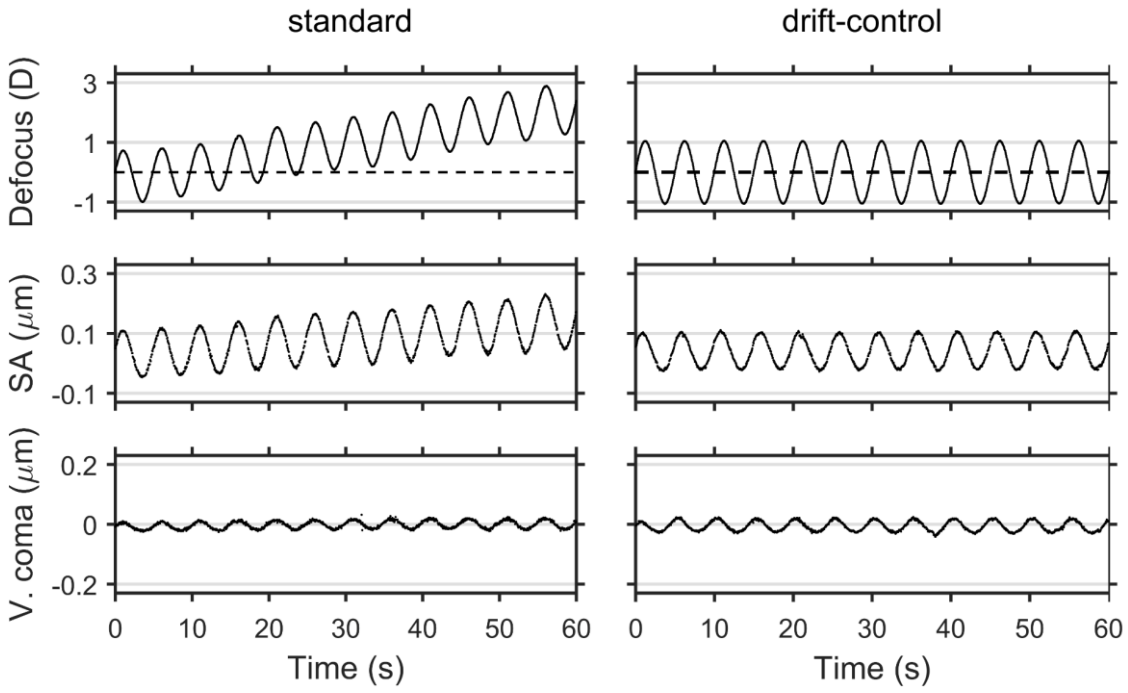

Figure 2.14. Zernike defocus in diopters (upper panels), spherical aberration in microns (middle panels), and vertical coma in microns (lower panels) for a 4-mm pupil for the standard (left panels) and drift-control (right panels) algorithms. The closed loop algorithm was intended to leave spherical and all other even-order aberrations uncorrected, while correcting odd-order aberrations, and while changing Zernike defocus sinusoidally. The dashed horizontal line in the upper panels represents 0 D of defocus.

Figure 2.15 shows the accommodative demand (upper panel), together with the response of a real eye (middle panel) measured with the infrared diode. In this trial, the phase plate was removed. A drift in the demand can be seen at almost the end of the trial. At first sight, differences in the responses are difficult to see, however, care is needed when measuring young eyes that can accommodate, since if the drift occurs towards negative vergences, the eye will accommodate, masking the drift to the Shack-Hartmann aberrometer. The correction of the desired aberrations is optimal in both algorithms, as can be seen in the example of the vertical coma (lower panel).

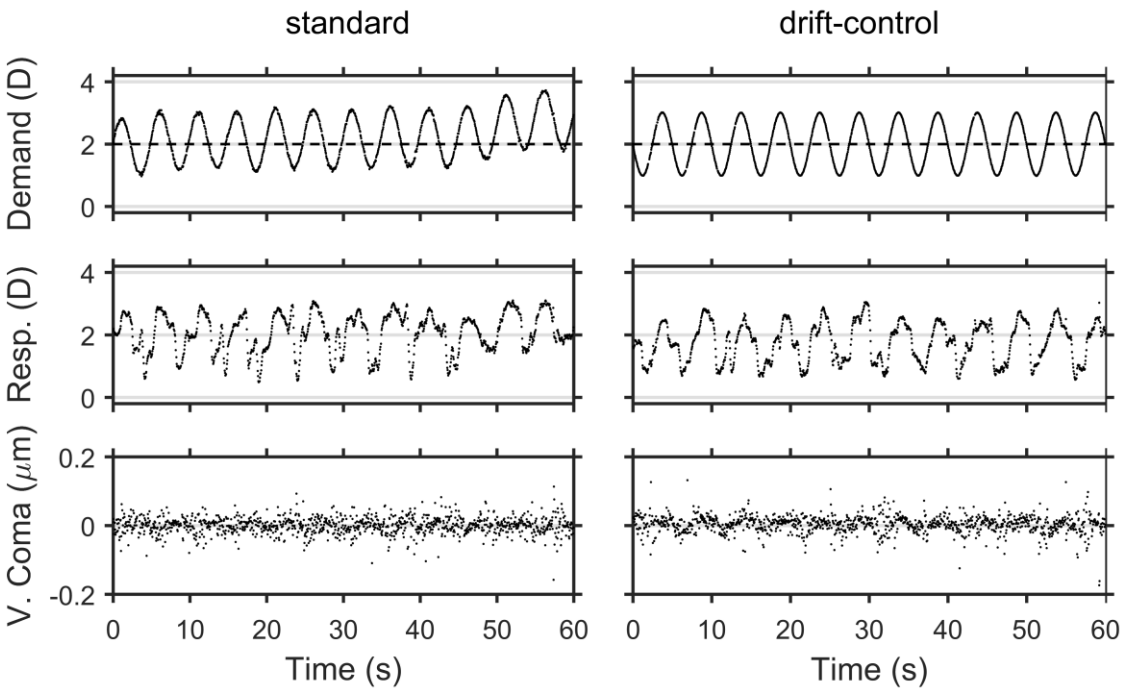

Figure 2.15. Accommodative demand in diopters (upper panels), accommodative response in diopters (middle panels), and vertical coma in microns (lower panels) for the standard (left panels) and drift-control (right panels) algorithms when measuring a real eye. The closed-loop algorithm was intended to leave spherical and all other even-order aberrations uncorrected, while correcting odd-order aberrations, and while changing Zernike defocus sinusoidally. The dashed horizontal line in the upper panels represents 2 D of defocus.

3. Preliminary trials

The main experiments of the thesis (see Section 1.4) are conducted under deprived viewing conditions. These conditions were characterized by the removal of binocular cues, since all the measurements were taken monocularly, as well as the removal of monocular cues by using the Badal optical system, and the elimination of chromatic cues, by using a monochromatic Maltese cross as the stimulus. Because only between 65% and 85% accommodate under these conditions (Fincham, 1951; Chen et al. 2006; Chin et al. 2009a; Marín-Franch et al. 2016; Del Águila-Carrasco et al. 2017), preliminary trials were run to identify those who could accommodate. In Marín-Franch et al. (2016), the study with greater number of subjects, 5 out of 14 subjects (35%) could not accommodate in monochromatic light. In Chin et al. (2009a) the number of subjects who could not accommodate in monochromatic light was 1 out of 5 (20%), and in Chen et al. (2006), 1 out of 6 (17%).

3.1. Methods

3.1.1. Subjects

Sixteen subjects were screened for accommodation under the stringent conditions described before. Nine of these subjects were screened in the University of Valencia using the crx1, a commercial AO system (Rocha et al. 2010; Madrid-Costa et al. 2012; Montés-Micó et al. 2012) that works similarly to the one described in Chapter 2. The remaining seven subjects were screened in the University of Murcia with the custom-made AO system described in Chapter 2. None of the subjects had ocular pathologies or accommodation anomalies. The mean age (± SD) of the participants was 30 (± 8) years and their refractive errors ranged from −5.0 to +0.75 diopters (D). None of the participants had astigmatism greater than 1 D. The study adhered to the tenets of the declaration of Helsinki and Ethics Committee approval from both the University of Valencia and the University of Murcia was obtained. Informed consent was collected from all the subjects after explanation of the nature and possible consequences. All the subjects were naïve as to the aim and the conditions of the experiments described in the present thesis.

3.1.2. Determination of the far point

Before starting the preliminary trials, the AO system aberrations were corrected, the subject bit the dental mould and was properly aligned using the pupil

camera. The contralateral eye was occluded with an eye patch and a 4-mm artificial pupil was placed in front of the microdisplay conjugated with the eye. Participants were then asked to find their far point, or the point in which they saw a letter chart through the system sharply. This was done using a fogging methodology (Benjamin, 2006) with the help of the Badal system, while the aberrations of the system were corrected. More precisely, participants were instructed to move the target far enough away from them beyond their far point, so they could not see it clearly. Then, they were asked to move the target slowly towards the eye until it first became clear, thus avoiding unintentional use of their accommodation. The average of three repetitions was taken as the subject's far point. The same procedure to obtain the subjects' far point was used in all other experiments in the present thesis.

3.1.3. Procedure and data analysis

These preliminary trials consisted of a Maltese cross moving sinusoidally from 1 to 3 D of accommodative demand with respect to the subjects' far point at a temporal frequency of 0.2 Hz during 25 seconds. The trials were run under the conditions described at the beginning of this Chapter, with habitual subjects' monochromatic aberrations present. The starting direction of the sinusoidal was randomized for each trial. The instruction given to the subjects was to try and see the target as clear as possible by making the same effort as if they were reading a book.

Aberrations were measured during the trials with the Shack-Hartmann sensor at a frequency of 20 Hz. The sensor measured accommodative error (lag or lead) of the eye with respect to the defocus generated with the deformable mirror (sinusoidal accommodative demand), as explained in Section 2.1.3. Then, the minimum root mean square (RMS) accommodative response (Thisbos et al. 2004; Tarrant et al. 2010) was obtained by subtracting the accommodative lead or lag measured with the wavefront sensor from the defocus generated by the deformable mirror with eq. 2.5.

A sinusoidal function with a temporal frequency of 0.2 Hz was fitted to the calculated accommodative responses over the 25 seconds of each trial. These fitted sinusoidal was characterized by two parameters: amplitude, which identifies the maximum variation in the magnitude of the sinusoidal; and temporal phase, defined as the difference in seconds between the peak locations of the demand and the response. Figure 3.1 shows a graphic depiction of these two parameters in a real trial

performed to a subject. From the amplitude of the fitted sinusoidal, gain, defined as the ratio between the amplitude of the response and the amplitude of the demand, was computed.

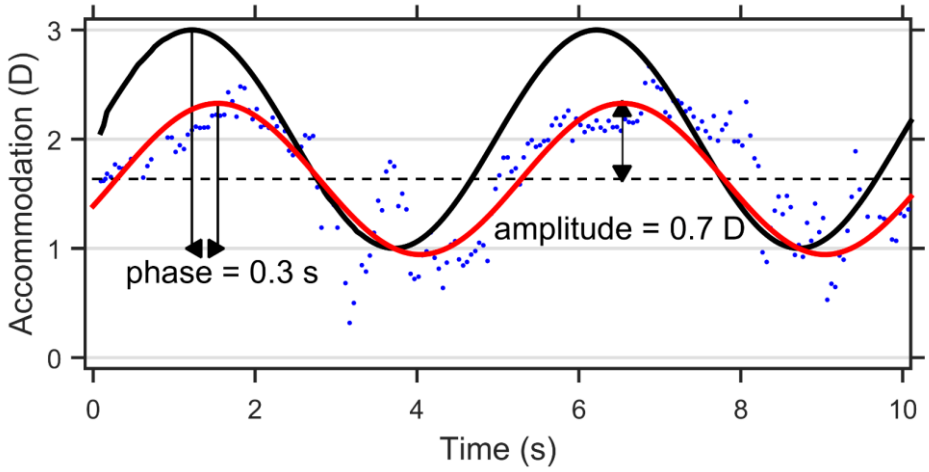

Figure 3.1. Recorded accommodation response (blue dots) and fitted sinusoidal function (red curve) for one typical subject. Accommodative demand (black curve) and graphic definitions for amplitude and temporal phase are also shown. The gray dashed line indicates the mean value of the fitted sinusoidal.

A gain value of 0.2 was selected as the threshold so that participants with smaller gain were excluded from the rest of experiments.

Since the sinusoidal change in vergence is repetitive, subjects could potentially show learning effects and therefore accommodate better in successive cycles. To evaluate if there was any learning effect, or even fatigue effects due to the constant use of accommodation, gain, temporal phase, and mid point obtained for the first cycle in each trial were compared against the ones obtained in the last cycle of each respective trial (see Figure 3.2).

3.2. Results and comment

After running the preliminary trials, 9 out of the 16 subjects (56%) showed gain greater than 0.2. Mean gain and temporal phase obtained for each of the mentioned subjects is shown in Figure 3.3. All nine subjects that passed this screening experiment took part in the main experiments, which are described in detail in the remainder of the present thesis.

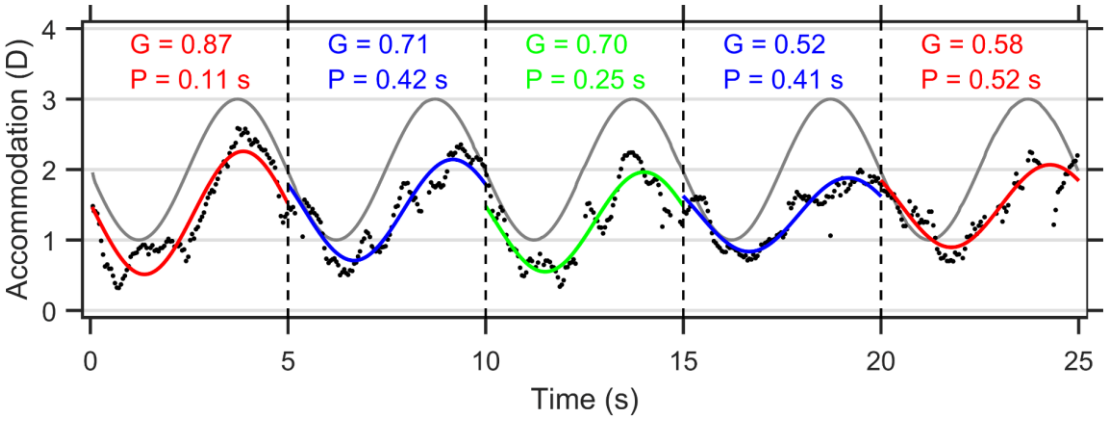

Figure 3.2. Accommodative response in D over time obtained in a trial. Black dots show the response recorded from one subject, gray solid curve shows the sinusoidal accommodative demand. The signal was split into five parts, each one corresponding to a cycle of the sinusoidal. A sinusoidal function with the same characteristics as the demand was then fitted to the experimental data in each cycle. G stands for gain and P stands for temporal phase. The first and last fits, showed in red, were compared against each other to study potential learning or fatigue effects.

A gain threshold of 0.2 seemed reasonable because of two reasons. The first one is that many eyes showed microfluctuations in accommodation. The energy of these microfluctuations at 0.2 Hz is added to the amplitude of the accommodative response at that frequency, and therefore gain can increase even when the response does not follow the sinusoidal accommodative demand (see Figure 3.4). The second one is that, when a sinusoidal is fitted to noisy data, the amplitude will rarely be zero, and due to the fact that gain is a positive-defined parameter, the average over repetitions will yield values greater than zero. For non-responsive subjects, both factors yield gains that are close to 0.1. The threshold chosen is twice as big to be sure that the subjects' measured response is real, not artefactual or due to microfluctuations (Del Águila-Carrasco et al. 2017).

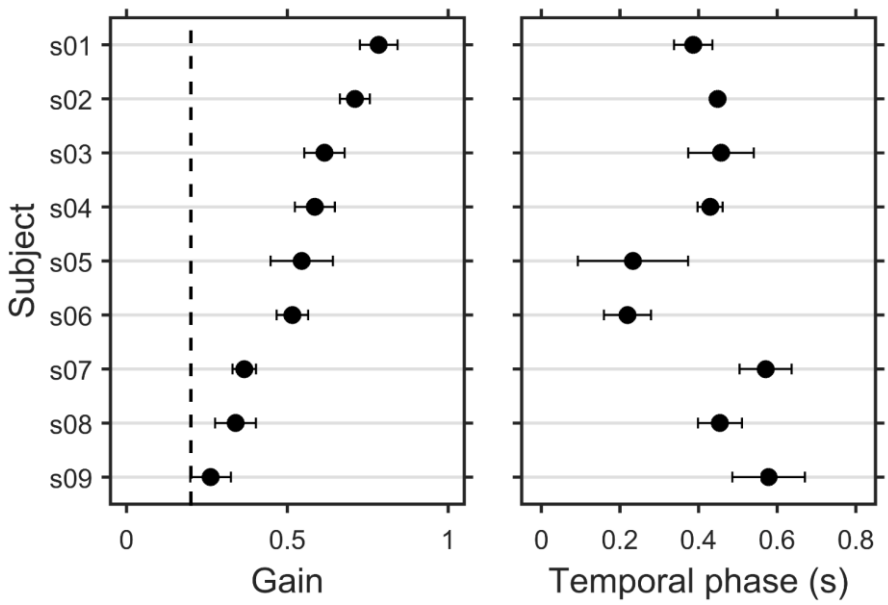

Figure 3.3. Mean gain obtained for each subject sorted in descending order (left panel) and their mean temporal phase (right panel). Error bars represent ±2 standard errors of the mean. Vertical dashed line on the left panel represents the threshold in gain of 0.2.

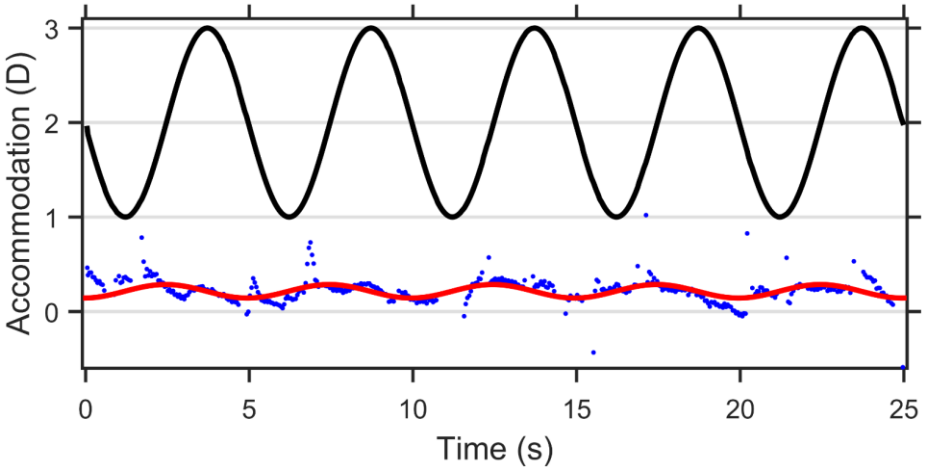

Figure 3.4. Example of a trial from a subject who could not accommodate under monocular and monochromatic conditions. The fitted sinusoidal (red curve) had an amplitude of 0.07 D, due to the small fluctuations and noise in the response (blue dots). The black curve represents the accommodative demand.

Figure 3.5 shows the mean gain (left panel), mean temporal phase (mid panel), and mean mid point (right panel) obtained for the first and the last cycles of the sinusoidal. Data from the analysis of the whole sinusoidal are also shown for comparison. These results show that on average there were no learning effects and

no fatigue effects either, since the means of the first and last cycles were practically the same for each subject. It seems that subjects could not anticipate the sinusoidal change in vergence, despite being a repetitive pattern, hence not affecting the outcomes of this thesis. Fatigue effects between trials were not expected, since subjects were given the possibility of taking a break whenever they required it.

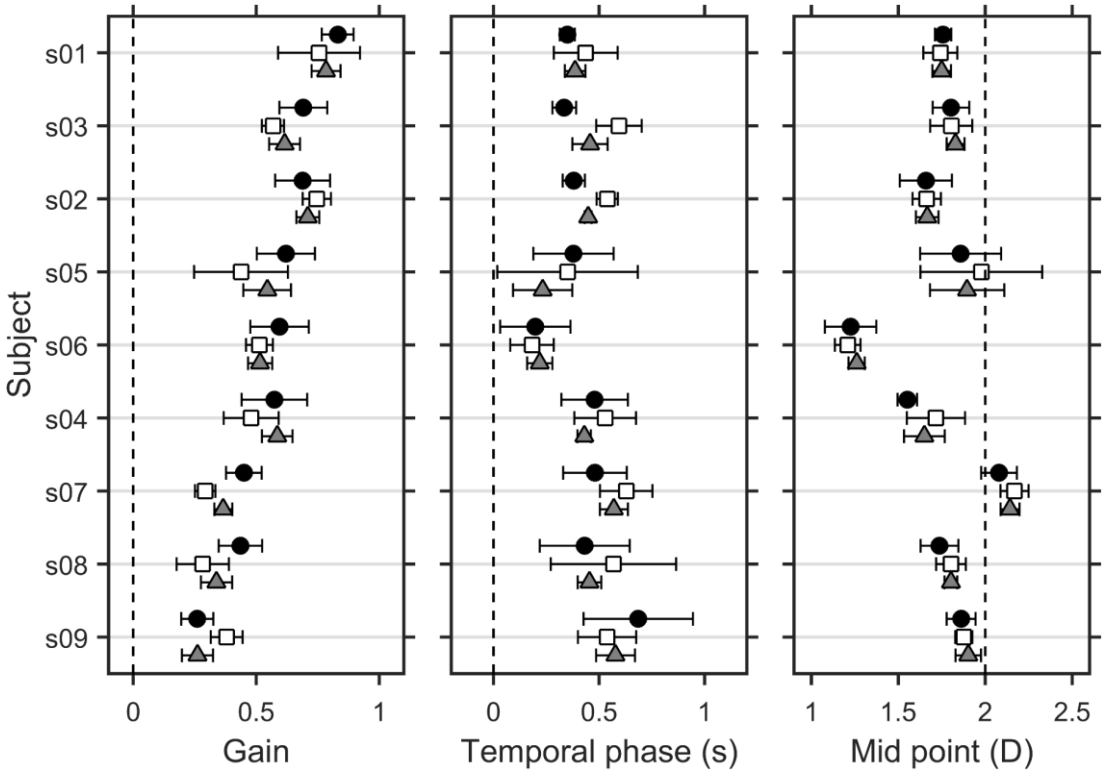

Figure 3.5. Mean obtained over the six trials for each subject of the parameters analysed for the learning and fatigue effects. Left panel shows the mean gain, mid panel shows mean temporal phase in seconds, and right panel shows mid point in D. Black circles represent the mean obtained for the first cycle, whereas empty squares represent the mean obtained for the last cycle of the sinusoidal. Gray triangles are the mean values obtained for the whole sinusoidal. Error bars are ±2 standard errors of the mean.

4. Accommodation to aberrated target blur alone

Some monochromatic aberrations cause the retinal image to be different whether the target is focused in front of or behind the retina, as already discussed in Section 1.1.3. These monochromatic aberrations are even-order aberrations (except defocus) and provide signed cues for accommodation (Campbell & Westheimer, 1959; Wilson et al. 2002; López-Gil et al. 2007). This Chapter shows an experiment about the effect of monochromatic aberrations in accommodation (Chen et al. 2006; Chin et al. 2009a; Chin et al. 2009b; Bernal-Molina et al. 2017).

The aim of this study was to elucidate whether accommodation responds to the shape of the blurred image itself without real changes in light vergence. The shape of blur refers to a target that is itself blurred with different combinations of aberrations and defocus. For this experiment, a small pinhole was used in order to remove feedback from changes in accommodation, thus opening the accommodation loop. This open-loop configuration allows the assessment of accommodation, while removing any potential feedback from trial-and-error changes in focus (microfluctuations of accommodation), from voluntary changes of accommodation, and from microfluctuations of accommodation. The present experiment follows the same approach as a previous study performed by Stark et al. (2009), where a stationary target was simulated at near and far distances. Here a dynamic target was simulated moving towards and away from the eye following a sinusoidal with an amplitude of 1 D at a frequency of 0.2 Hz, as opposed to the static ones used by Stark et al.

4.1. Methods

To blur the target itself, computer-generated videos were created off-line in which the Maltese cross was artificially blurred. Different target blur videos were generated: taking into account the subjects' natural aberrations (N); sinusoidal spherical defocus without aberrations, or perfect eye (P); sinusoidal defocus plus 0.2 μm of spherical aberration (SA); and sinusoidal defocus plus 0.1 μm of oblique astigmatism (AST). In order to simulate each subject aberrations, a typical accommodation stimulus-response curve (López-Gil et al. 2009; Bernal-Molina et al. 2014; Chen et al. 2017) was measured with the Shack-Hartmann aberrometer. From here, aberrations for each subject were obtained, so they could be added later to the videos.

4.1.1. Variation of aberrations with accommodation

Three accommodation curves were obtained for each subject in order to obtain the aberrations of the participants under different accommodative demands. Before starting these measurements, the same procedure as the one described in Section 3.1.2 was performed. Then, the subjects' accommodative responses, starting at each subject's far point (0 D of accommodative demand) up to 5 D of accommodative demand in steps of 0.5 D, were measured with the Shack-Hartmann wavefront sensor. The response was obtained using the minimum-RMS refraction (see eq. 2.5) (Thibos et al. 2004; Tarrant et al. 2010), as explained in Section 2.1.3.

Zernike coefficients were rescaled (Schwiegerling, 2002; Lundström & Unsbo, 2007) from the measured pupil diameter to the viewing 4-mm pupil diameter. The median of each aberration in each accommodative demand among the three curves obtained for each subject was calculated. After this, a linear regression was performed to each Zernike coefficient from second order up to and including sixth order (except spherical defocus) with respect to the accommodative demand. This was done to account for the possible variations of these coefficients with accommodation. These variations were taken into account when making the video with the subject's aberrations included.

4.1.2. Generation of videos with aberrations

All the videos were generated using custom Matlab software based on the Fourier Optics Calculator (Thibos et al. 2004). A Maltese cross was convolved with a point spread function (PSF) including defocus that changed sinusoidally from −1 to +1 D at a frequency of 0.2 Hz. Depending on the condition, the PSF was affected only by this defocus, or together with other monochromatic aberrations. When the subjects' aberrations were considered (N), the Zernike coefficients obtained for each subject and accommodative demand after the linear regression were taken into account, so the PSF, and thus the Maltese cross, were aberrated. In P, only the sinusoidal spherical defocus was added to the video. In SA, 0.2 μm of fourth order spherical aberration was added, along with $\sqrt{15} \cdot 0.2$ μm of spherical defocus, so as to add only the effect of Seidel-like shape (unbalanced) spherical aberration and not the defocus that this Zernike polynomial contains (Xu et al. 2015). For the video of the Maltese cross with astigmatism (AST), only 0.1 μm of oblique astigmatism was added to the sinusoidal spherical defocus. Figure 4.1 shows a set of frames of each video.

All the videos were the same for every subject except for (N), where each video had the aberrations of each subject.

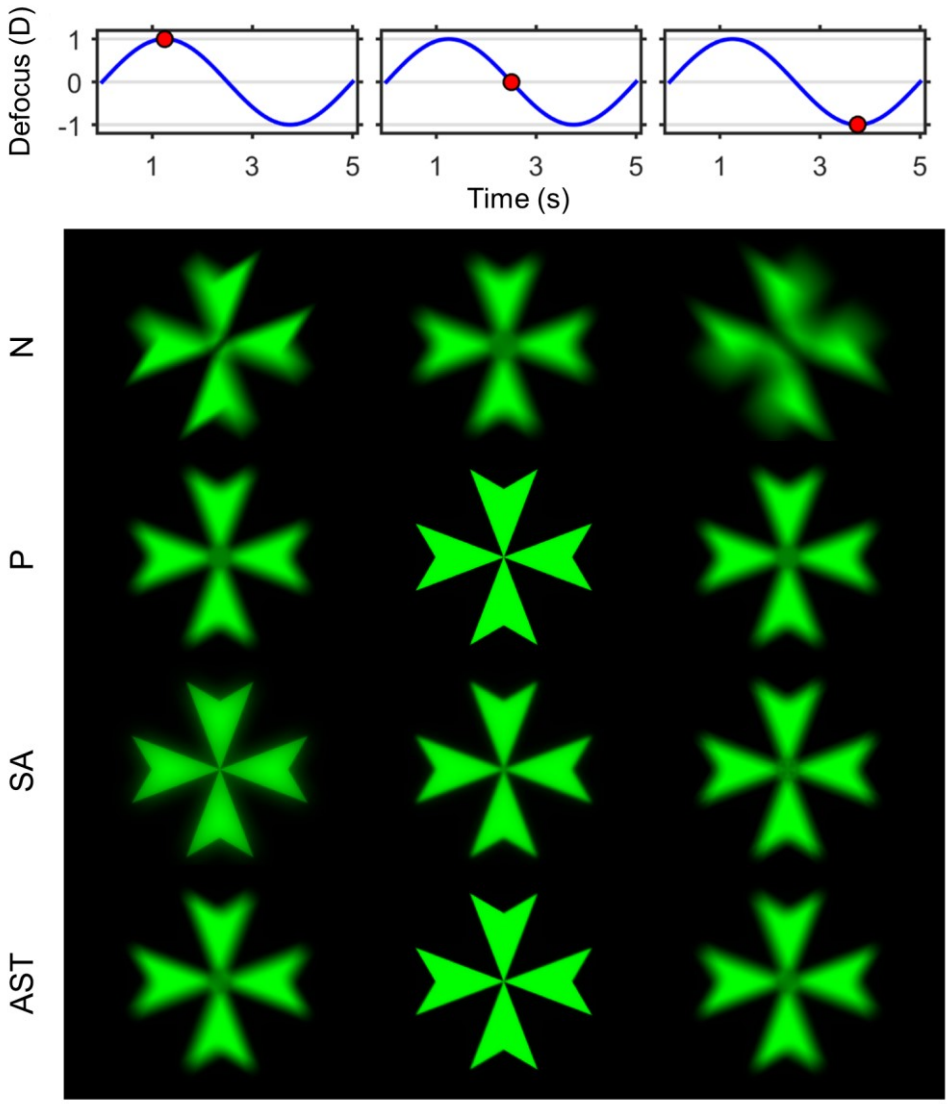

Figure 4.1. Frames extracted from the different videos used in this experiment. Upper row shows the sinusoidal variation experienced by the defocus blur during five seconds (one cycle). Red dots indicate the point where the frames were obtained. The rest of the rows shows frames at +1 D, 0 D and −1 D of target blur for the four conditions tested: natural aberrations (N), perfect eye (P), spherical aberration (SA), and oblique astigmatism (AST). The crosses subtend approximately 1.95°, as in the experiment, if they are seen from 1 m away.

4.1.3. Experimental procedure

Once the videos had been created, the 4-mm pupil in P2 was replaced by a pinhole that produces an effective pupil in the subject's pupil plane of 0.8 mm. This small aperture increased the depth of focus of the subjects as illustrated in Figure

4.2, removing feedback from accommodation, and thus opening the accommodative loop.

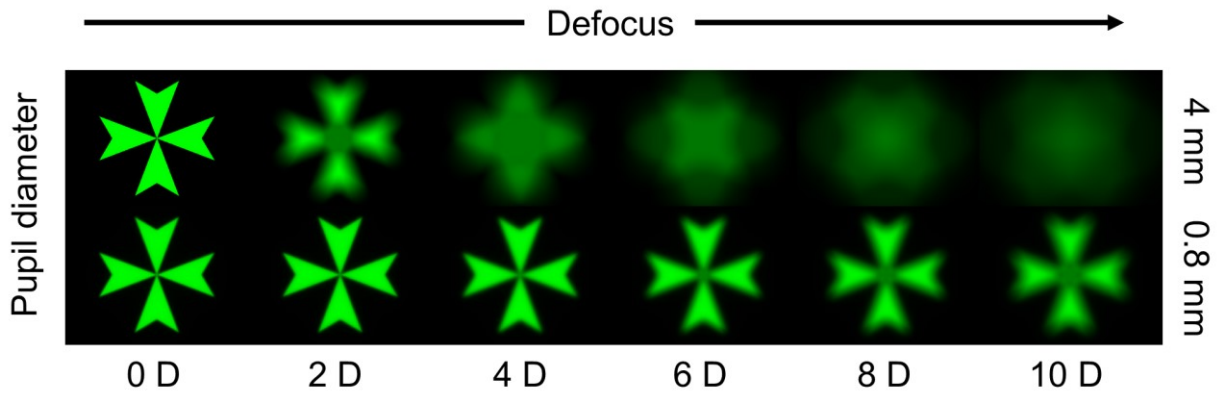

Figure 4.2. Effect of the aperture size on the image of the Maltese cross. Upper row shows retinal image simulations when the pupil has a diameter of 4 mm, whereas the lower row shows the same simulations, but when the pupil has a diameter of 0.8 mm. The increase in depth of focus when the pupil is small is evident.

In order to ensure that the light reaching the retina was always enough to elicit accommodation, the luminance of the microdisplay was increased from an approximate value of 260 cd/m^2 for the 4-mm pupil to a value close to 3400 cd/m^2. These values correspond roughly to 20 and 260 cd/m^2 in the corneal plane, due to the loss experienced when passing through all the optical elements (about 93%). This way a retinal illuminance (luminance multiplied by pupil area) of about 100 Troland was achieved in every experimental condition, thus not affecting accommodation (Cabello, 1945; Otero, 1951; Johnson, 1976).

Subjects were asked to bite the dental mould again and they were aligned with the system with the help of the pupil camera. The contralateral eye was occluded again and the Badal was set at the far point of the subject. Then, the Badal was moved 2 D closer to the subject's eye from the far point to induce an accommodative demand of 2 D. At this position, aberrations of the subjects were corrected with the AO system. Aberrations measured before and after the correction were recorded. After 5 seconds, the simulations were displayed in the microdisplay in a randomized order. There were 6 trials for each of the four conditions, and each trial lasted 25 seconds. The initial direction of the sinusoidal in the videos was also randomized, and the subjects were instructed to try to keep the target clear using the same effort as when reading a book.

4.1.4. Data analysis

4.1.4.1. Characterization of the accommodative response

The accommodative responses in each trial were computed using the minimum RMS refraction (Thibos et al. 2004; Tarrant et al. 2010). Sinusoidal functions with a frequency of 0.2 Hz were fitted to the recorded responses and then gain and temporal phase (see Figure 3.1) calculated as described previously in Section 3.1.3. Since the majority of responses did not follow a sinusoidal trend, temporal phase is meaningless, and hence not shown in Results.

4.1.4.2. Frequency spectrum characteristics

Because in this experiment some subjects showed a great deal of activity, a Fourier analysis was performed to see whether these subjects were effectively following the accommodative stimulus or they were just on a search quest. For this purpose, a cubic interpolation was performed to the responses before applying the Fourier transform. The result of this operation gives information about the temporal frequency content of the accommodative responses. Since the accommodative demand, either real (preliminary trials) or simulated (videos used in this experiment), follows a sinusoidal pattern, its Fourier transform is a delta function (Bracewell, 2000), that is, it presents an isolated peak at the frequency of the sinusoidal, 0.2 Hz. Hence, if the accommodative response follows the demand closely, its Fourier transform should show a distinct peak at the same sinusoidal temporal frequency. Otherwise, the Fourier transform would show energy at many frequencies.

4.1.4.3. Statistical analysis

Since data were not satisfactorily described by a normal distribution according to the Shapiro-Wilk test, the Friedman's test, which is the non-parametric version of ANOVA, was performed to the gain values to evaluate whether there were any differences in accommodative responses among conditions. The significance level was set at 0.05.

4.2. Results

4.2.1. Change in aberrations with accommodation

The left panel in Figure 4.3 shows the stimulus-response curves obtained for each subject (gray lines) and the mean curve (black line). The right panel shows the mean change experienced by each Zernike coefficient with accommodation for a 4-mm pupil. Each data point represents the average slopes over subjects obtained after

performing a linear regression between each Zernike coefficient and the accommodative response. The individual linear regressions were used to calculate the coefficients at each demand and generate the videos, as described in Section 4.1.2.

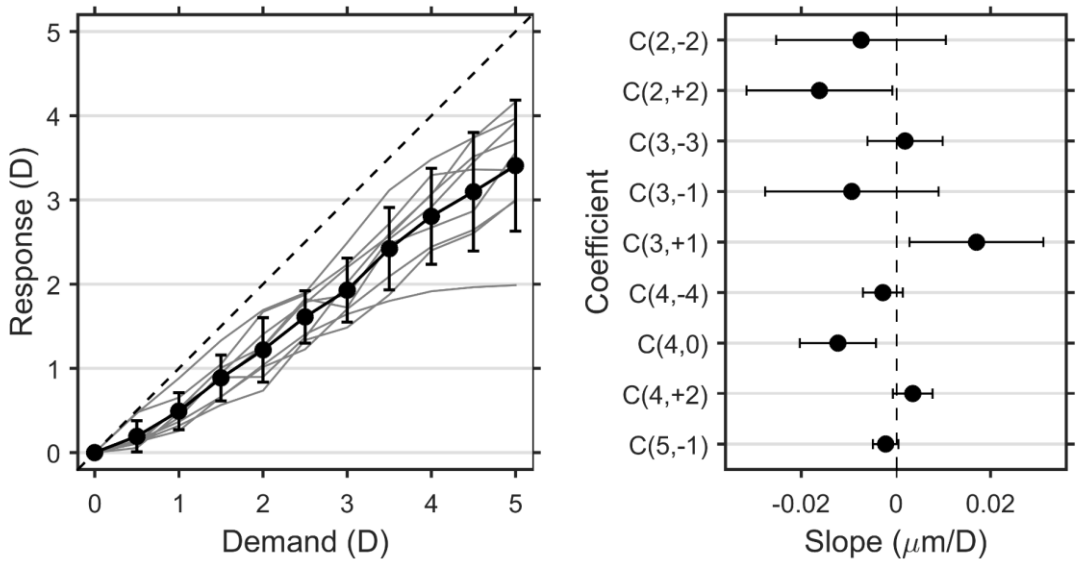

Figure 4.3. Left panel shows in gray the stimulus-response curves for each subject, along with the mean response (solid black line). The dashed line represents the ideal response, with unit slope. Right panel shows the mean slope obtained in the linear regression among subjects for each Zernike coefficient that on average is different from zero, except defocus. The coefficients not shown showed slopes of zero. Values correspond to a 4-mm pupil diameter. Error bars in both panels represent ±2 standard errors of the mean.

4.2.2. Accommodation to target blur without feedback

Figure 4.4 shows the mean gain values obtained for the 4 experimental conditions and for the preliminary trial for comparison for the 9 participants. The responses in the preliminary trials were always greater than the ones obtained in any of the conditions of this experiment. Only one (s05) out of nine subjects showed roughly similar gain as in the preliminary trials.

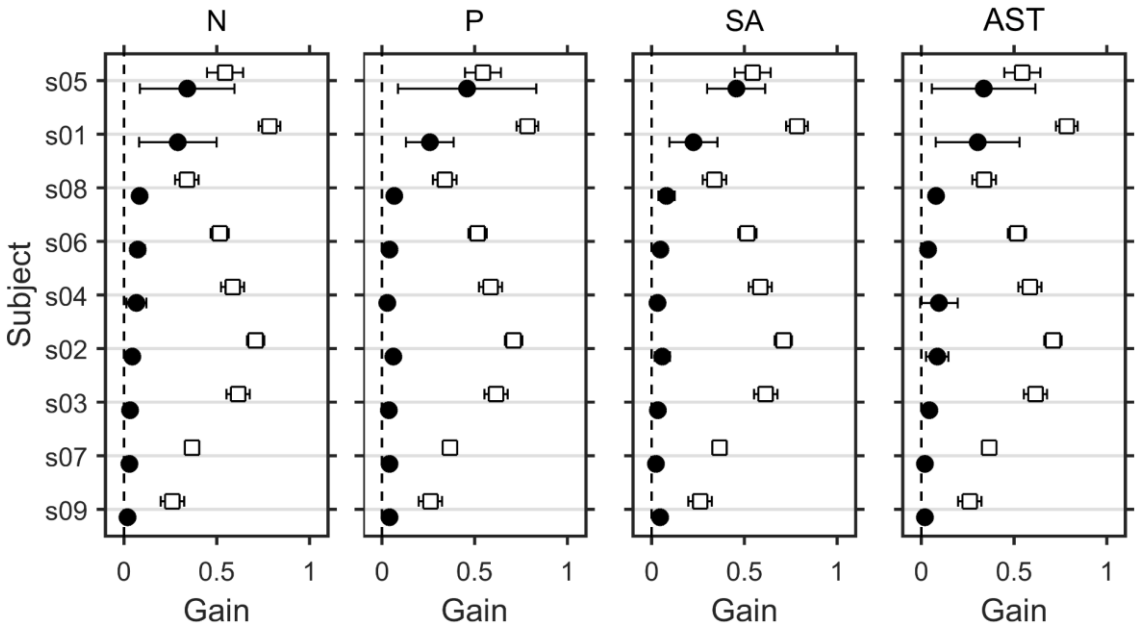

Figure 4.4. Mean gain among the six trials per subject and condition under study. Each panel represents a different condition for the simulated target blur experiment; from left to right: N, P, SA, and AST. Black solid circles stand for the gain obtained in the simulated target blur condition without feedback from accommodation, whereas white empty squares stand for the gain obtained in the preliminary trials (see Section 3.2). Subjects are arranged in descending order of gain obtained in the subjects' aberrations condition. Error bars represent ±2 standard errors of the mean.

No statistically significant differences were found among experimental conditions with the non-parametric Friedman's test (p = 0.99). Three subjects (s03, s07 and s09) did not show any response at all in any of the four conditions. Four subjects (s08, s06, s04 and s02) showed little to no response among conditions. Two subjects (s05 and s01) showed mean gains ranging from 0.23 to 0.46.

The overall mean gain in the preliminary trials was 0.52, dropping to 0.11 when removing real changes in vergence and feedback from accommodation. This result highlights their importance within the accommodative process.

Subject s09 did not show any response to the change in target blur, merely some small fluctuations. On the contrary, subject s05 showed a great deal of activity in the target blur conditions, however this subject could not follow the sinusoidal pattern properly. As can be seen in the four lower panels at the left in Figure 4.5, it seemed as this subject was trying very hard to follow the stimulus, although erratically and unsuccessfully, as if searching for the position to clear the image.

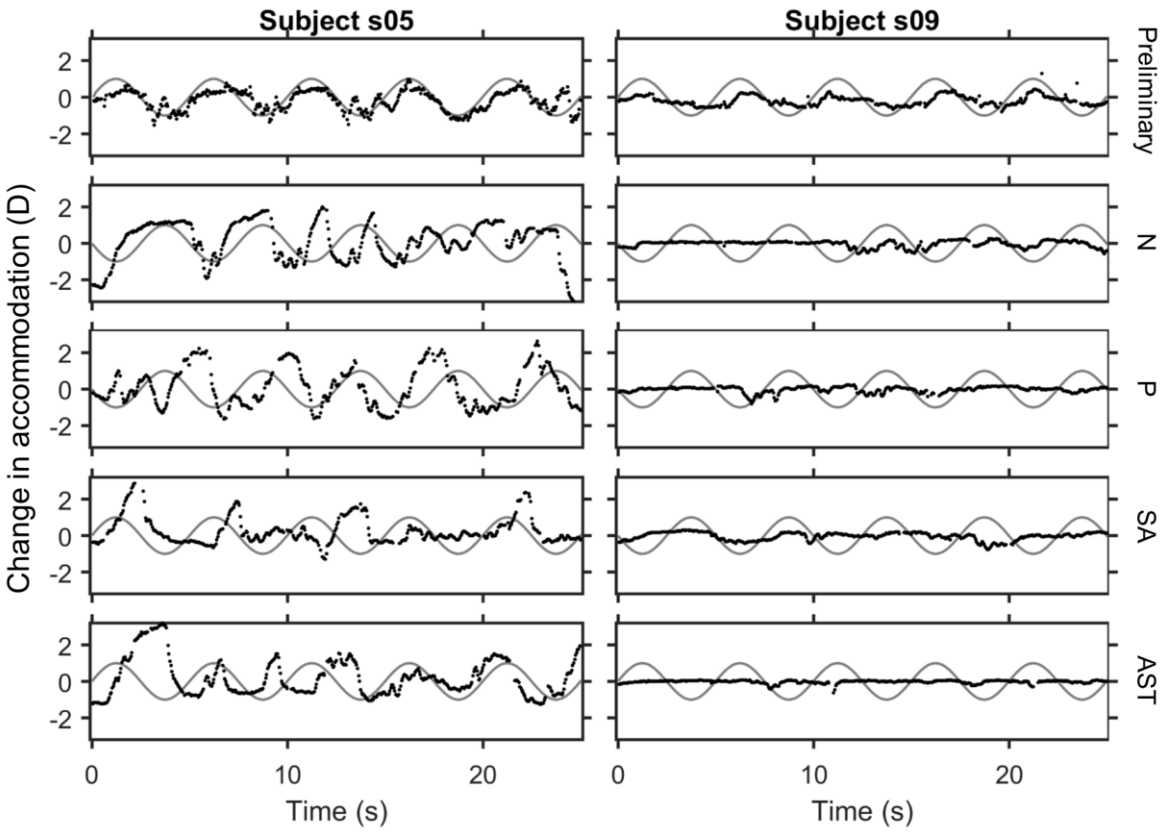

Figure 4.5. Variation in accommodative response for the subject who showed the greatest gain (left column) and for the subject who showed the smallest gain (right column) for accommodation to target blur. Rows represent different experimental conditions. From top to bottom: trial corresponding to the preliminary experiment, target blur with subjects' aberrations, target blur with defocus only, target blur with unbalanced spherical aberration, and target blur with oblique astigmatism. Gray solid curve is the sinusoidal accommodative demand, whether it is real (upper row) or simulated (rest of the rows).

Figure 4.6 shows the median temporal frequency spectra obtained for the preliminary trials (in the left column) and two conditions (subjects' HOAs in the middle column and only defocus in the right column). When the subjects could follow the stimulus correctly and at the right frequency, there was a distinct peak at 0.2 Hz, as in the left column of Figure 4.6. For the simulations, the subjects who showed little gain presented a flat spectral distribution, whereas for subjects who showed greater gain (s05 and s01), there was plenty of activity up to 0.8 Hz. The fact that the energy is not concentrated only in 0.2 Hz suggests that these subjects were probably searching unsuccessfully for a sharp retinal image. Subject s05 showed peaks at 0.2 Hz when its aberrations were included in the video, and close to 0.2 Hz when there was only defocus; however, this subject also showed a great deal of

energy at other frequencies, unlike the characteristic isolated peak shown in the preliminary trials.

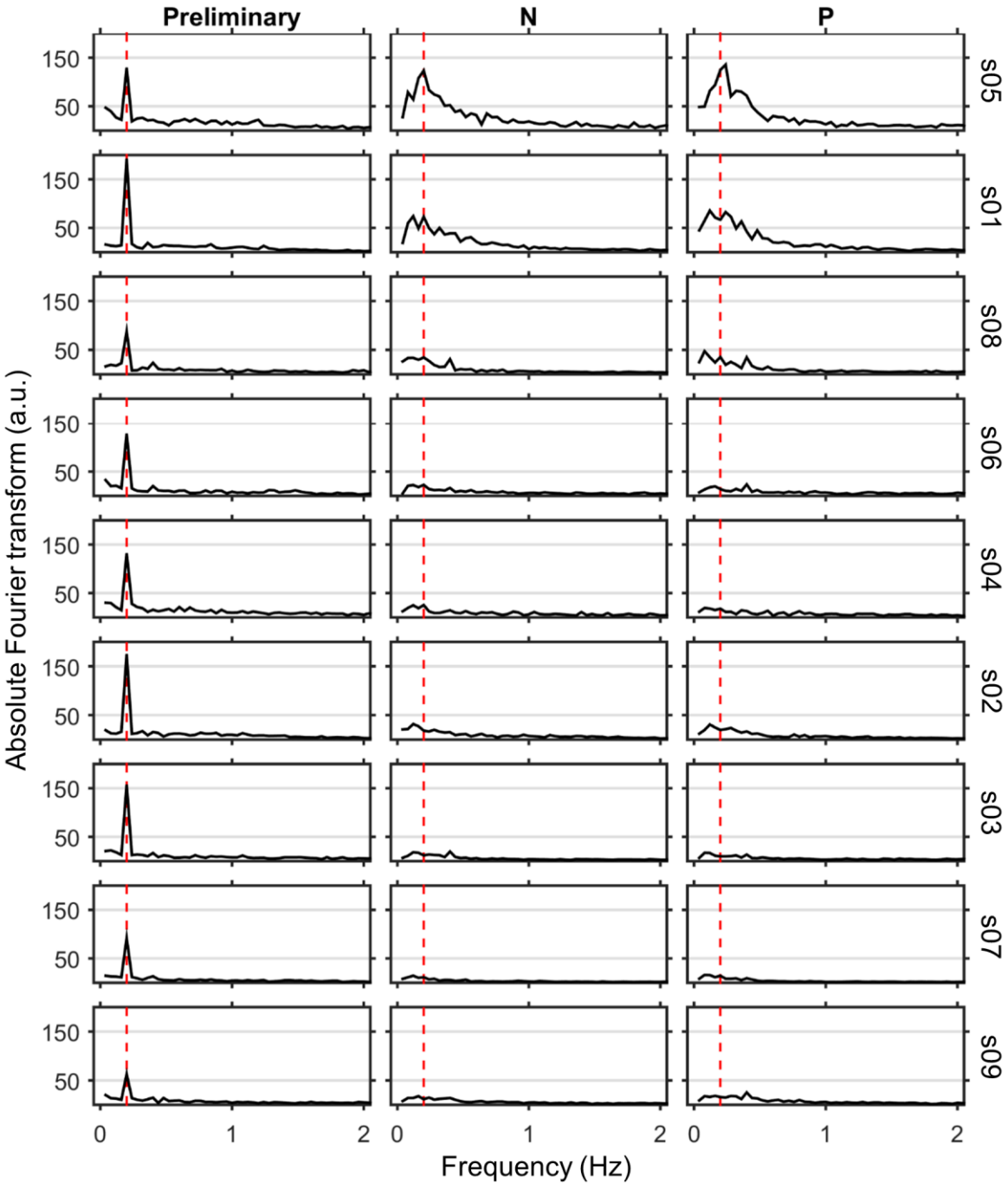

Figure 4.6. Median temporal frequency spectra of the responses for each subject for the preliminary trials (left column) and for two target blur experimental conditions (middle and right columns). Dashed red vertical line shows the frequency of the sinusoidal, that is 0.2 Hz. Subjects are arranged in descendent order of gain obtained in the subjects' aberrations condition.

4.3. Discussion

From the experimental results shown here, the hypothesis that the differences in the shape of the blur in retinal images is enough for the eye to accommodate is unlikely true. Although some subjects responded with a lot of activity in their accommodation to defocus blur alone, their response was erratic and could not follow the stimulus.

A possible limitation of this study is the fact that the changes in aberrations with accommodation were calculated from the stimulus-response curves by means of linear regressions. This assumes that aberrations change linearly with accommodation, which could oversimplify the real variation. Nonetheless, other than an astigmatism term, coma and the fourth order spherical aberration, the rest of aberrations changed very little or nothing with accommodation (see Figure 4.3). Spherical aberration became more negative with accommodation, which is in agreement with previous studies (Atchison et al. 1995; Bernal-Molina et al. 2014). Astigmatism and coma have also been shown to change with accommodation, although the trend of the variation remains unclear (Ukai & Ichihashi, 1991; Cheng et al. 2004). In addition, possible variations of aberrations over time (Iskander et al. 2004; Montés-Micó et al. 2004) are not taken into account with the method used here. But these changes are not expected to be large. Since the goal of this study was to elucidate whether different shape of blur in retinal images could drive accommodation, the setup used here is sufficient for this end.

The appropriateness of the correction of the subjects' aberrations before the start of each trial can be found in Figure 4.7. The mean HOAs and astigmatism RMS for all conditions and subjects is smaller after correction of the aberrations, except in one subject in the condition where the target was blurred with the subject's own aberrations. Apart from subject s04, who showed the highest RMS among all and a high variability in the correction of aberrations, the rest of the subjects had their aberrations corrected optimally, with RMS values very close to zero. The corrections of aberrations for s04 in the first condition were generally suboptimal; however, it probably did not

affect the outcomes since the 0.8-mm pinhole also reduced the aberrations greatly.

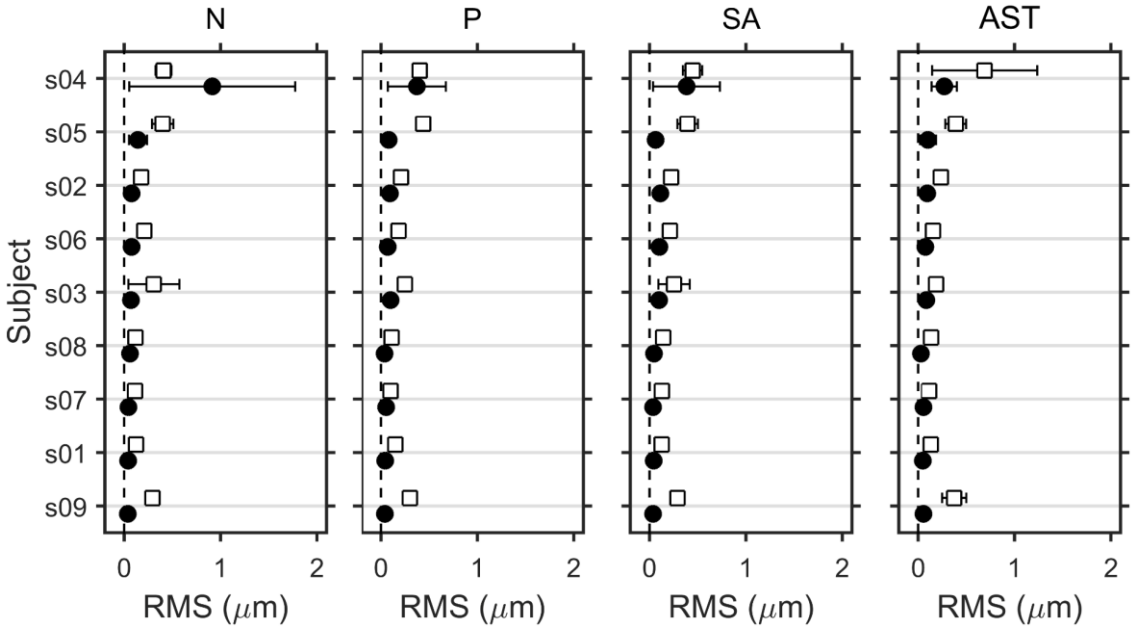

Figure 4.7. Mean HOAs and astigmatism RMS before (empty squares) and after (black solid circles) AO correction for each subject and condition. Subjects are arranged in descending order of RMS before correction in the subjects' HOAs condition. Error bars correspond to ±2 standard errors of the mean.

This experiment provides further support to the observation that monochromatic even-order aberrations are weak cues for accommodation (Campbell & Westheimer, 1959; Wilson et al. 2002; Bernal-Molina et al. 2017), if used at all (Chen et al. 2006; López-Gil et al. 2007; Chin et al. 2009a, 2009b). There were no significant differences between the condition with only defocus, where the resulting retinal image is the same from either over- or under-accommodation and the rest of conditions with simulated monochromatic aberrations. And since the responses were either negligible or erratic, it can be concluded that subjects do not respond to defocus blur that includes the effects of monochromatic aberrations.

5. Accommodation to optical blur and target blur without feedback

The fact that the shape of blur in the retinal image does not drive accommodation was demonstrated in the previous Chapter. It is also known that eyes can still accommodate in monocular and monochromatic conditions while astigmatism and monochromatic HOAs are corrected (Chen et al. 2006; Chin et al. 2009a; Bernal-Molina et al. 2017). Under such stringent conditions, the driving force of accommodation ought to be light vergence or feedback from microfluctuations in accommodation or both in concert.

In this Chapter, an experiment is presented that aims at testing whether accommodation is driven by light vergence, which produces real out-of-focus retinal images (optical blur).

5.1. Methods

5.1.1. Experimental conditions

Two different stimulus conditions, which are presented in Figure 5.1, were part of this experiment. In both conditions the deformable mirror corrected subjects' HOAs and astigmatism at 20 Hz. In the first condition, which is referred throughout this thesis to as vergence-driven condition without feedback, the deformable mirror also compensated for changes in accommodation and additionally it provided sinusoidal changes in defocus that changed between −1 and +1 D at a temporal frequency of 0.2 Hz. The induction of fixed amount of defocus at the retina opened the accommodative loop and removed feedback, so that the eye could not use trial-and-error changes or small fluctuations in accommodation to determine the direction in which to accommodate. Therefore, the only cue available in this condition was changes in light vergence. In the second condition, which is referred throughout this thesis to as blur-driven condition without feedback, sinusoidal blur between −1 and +1 D was simulated in the Maltese cross at 0.2 Hz, using the Fourier optics calculator. This is the same as the second condition in Section 4.1.2. The same profile of defocus blur was presented in the blur-driven condition as for the vergence-driven condition, except this time it was target blur, not optical blur.

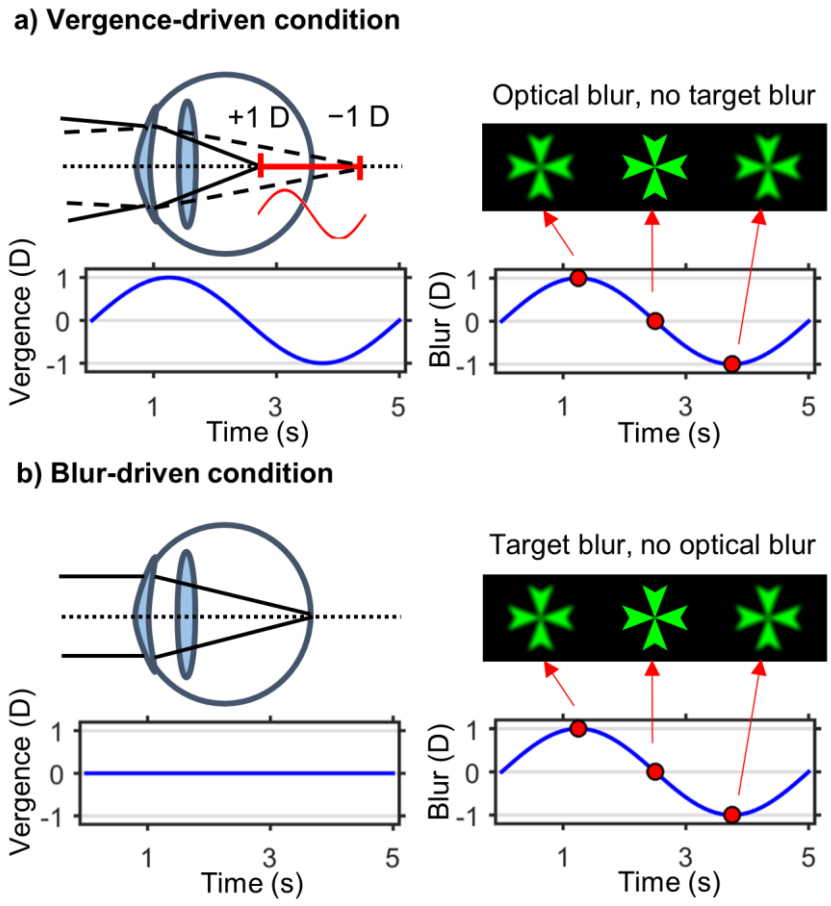

Figure 5.1. Schematic representation of the two conditions tested in this experiment. The upper row illustrates the vergence-driven condition, in which the level of defocus without feedback provided by the deformable mirror at the retina varied sinusoidally between −1 and +1 D at 0.2 Hz, regardless of the accommodative state of the eye. This sinusoidal change in light vergence caused the Maltese cross to be blurred at the retinal plane as well, as shown at the right. The lower row illustrates the blur-driven condition, in which the defocus provided at the retina was always zero during the trials, while the Maltese cross was sinusoidally blurred without feedback by means of simulations.

5.1.2. Experimental procedure

A 4-mm pupil in front of the microdisplay was used in all trials and conditions, and its luminance was set to approximately 260 cd/m^2, which corresponds to about 20 cd/m^2 at the corneal plane and to a retinal illuminance of about 100 Troland (see Section 4.1.3).

As in the experiment presented in Chapter 4, the subject bit the dental mold and was properly aligned using the pupil camera after the aberrations of the optical system were corrected. The contralateral eye was occluded with an eye patch and

the far point of each subject was determined as described in Section 3.1.2. Once the far point was obtained and after a short break if necessary, subjects were aligned with respect to the optical system again. Then the Badal was set at the far point of the subject. Once the subject was ready, the Badal moved 2 D closer to the subject's eye from the far point to induce an accommodative demand of 2 D. The instruction given to the subjects was to try and clear the Maltese cross by using the same effort as if they were reading a book. After a few seconds, measurements for the three conditions started in a randomized order. There were six trials for each condition, making a total of 18 trials per subject. The duration of each trial was 25 seconds (5 cycles as the ones shown in Figure 5.1). The initial direction of the sinusoidal, both in the vergence-driven and in the blur-driven conditions, was randomized.

A correction speed of 20 Hz is more than fast enough to eliminate any non-negligible cues from microfluctuations, since microfluctuations of accommodation with temporal frequency greater than 5-6 Hz are quite small in magnitude (Denieul, 1982; Charman & Heron, 1988). This speed was also sufficient for the simulated blur of the target to appear to change smoothly in the blur-driven condition. The assessment of the corrections made with the AO system can be found in Appendix A.

5.1.3. Data analysis

5.1.3.1. Characterization of the accommodative response

In this experiment the accommodative error of the subjects had to be corrected and a certain level of defocus provided at the retina at any given moment in time (as the stimulus was required to change sinusoidally between −1 and +1 D at the retina). Thus, the accommodation response could not be extracted directly from the accommodative error measured by the Shack-Hartmann, since it was always zero (in the blur-driven condition) or a sinusoidal between −1 and +1 D (in the vergence-driven condition). So the response of the eye had to be extracted from the shape of the deformable mirror that had been used to compensate for the response. A subtraction was performed between the defocus induced by the deformable mirror, which was calculated from the actuators voltage values (see eq. 2.4), and the defocus measured with the Shack-Hartmann sensor. As in the analysis presented in Chapter 3, the accommodative response was computed using the minimum-RMS refraction (Thibos et al. 2004;Tarrant et al. 2010). A sinusoidal function with a frequency of 0.2 Hz was then fitted to the responses. Gain and temporal phase (see Figure 3.1) were calculated from the fitted functions as

described previously in Section 3.1.3. Temporal phase was only analysed if the responses did follow a sinusoidal, since otherwise temporal phase would be rendered meaningless, as noted in Section 4.1.4.1.

5.1.3.2. Statistical analysis

Data were first tested for normality using a Shapiro-Wilk test and because the data were not found to be normally distributed, the non-parametric version of the paired t-test, the Wilcoxon signed-rank test, was performed. The significance level was set to 0.05.

5.2. Results

Figure 5.2 shows the mean gain obtained for both conditions tested in this experiment, as well as from the preliminary trials for all the subjects. The mean gain ±2 standard errors of the mean for the vergence-driven condition without feedback over all subjects was 0.50±0.19, whereas for the blur-driven condition without feedback was much smaller at 0.07±0.02, as expected.

In the vergence-driven condition, 8 out of 9 subjects responded to the sinusoidal changes in light vergence. The gain values varied considerably between subjects: subjects s01 and s07 showed greater gain than in the preliminary trials; subjects s03, s04, s05, and s09 showed about the same mean gain, and subjects s02, s06, and s08 showed smaller gain. In general, the variability was greater in the vergence-driven condition than in the preliminary trials, which was expected since in this experiment there was no feedback from accommodation. Gains were significantly different between the vergence-driven condition and the blur-driven condition ($p = 0.004$). In the vergence-driven condition, only 1% of the responses were in counter-phase with the demand, and only for subject s08, who showed negligible gains in this experiment. In the blur-driven condition, however, about 46% of the responses were in counter-phase, showing that subjects could not follow the sinusoidal blur pattern when light vergence was not present.

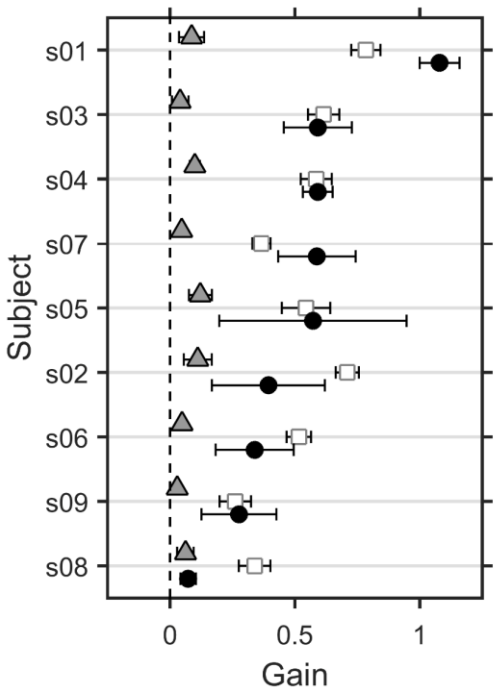

Figure 5.2. Mean gain over the six trials per subject and experimental condition under study. Black solid circles represent the gain obtained in the vergence-driven condition without feedback, gray triangles represent the gain for the blur-driven condition without feedback, and gray empty squares represent the gain obtained in the preliminary trials (see Section 3.2). Subjects are arranged in descending order of gain obtained in the vergence-driven condition. Error bars represent ±2 standard errors of the mean.

Temporal phase was calculated only for the vergence-driven condition, since it was the only condition were subjects showed sinusoidal responses to the stimulus. Figure 5.3 shows the mean temporal phase over the six trials obtained for the vergence-driven condition and that obtained in the preliminary trials for comparison. Temporal phase was generally greater in the vergence-driven condition than in the preliminary trials. Only 2 out of 9 subjects showed less mean temporal phase in their responses in the vergence-driven condition than in the preliminary trials.

To illustrate responses to the different conditions and to show an example of variability among subjects, Figure 5.4 shows the same trial for the two conditions plus the preliminary experiment for the subjects with greatest (s01) and smallest gain (s08) in the vergence-driven condition, respectively.

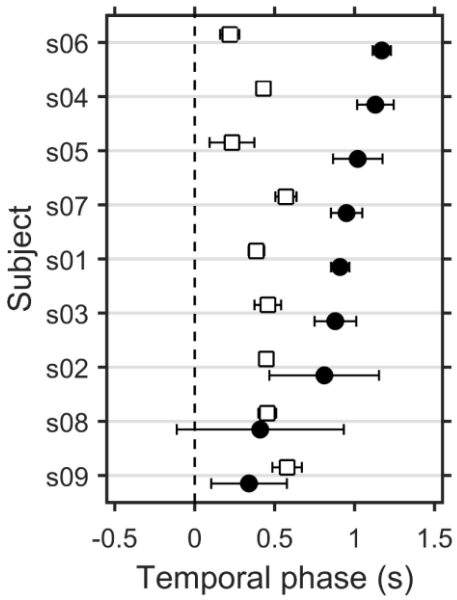

Figure 5.3. Mean temporal phase among the six trials per subject for the vergence-driven condition. Other details as in Figure 5.2.

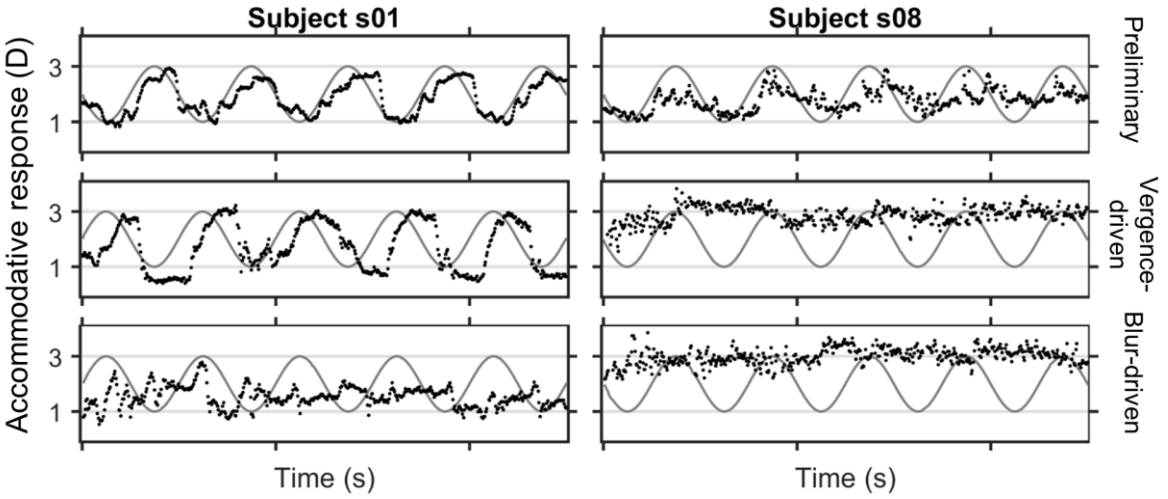

Figure 5.4. Accommodative response for the subject with the greatest gain (left column) and for the subject with the smallest gain (right column) in the vergence-driven condition. Rows represent different experimental conditions. From top to bottom: a trial corresponding to the preliminary experiment, and trials corresponding to the vergence-driven, and blur-driven conditions. Gray solid curves are the sinusoidal accommodative demand, whether real with feedback (first row), real without feedback (second row), or simulated (third row).

The greater temporal phase in the vergence-driven condition (second row) compared to the preliminary trials (first row) can be seen in the left panel (s01) of the two first rows of Figure 5.4. The behaviour of these two subjects among

conditions is radically different. Subject s08 seemed to repeat the same accommodative behaviour in the vergence-driven and blur-driven conditions. The subject increased the accommodative response up to a level where the response remained practically constant. In contrast, subject s01 could follow the sinusoidal change remarkably well even without feedback as in the vergence-driven condition, albeit with a greater temporal phase than for the preliminary experiment. This subject could not follow the sinusoidal change in the blur-driven condition (third row), as expected, despite the evident effort the subject made in seeking the correct direction in which to accommodate.

Figure 5.5 shows the median temporal frequency spectra obtained for the preliminary trials and the two conditions; that is vergence-driven and blur-driven conditions. All but subject s08 showed the characteristic peak at 0.2 Hz both in the preliminary experiment and in the vergence-driven condition, highlighting that 8 subjects could follow the sinusoidal change in light vergence properly. Note that subject s08 did not show that peak in the vergence-driven condition, and consequently its gain was very close to zero. In the blur-driven condition, none of the subjects showed a clear peak at 0.2 Hz. Moreover, except for subjects s04 and s05, they showed very little to null activity.

5.3. Discussion

The experiment presented here is the first of its kind to use light vergence to drive accommodation while all the other potential directional cues for the sign of defocus were eliminated with AO. The main conclusion of this study was that the human visual system is capable of detecting the vergence of the light incoming to the eye, which is different whether the light is focused in front or behind the photoreceptor plane (see Section 1.1.4.3).

In this experiment, binocular and monocular depth cues were removed by using the Badal optical system, cues from chromatic aberration, astigmatism and monochromatic HOAs of the eye were removed by using a monochromatic target and adaptive optics in real time at 20 Hz. Fluctuations of accommodation were also compensated for with the AO system. The circular artificial pupil through which the subject viewed the stimulus prevented signed cues for accommodation that could appear from the irregular shape of natural pupils (López-Gil et al. 2007).

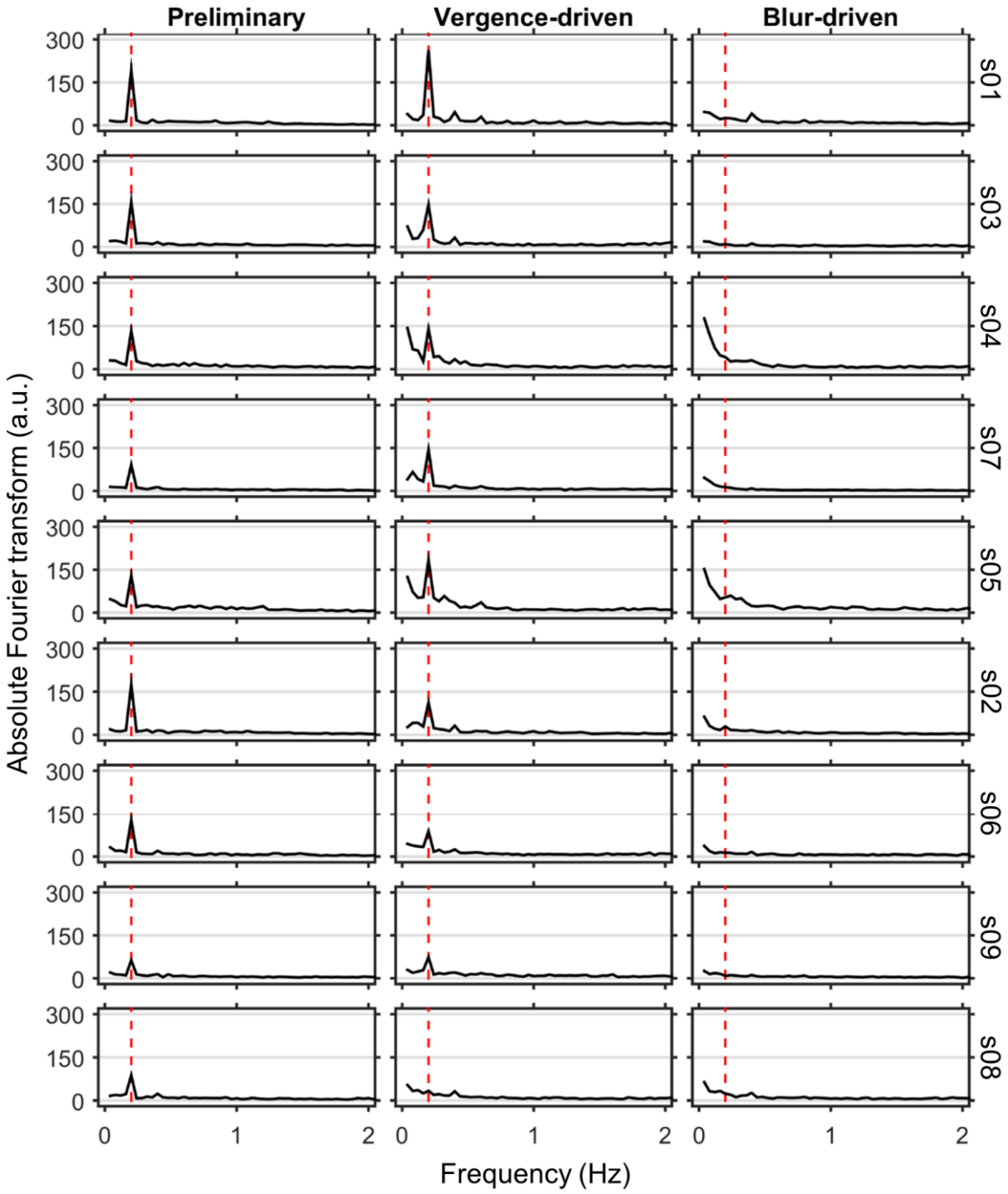

Figure 5.5. Median temporal frequency spectra of the responses for each subject for the preliminary trials (left column) and for the vergence-driven (middle condition) and the blur-driven (right column) conditions. Dashed red vertical line shows the frequency of the sinusoidal demand at 0.2 Hz. Subjects are arranged in descending order of gain obtained in the vergence-driven condition.

Therefore, defocus blur caused by inaccurate focus or light vergence, acted as the fundamental accommodation cue and it was carefully isolated from any other potential cue.

Subjects generally showed greater temporal lag in the open-loop condition than in the closed-loop condition of the preliminary experiment (see Figure 5.3). These results are in agreement with those obtained by Kruger et al. (1997) in an open-loop dynamic accommodation experiment.

In the vergence-driven condition, 8 out of 9 subjects showed clear sinusoidal responses, whereas in the blur-driven condition, where no changes in light vergence occurred and only defocus blur was present, the accommodation response was negligible. Therefore, the results of this study present further evidence in support of the hypothesis that accommodation responds directly to light vergence (Fincham, 1951; Campbell & Westheimer, 1959), not indirectly via defocus blur (Heath, 1956; Phillips & Stark, 1977).

6. Accommodation to optical blur and target blur with feedback

It was demonstrated in Chapter 5 that light vergence plays an important role in driving accommodation. However, the experiment was performed when feedback from accommodation was eliminated (open-loop setup). In the experiment described in detail in this Chapter, feedback from accommodation was present. Depending on the type of feedback there were two experimental conditions: one in which the feedback from accommodation comes from the accommodative error or light vergence, together with the blur associated to the accommodative error; and another condition in which the feedback comes only from the blur of the target.

The aim of this experiment was to test directly two hypotheses about what drives human accommodation. Is it driven by changes in light vergence (accommodative error) as Fincham suggested (Fincham, 1951), or is it driven by a trial-and-error strategy that minimizes retinal blur and thus maximizes retinal contrast, as it is generally accepted (Heath, 1956; Troelstra et al. 1964; Phillips & Stark, 1977)?

6.1. Methods

Three experiments were carried out. In the first one, referred here to as the steady-state experiment, the accommodative demand remained constant throughout the trials. In the second one, referred here to as the step-change experiment, the demand was modified in random rectangular steps. In the third experiment, referred here to as the sinusoidal experiment, the accommodative demand changed sinusoidally.

6.1.1. Experimental conditions

There were two different experimental conditions in all three experiments. In both conditions subjects' astigmatism and HOAs were corrected at 20 Hz with the AO system, while they were viewing monocularly the green Maltese cross through a 4-mm circular pupil. Therefore, cues from binocular vision, chromatic and monochromatic aberrations, irregularities in pupil shape, and monocular depth cues were absent.

In the first condition, namely the vergence-driven condition with feedback, the deformable mirror provided the necessary amount of light vergence, whether this remained constant (steady-state stimulus), or it changed over time (step-change and sinusoidal stimuli).

In the second condition, namely the blur-driven condition with feedback, the deformable mirror was always compensating the accommodative error of the subjects, so the Maltese cross was always focused accurately at the retina. However, depending on the response of the eye, the Maltese cross was artificially blurred to appear as it would be under normal conditions. Thus, in both conditions, the Maltese cross appeared blurred to the subjects if they were not accommodating to the required accommodative demand as a result of the inaccurate focus at the retina. The difference between conditions is that in the vergence-driven condition the blur is a consequence of accommodative error (optical blur), whereas in the blur-driven condition the target itself is blurred (target blur).

To understand better the difference in the nature of blur in both conditions, consider the following example. In the vergence-driven condition, a Maltese cross is presented at an accommodative demand of 0 D and the eye is fixating at that distance so that there is no accommodative error. The Maltese cross moves from an accommodative demand of 0 D to one of 1 D. At the exact moment that the change in vergence happens, the eye presents an accommodative error of −1 D. This accommodative error causes a blur in the retinal image of 1 D. If the eye responds in the right direction (accommodating), the accommodative error would decrease in magnitude, thus decreasing the blur in the retinal image and maximizing the contrast. If, however, the eye responds in the wrong direction (disaccommodating), then the accommodative error would increase, and the retinal image would become more blurred (see vergence-driven condition in Figure 6.1). In this condition, there is feedback from accommodation because of optical blur.

The example for the blur-driven condition would be the same, but this time the accommodative error is always zero, since the deformable mirror is compensating it in real time (see blur-driven condition in Figure 6.1). There are not real changes in light vergence, but the changes happen in the Maltese cross by blurring it by the proper amount. Then, if the eye responds correctly, the blur of the Maltese cross will decrease, and it will increase if the eye responds wrongly. In this condition, there is feedback from accommodation because of target blur.

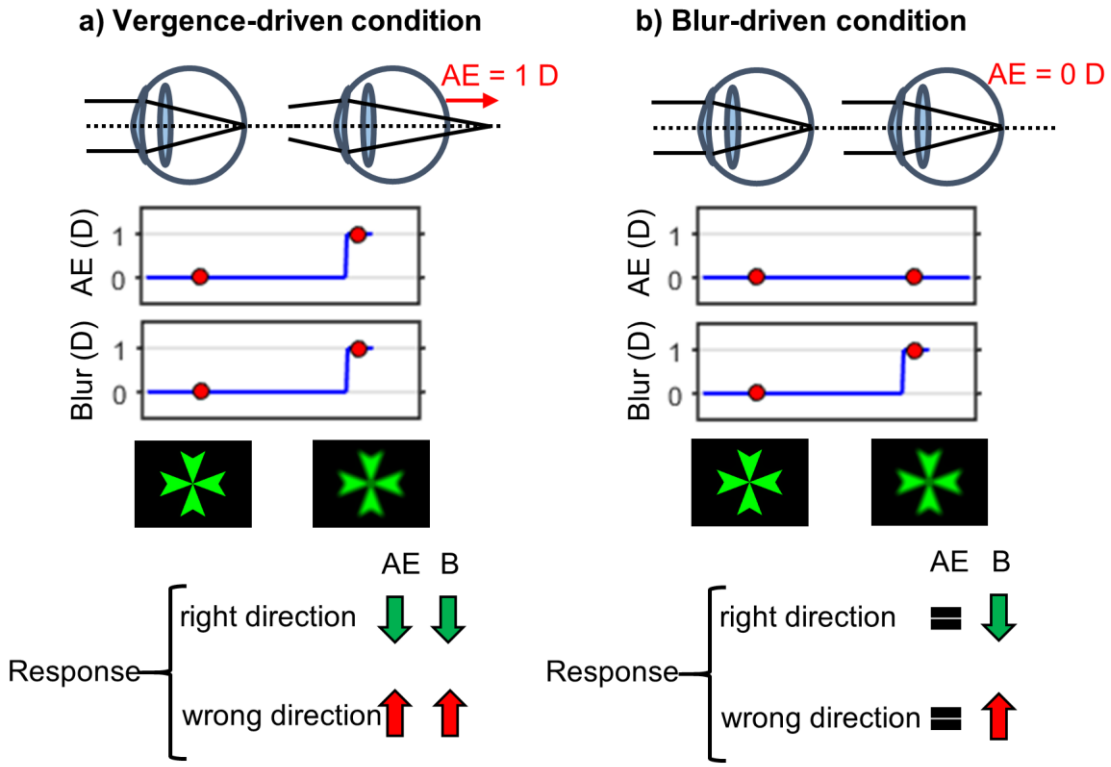

Figure 6.1. Schematic representation of the two conditions tested in this experiment. Panel (a) illustrates the vergence-driven condition with feedback, in which there is accommodative error on the retina when the eye's accommodative state does not match the stimulus demand. In this condition, there is feedback from accommodation because of optical blur. Panel (b) illustrates the blur-driven condition with feedback, in which the Maltese cross was always focused accurately on the retina, but the target itself is blurred when the eye accommodative state does not match the stimulus demand. In this condition there is feedback from accommodation because of target blur. Green arrows pointing down indicate decrease, whereas red arrows pointing up indicate increase. AE stands for accommodative error and B stands for blur. Note that in this example the change in demand was a step, however, depending on the experiment, it can also change sinusoidally or remain constant.

6.1.2. Experiments

6.1.1.1. Steady-state stimulus

For the steady-state experiment, the Maltese cross was presented with a stationary accommodative demand of 2 D. Six trials were performed per subject and experimental condition. Each trial had a duration of 50 seconds. Conditions were presented randomly.

6.1.1.2. Step-change stimulus

For the step-change experiment, the blur of the Maltese cross followed a pattern centered at 2 D of accommodative demand and presenting step changes in demand of 1 D of amplitude with random sign. The accommodative demand was always between 1 and 3 D. Steps were randomly introduced over time, with a mean Gaussian distribution of 10 seconds and a standard deviation of 1.25 seconds. With this standard deviation, 95% of the times, time change is between −2.45 and +2.45 s from the mean change time. Six trials per subject and experimental condition were performed, and each trial presented a different pattern. The same patterns were used in both condition of the same trial for comparison purposes, making a total of 6 different patterns per subject. Trials were presented randomly and each lasted 50 seconds.

6.1.1.3. Sinusoidal stimuli

For the sinusoidal experiment, the blur of the Maltese cross changed following a sinusoidal pattern centered at 2 D of accommodative demand and with an amplitude of 1 D, so the demand changed between 1 and 3 D. Four different temporal frequencies of the sinusoidal change were tested: 0.05, 0.1, 0.2, and 0.4 Hz. The initial direction of the sinusoidal was randomized. This is the same sinusoidal blur change pattern used in the preliminary trials (see Section 3.1.3), except this time aberrations were corrected and different temporal frequencies were used. Six trials per subject, condition, and frequency were performed in a random order, for a total of 48 trials per subject. The duration of the trials depended on the frequency of the sinusoidal, being 40 seconds for 0.05 Hz; 30 seconds for 0.1 Hz; and 25 seconds for 0.2 and 0.4 Hz. The different durations of the trials was a trade-off between the number of cycles of the sinusoidal and trial time. A longer trial time was needed for slower sinusoidal patterns in order to have at least 2 cycles.

6.1.2. Experimental procedure

Subjects were asked to bite their dental mold and were carefully aligned and centered with respect to the optical system. Once their far point was determined (see Section 3.1.2), the Badal was set at 2 D of accommodative demand from their far point. Trials started after giving the same instruction to the subjects as in the rest of experiments in this thesis, to make the same effort as if they were reading a book. Since this was a particularly long experiment, subjects were allowed to take multiple breaks whenever they required it.

The assessment of the corrections made with the AO system can be found in Appendix A.

6.1.3. Data analysis

6.1.3.1. Characterization of the accommodative response

Since in this experiment the deformable mirror was always providing a particular vergence, whether it was changing over time or it was zero, subjects' response was obtained as described in Section 5.1.3.1. Then, for the steady-state experiment, the response was evaluated by calculating the mean accommodative error throughout the trials. The RMS error (not to be mistaken with the aberrations RMS) of the accommodative error was also calculated for each trial, so as to quantify the stability of such responses. The responses to the step-change stimulus were characterized in a similar manner as the sinusoidal described in Section 3.1.3. Only this time the function fitted to the data was a step function with the same profile as the accommodative demand and parameters amplitude and latency. Gain then was calculated as the amplitude of the response divided by the amplitude of the demand. Amplitude here has the same interpretation as for sinusoidals, and latency takes the role of temporal phase and represents how long, on average, it takes the eye to respond to each step-change in demand. Lastly, the responses to the sinusoidal stimuli were characterized by means of the gain and temporal phase, as explained in Section 3.1.3 and Section 4.1.4.1. Since there were sinusoidal patterns with four different frequencies, the function fitted to the data in each case had the same frequency as the demand. The median frequency spectra over all trials and subjects in each condition was calculated for the steady-state and the sinusoidal stimuli and the two conditions were compared against each other.

The response to the step-change stimulus was further analysed by calculating the peak velocity of accommodation and disaccommodation to the step changes in vergence. The peak velocity was calculated as follows: first, the responses were split into as many parts as step changes the profile contained. Then, a Boltzmann sigmoid function was fitted to the data around the step change. This function is defined as

$$r = \frac{a - b}{1 + e^{\frac{t-c}{s}}} + b, \tag{6.1}$$

where r is the accommodative response at each moment in D, t is the time in seconds, a stands for the initial response and b for the final one, both of them are in D. The parameter c indicates the time at which the sigmoid function reaches 50% of the total change, and it is given in seconds. The parameter s is the slope of the change, and it is given in D/s. Accommodative responses to steps tend to fit well to this type of function (Chin et al. 2009b; Hampson et al. 2010). The peak velocity then can easily be calculated as the maximum or the minimum of the derivative of the sigmoid, depending on whether the eye accommodates or disaccommodates. Figure 6.2 shows an example of a subject's response to a step change in demand. The fitted Boltzmann sigmoid function is shown as a red curve in the left panel.

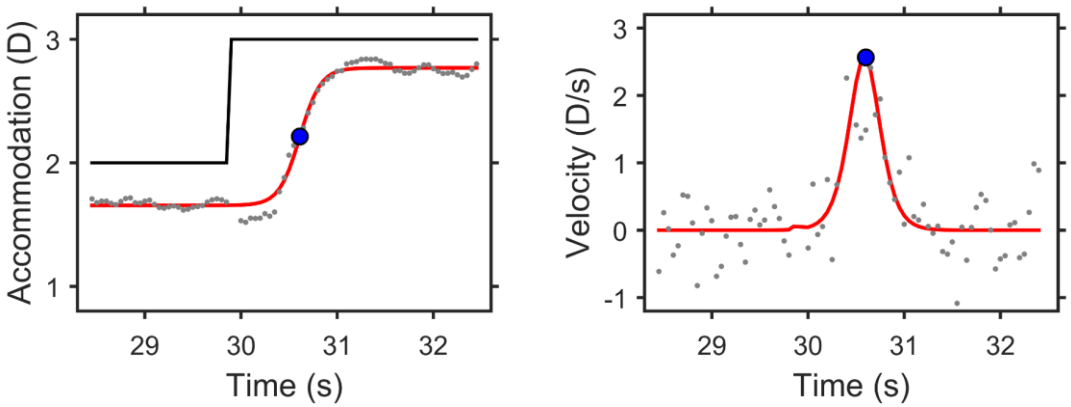

Figure 6.2. The left panel shows a fragment of a step-change stimulus trial where the demand (black line) changed suddenly from 2 to 3 D. The response of the subject is shown as gray dots. The sigmoid fitted to the response is shown as a red curve. Blue marker shows the parameter c of the sinusoidal, which indicates the time at which the sigmoid function reaches 50% of response. The right panel shows the derivative of the response (gray dots) and the derivative of the fitted sigmoid function (red curve), which corresponds to the velocity of the accommodation. The blue marker indicates the peak velocity.

Additionally, the first direction of the accommodative response to the step-change stimulus was assessed by performing a linear regression of the data right after a step in demand happened. The linear regression was performed for different time intervals. These time intervals were defined from the moment there was a step change in the demand to 5 seconds after it happened, in steps of 0.1 s. The sign of the slope was then compared with the sign of the demand to ascertain if the eye was accommodating in the correct direction depending on the condition.

6.1.3.2. Statistical analysis

Data were first tested for normality using a Shapiro-Wilk test and because the data were not found to be normally distributed, the non-parametric version of the paired t-test, the Wilcoxon signed-rank test, was performed. The significance level was set to 0.05.

6.2. Results

6.2.1. Steady-state stimulus

The left panel of Figure 6.3 shows the mean accommodative error obtained for each subject and condition under study for the steady-state stimulus. For this stationary stimulus, the accommodative error indicates how well subjects could focus on the Maltese cross. Except for subject s06, there were practically no differences between the two conditions. The mean difference in accommodative error (±2 standard errors of the mean) between conditions was −0.09±0.19 D, not significantly different from zero (p = 0.496).

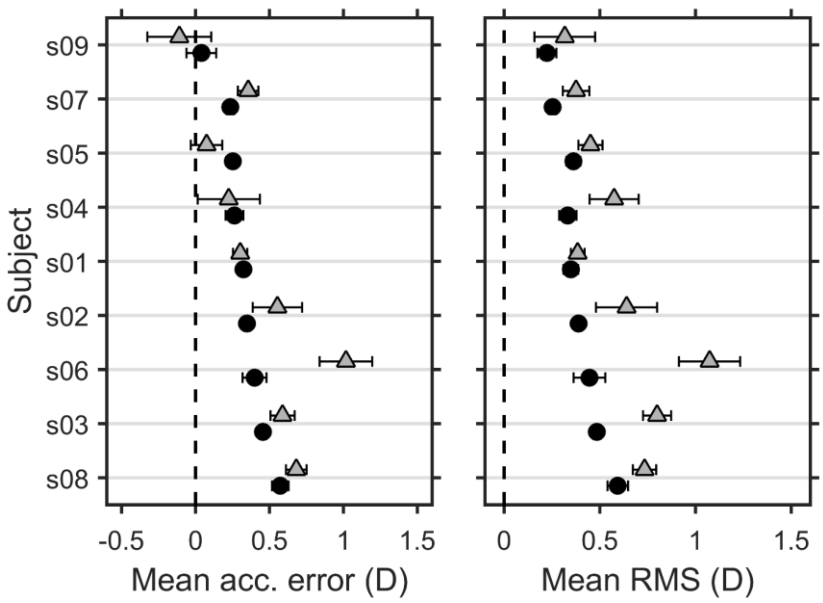

Figure 6.3. Left panel shows the mean accommodative error over the six trials per subject and condition under study. Right panel shows the mean RMS error. Black solid circles show results for the vergence-driven condition, whereas the gray triangles show the results for the blur-driven condition. Subjects are arranged in ascending order of accommodative error obtained in the vergence-driven condition. Error bars represent ±2 standard errors of the mean.

The right panel of the figure shows the mean RMS error of the accommodative error, which is an indicator of the stability of the responses. The mean difference in RMS error between conditions was −0.21±0.15 D, significantly different from zero (p = 0.004). A large RMS error indicates that accommodation fluctuates by a large amount around the mean accommodative error. Conversely, a small value of RMS error indicates that accommodation fluctuates little around the mean accommodative error.

To illustrate responses to the different conditions and to show an example of variability among subjects, left panels in Figure 6.4 shows the same trial for both conditions for the subject who accommodated closest to the stationary stimulus, whereas the right panel shows the same for the subject who accommodated furthest away. There is not much difference between the responses of subject s09 and those from subject s08. Microfluctuations are more evident in subject s09.

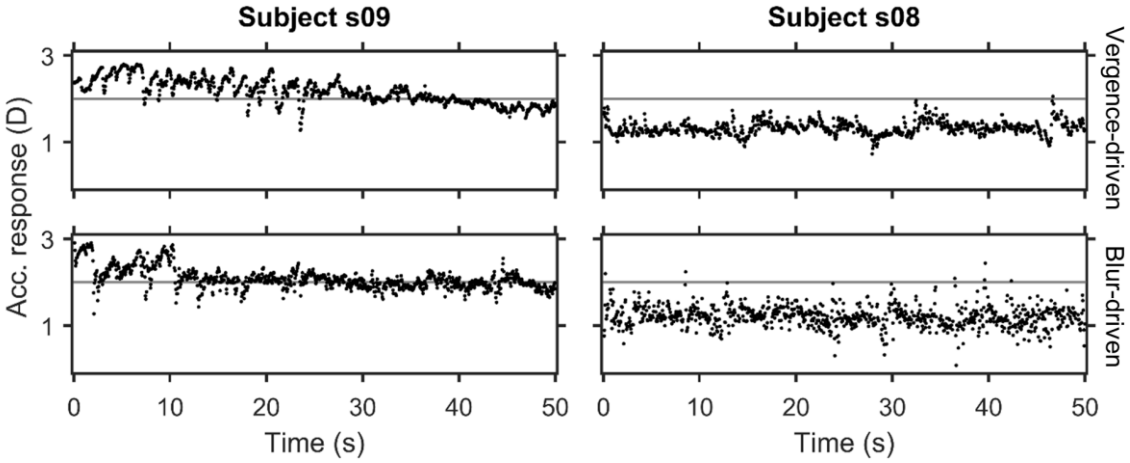

Figure 6.4. Accommodative responses to the stationary stimulus for the subject with the smallest average accommodative error (left column) and for the subject with the greatest accommodative error (right column) in the vergence-driven condition. Upper row shows responses for the vergence-driven condition, whereas lower row shows responses for the blur-driven condition. Gray solid line is the stationary accommodative demand, whether it is real (upper row) or simulated (lower row).

To further explore differences between conditions, Figure 6.5 shows the median frequency spectra over all trials and subjects in each condition. It can be seen that there is less energy (activity) at low frequencies in the vergence-driven condition than in the blur-driven one. The flatter spectra for the vergence-driven condition indicates that, in general, subjects needed to make more effort to accommodate

accurately to stationary targets when there was no light vergence information, and only blur available to the eye.

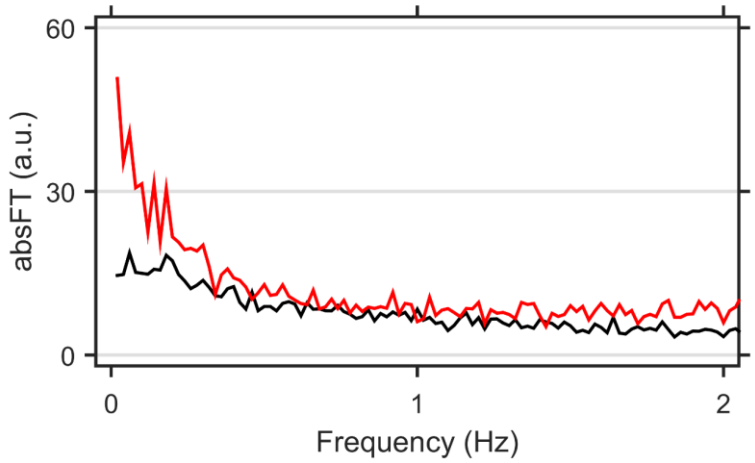

Figure 6.5. Median temporal frequency spectra over all trials and subjects in the vergence-driven condition (black solid line) and the blur-driven condition (red solid line).

6.2.2. Step-change stimulus

The left panel of Figure 6.6 shows the mean gain obtained for each subject and condition. The gain was consistently greater for all subjects for the vergence-driven condition. The mean difference in gain between the vergence-driven and the blur-driven conditions was 0.41±0.20, significantly different from zero (p = 0.004). There was also greater variability in the blur-driven condition, as indicated by the error bars. Subject s04 showed a negative mean gain for the blur-driven condition, since 3 out of 6 responses were in counter-phase with the demand, with gain slightly greater than those that were in phase.

The right panel of Figure 6.6 shows the average latency over the six trials for each subject and condition. The mean difference in latency between the vergence-driven condition and the blur-driven condition was −1.11±0.69, significantly different from zero (p = 0.004).

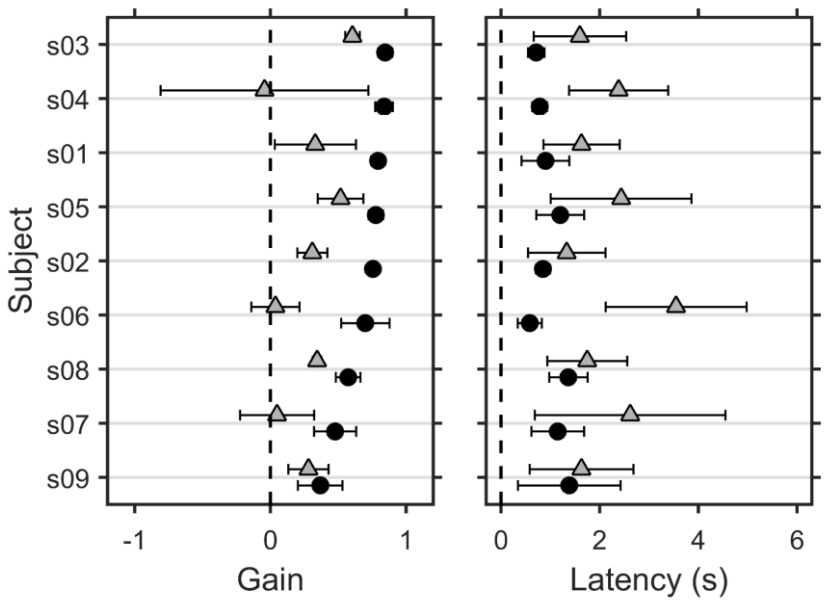

Figure 6.6. The left panel shows the mean gain over the six trials per subject and condition. The right panel shows the mean latency in seconds over the six trials per subject and condition. Subjects are arranged in descending order of gain obtained in the vergence-driven condition. Other details as in Figure 6.3.

Figure 6.7 shows examples of accommodative responses when the stimulus was changing in steps. The subject who showed the greatest gain when light vergence was present (s03) responded very well to the steps pattern, as can be seen in the upper left panel. The response became more erratic when there was no light vergence available, however this subject could still follow the demand. On the other hand, subject s09 showed great difficulty in following the demand in both conditions.

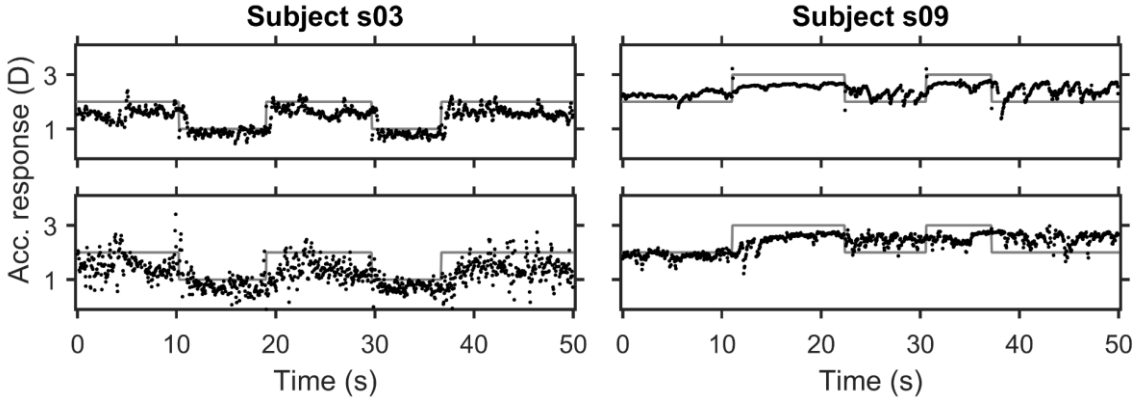

Figure 6.7. Accommodative responses to step-change stimuli for the subject with the greatest gain in the vergence-driven condition (left column) and for the subject with the smallest gain (right column) in the vergence-driven condition. Other details as in Figure 6.4.

Figure 6.8 shows the average peak velocity of accommodation (left panel) or disaccommodation (right panel) over steps and trials for each subject and condition. In general, subjects showed greater velocity in both accommodating and disaccommodating for the vergence-driven condition than for the blur-driven condition, which indicates that they reached the required level of response faster. However, the great error bars shown in some subjects showed the large variability in velocity among steps and trials.

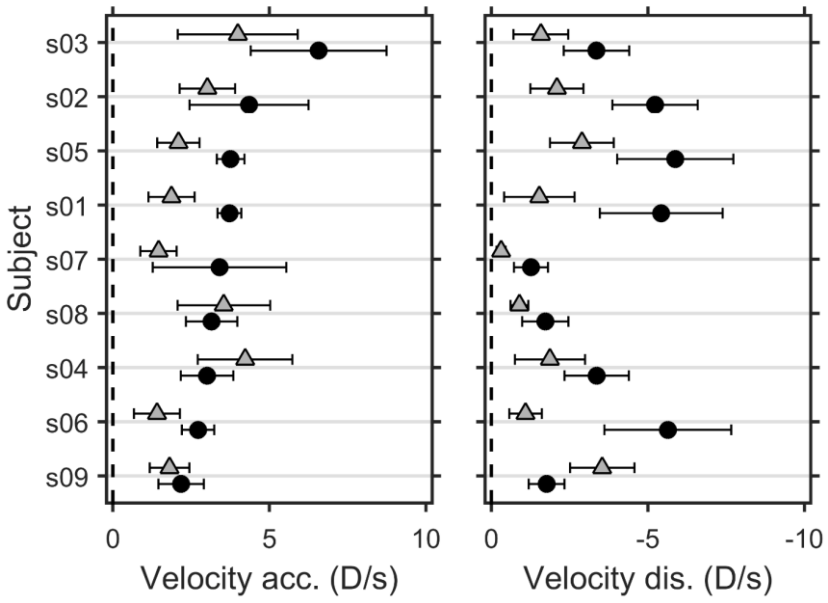

Figure 6.8. The left panel shows the mean velocity of accommodation over the step changes in the six trials per subject and condition under study. The right panel shows the same but for disaccommodation. Subjects are arranged in descending order of velocity of accommodation obtained in the vergence-driven condition. Other details as in Figure 6.2.

In 7 out of 9 subjects, mean peak velocity of accommodation was greater in the vergence-driven condition. In 8 out of 9 subject, peak velocity of dis-accommodation is greater in the vergence-driven condition.

Figure 6.9 shows the changes over time in the proportion of responses in the correct direction after the step changes in demand. In the vergence-driven condition, subjects generally reached values close to 100 % after less than one second, whereas in the blur-driven condition the majority of the subjects showed smaller proportions of responding correctly, even after 5 seconds. Four out of 9 subjects showed proportions close to 50 %, almost independent of the time.

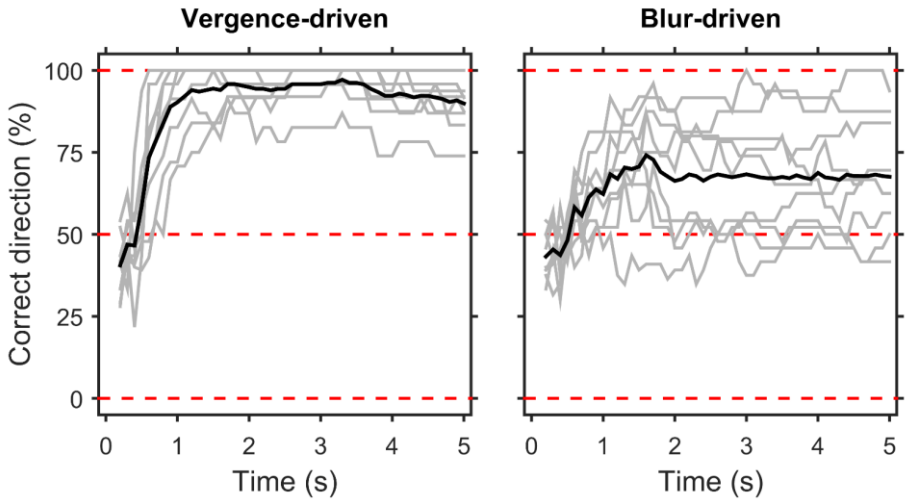

Figure 6.9. Percentage of responses in the correct direction with respect to the length of the time passed after a step-change in demand happened. The left panel shows the vergence-driven condition, whereas the right panel shows the results for the blur-driven condition. Gray lines show the results for each subject and black thick line shows the mean over subjects. Red dashed lines indicate percentages of 0, 50, and 100.

6.2.3. Sinusoidal stimulus

Figure 6.10 shows the mean gain over the six trials obtained for every subject, and condition at temporal frequencies of 0.05, 0.1, 0.2, and 0.4 Hz, and also the mean gain obtained in the preliminary trials at 0.2 Hz (see Section 3.2) for comparison.

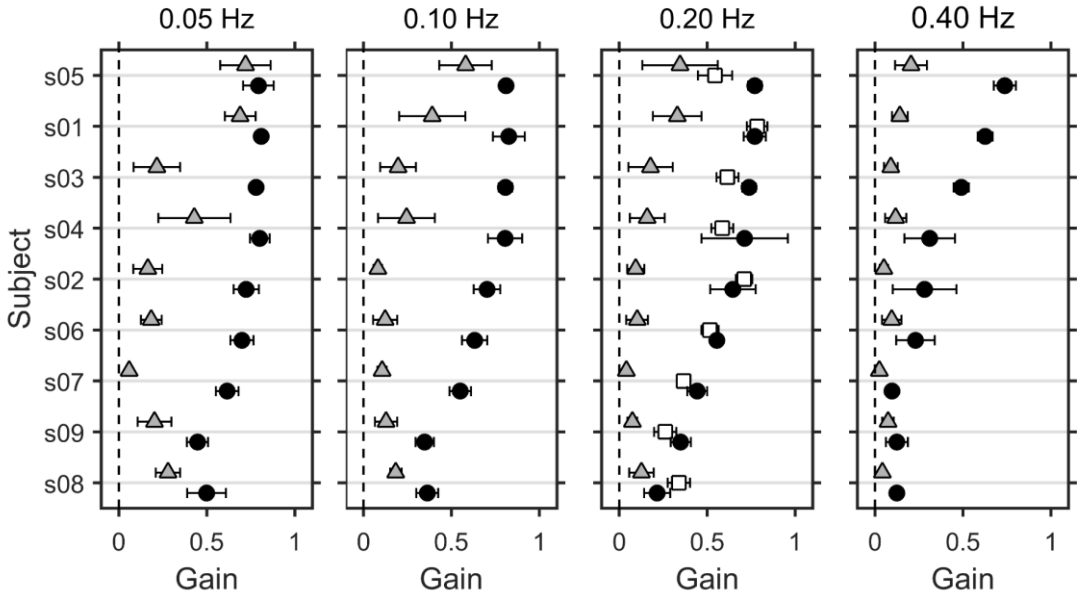

Figure 6.10. Mean gain over the six trials per subject and condition under study. Each panel shows the results for a different frequency of the sinusoidal. From left to right: 0.05, 0.1, 0.2, and 0.4 Hz. Subjects are arranged in descending order of gain obtained for 0.2 Hz in the vergence-driven condition. Empty squares in the 0.20 Hz panel are the mean gain obtained in the preliminary experiment described in Section 3.2. Other details as in Figure 6.2.

At 0.05 Hz, subjects s05 and s01 showed almost no differences in mean gain between conditions. The remaining 7 subjects showed systematically greater mean gain when light vergence was present. The difference between conditions became greater for subjects s05 and s01 when the temporal frequency increased. The mean difference in gain between conditions was 0.36±0.17, 0.43±0.15, 0.44±0.13, and 0.19±0.23 for 0.05, 0.10, 0.20, and 0.40 Hz, respectively. The results between conditions were significantly different for all temporal frequencies (all p = 0.039). When the temporal frequency of the sinusoidal increased, the mean gain in the blur-driven condition decreased more rapidly than the gain obtained in the vergence-driven condition. At 0.4 Hz, only one subject (s05) could follow the sinusoidal change in demand in the blur-driven condition, although with small gain. Six subjects could follow the changes in the vergence-driven conditions, three of them remarkably well.

Figure 6.11 shows responses obtained when the stimulus was changing demand sinusoidally. Subject s05 always was able to properly follow the sinusoidal changes in demand, except for the sinusoidal with the greatest frequency in the blur-driven condition. Even in this condition, this subject could follow the demand at times (see left lower panel). In contrast, subject s08 could follow changes in demand up to 0.2 Hz, but with little gain.

Figure 6.12 shows the frequency spectra for the vergence-driven condition. The peaks show that the activity was concentrated at the temporal frequency of the sinusoidal. The peak became smaller in magnitude as the temporal frequency of the sinusoidal increased, showing that the average response is reduced as the sinusoidal changes in demand happened faster. In the vergence-driven condition, the peaks were absolute maxima, whereas in the blur-driven condition, the peaks were smaller and were local maxima, except for 0.05 Hz.

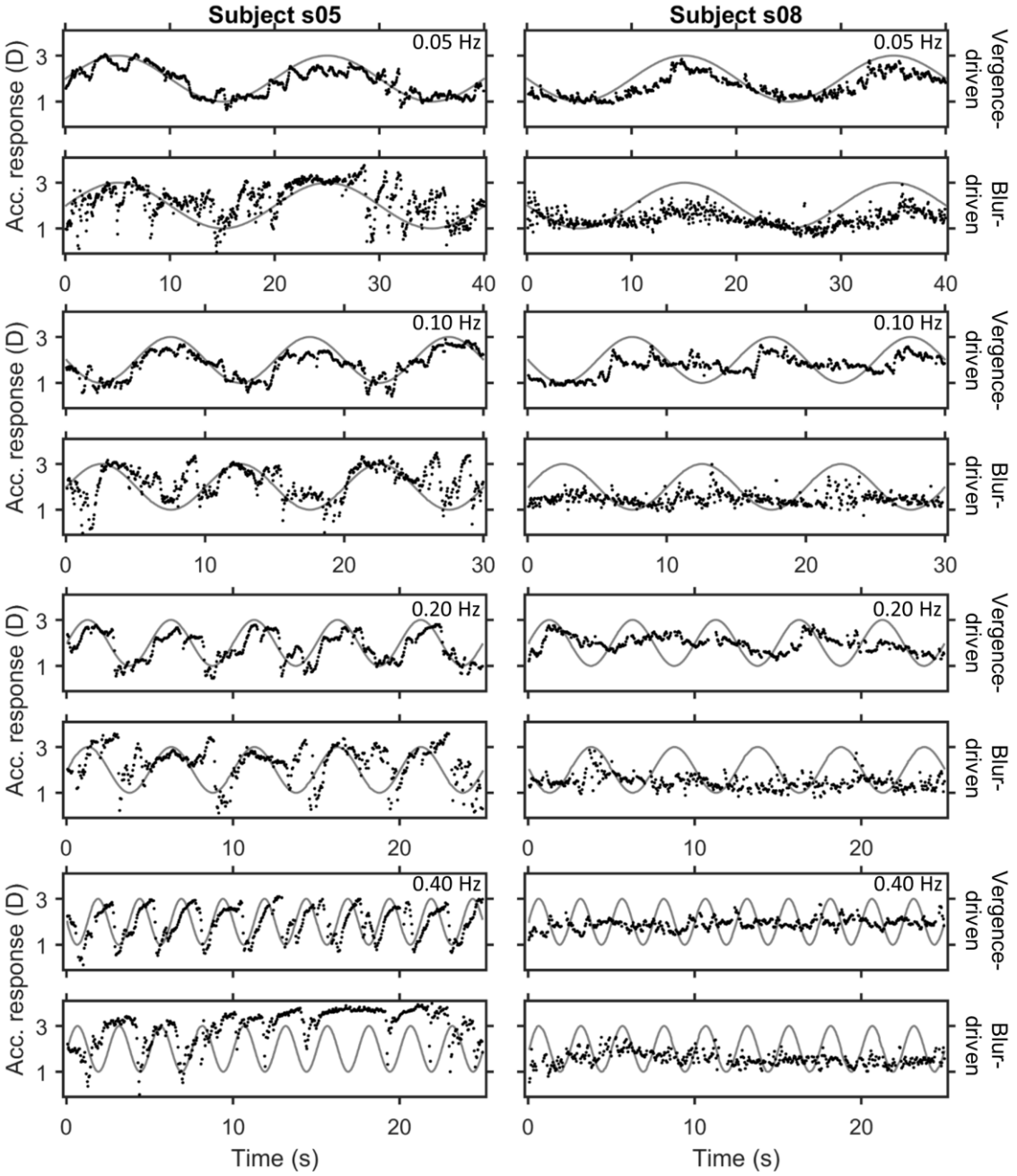

Figure 6.11. Accommodative responses to sinusoidal stimuli for the subject with the greatest gain in the 0.2 Hz sinusoidal in the vergence-driven condition (left column) and for the subject with the smallest gain (right column). Every two rows the frequency of the sinusoidal was different, from top to bottom: 0.05, 0.1, 0.2, and 0.4 Hz. Note that the scale of the x-axis is different, since the duration of the trials depended on the frequency of the sinusoidal. Other details as in Figure 6.4.

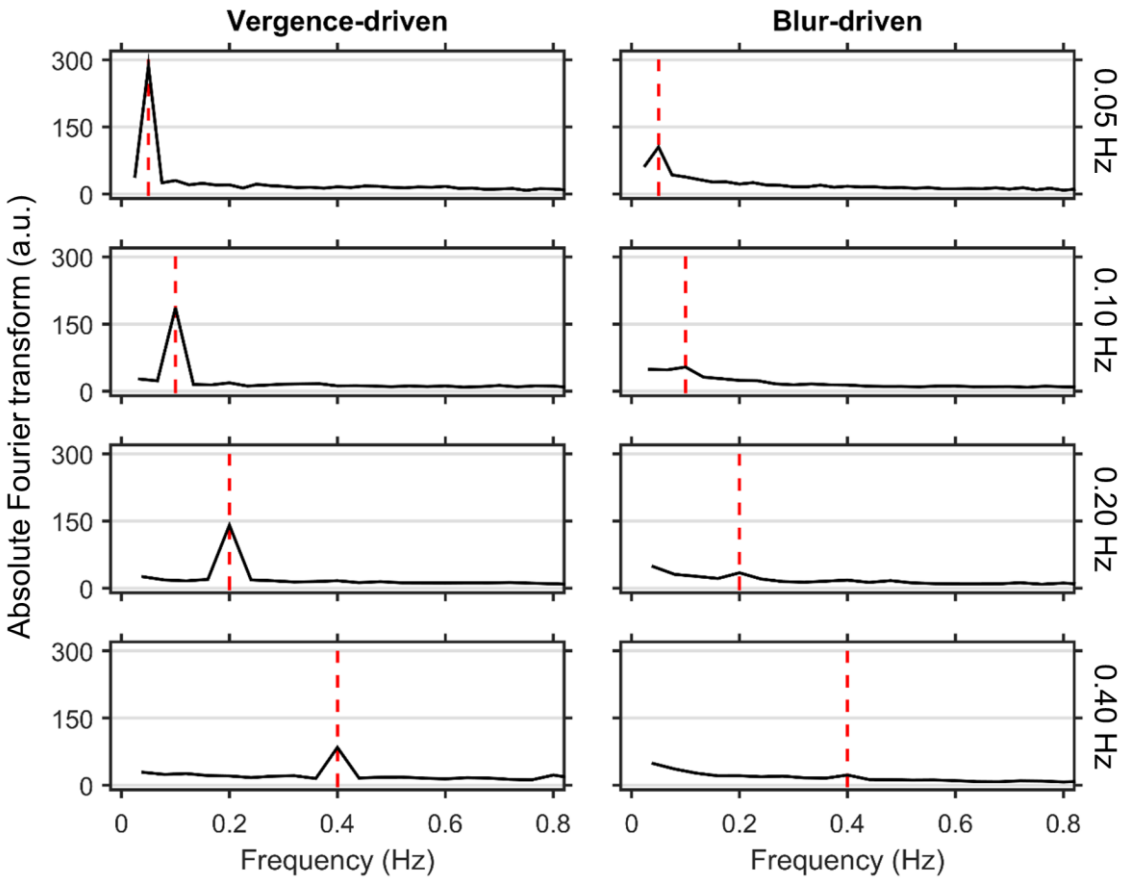

Figure 6.12. Median temporal frequency spectra of the responses in each condition. Left column represents the vergence-driven condition, whereas the right column represents the blur-driven one. Each row corresponds to a different temporal frequency. Red dashed lines indicate the frequency of each sinusoidal accommodative demand.

6.3. Discussion

The results obtained in this experiment show that the accommodative system goes beyond trial and error to minimize retinal blur and thus maximize retinal contrast. In general, accommodation functions better when changes in light vergence are present.

This experiment shares similarities with that performed by Phillips and Stark (1977). However, nowadays thanks to the AO technology and high-speed aberrometry, it is possible to correct the subjects' aberrations and measure the accommodative response in real time in a precise manner. The results obtained here for the blur-driven condition are in agreement with those obtained by Phillips and Stark. They concluded that blur alone activated and controlled accommodation. Yet,

as it was made evident in the present experiments, subjects consistently accommodate better when light vergence is available to them.

In the steady-state experiment, except for subject s06, there were practically no differences between the two conditions, meaning that for stationary targets subjects can generally use both trial and error and light vergence to keep the target clear. A larger RMS error indicated that accommodation fluctuates more around the mean accommodative error. Generally, when light vergence was not present, subjects showed less stable accommodation than when it is present.

In the step-change experiment, subjects showed consistently greater gain and smaller latency in the vergence-driven condition than in the blur-driven condition. There was also greater variability in the blur-vergence condition, as indicated by the error bars, suggesting a more erratic behaviour in the responses when no light vergence is present. The peak velocity showed by the subject was also generally greater for the vergence-driven condition, both for accommodation and disaccommodation, which mean that subjects normally accommodated faster when light vergence was present. Light vergence also helped subjects to discern the correct direction in which to accommodate, as showed in Figure 6.9.

In the sinusoidal experiment, subjects showed greater gain in the vergence-driven condition. As the frequency of the sinusoidal movement increased, the gain generally decreased, but it did it more rapidly for the blur-driven condition.

In the blur-driven condition, the results showed weaker responses consistently in every aspect of the accommodation analysed. These results, together with those obtained in Chapter 5, show unambiguously the major role played by light vergence, since when it is present, subjects seem to accommodate better in the majority of the trials. According to the results obtained here, it seems that light vergence is used by the accommodative system in concert with trial and error trial and error to minimize retinal blur and maximize contrast.

7. General conclusions and future work

7.1. General conclusions

The goal of this thesis was to test different theories about the mechanism of accommodation. Particularly, whether accommodation is driven by changes in light vergence, by the differences in shape of retinal blur due to optical imperfections of the eye, or by a trial-and-error strategy, which aims to minimize retinal blur and maximize retinal contrast.

Do differences in the shape of the retinal blur caused by monochromatic aberrations help accommodation? As shown in Chapter 4 of the present thesis, subjects' responses to the changes in blur did not follow the sinusoidal change in blur without feedback. From here and previous studies (Chen et al. 2006; Chin et al. 2009a, 2009b; Marin-Franch et al. 2016; Bernal-Molina et al. 2017), it can be concluded that the shape of the blur produced by eye imperfections in the retinal image does not drive accommodation. In other words, the different PSFs generated by monochromatic even-order aberrations (signed cues), such as astigmatism or spherical aberration do not drive human accommodation without feedback.

Do changes in light vergence drive accommodation when feedback is absent? In Chapter 5, the majority of the subjects followed the sinusoidal change in light vergence optimally, whereas none of them followed the sinusoidal change in target blur. Thus, the conclusion is that subjects do accommodate properly when light vergence is present without feedback, however they do not accommodate when only defocus target blur is present, without feedback from accommodation. This result showed that light vergence is used to drive accommodation when feedback is not available to the eye.

Does the eye accommodate thanks to changes in light vergence or to changes in blur? In Chapter 6, subjects systematically showed equal or better accommodative responses in every experiment when light vergence was available to them. These results represent further proof that light vergence is an important cue that drives accommodation. Yet some subjects could accommodate when no light vergence was present and the accommodative loop was closed, but their accommodation was generally weaker than when light vergence was present.

The key result that light vergence is a driving force for accommodation has been shown in this thesis. Light vergence is thus an important cue used by the eye, presumably in concert with all other binocular and monocular cues and mechanisms, including trial and error to reduce blur and maximize contrast, and chromatic aberration. The human eye does not necessarily require feedback to accommodate, as shown in Chapter 5; however, it does need light vergence to accommodate correctly.

7.2. Generalization and implications of the results

All subjects tested here could accommodate to the stringent conditions imposed. Accommodation was assessed monocularly, without monocular depth cues and without chromatic cues. In addition, in each of the experiments more cues were removed, depending on the conditions, such as monochromatic aberrations, light vergence, or feedback from accommodation. It can be estimated that approximately 65% to 85% of subjects can accommodate to changes in light vergence in monochromatic light (Del Águila-Carrasco et al. 2017). In this thesis, 56% of the subjects tested could accommodate in monochromatic light.

However, it is reasonable to speculate that in white light, some of these subjects also use light vergence to compute differences in the amount of defocus between long-, medium-, and short-wavelength-sensitive cone photoreceptors. Chromatic aberration does help the eye to accommodate, so perhaps it does so by detecting the differences in light vergence for each type of cone photoreceptor.

7.2.1. Implications for emmetropization and myopia

In addition to the implications of these results in the accommodation process *per se*, there may be consequences for the emmetropization, which is the long-term focusing process of the eye (Wildsoet, 1997; Seidemann & Schaeffel, 2002; Mutti et al. 2009). The emmetropization process is the coordinated growth and development of the optical components of the eye (cornea and lens) and its axial length, with the goal of focusing the incoming light from targets at infinity on the retina (emmetropia). If emmetropization fails, it can lead to myopia. Accommodation and emmetropization may share a similar feedback loop to focus the image of an object on the retina. In emmetropization, ocular adjustments of axial length are made for this purpose, evidently at a much slower pace than in accommodation.

In the last decades, myopia prevalence has increased drastically in developing countries (Williams et al. 2015; Holden et al. 2016; Guo et al. 2016; Jorge et al. 2016). This fact seems to be related to the dramatic increase in the use of near vision among young people, whose eyes are still growing. Thus, it seems reasonable to link the over-use of accommodation to the development of myopia. Myopia is a significant public health problem (Seet et al. 2001) and a leading cause of blindness from diseases secondary to the development of high amounts of myopia. Research has been carried out on the eyes of different animals, such as fishes, chicks, kestrels, squirrels, rabbits, guinea pigs, tree shrews, cats, marmosets, and monkeys. Those research works showed that the vertebrate eye compensates for positive and negative light vergence by altering its axial length (Diether & Wildsoet, 2005; Hammond et al. 2013). Negative light vergence produced by placing negative lenses in front of the animals' eyes increases the rate of elongation of the eye by thinning the choroid of chicks, while myopic defocus from positive lenses slows the rate of elongation and thickens the choroid. The findings in this thesis suggest that the eye must have an internal mechanism to detect or infer the light vergence of light, in addition to the role played by blur, contrast, spatial frequency, and color signals from chromatic aberration.

7.3. Theoretical models for light vergence detection

The way in which the eye can extract the sign information from light vergence is still unknown. There are some recent theoretical models that have tried to shed light onto this matter. One of those models is based on the antenna-like properties of cone photoreceptors (Toraldo di Francia, 1949) and the possibility of differentiating between convergent and divergent light by scattering and internal reflections taking place in these cone photoreceptors (Vohnsen, 2014). Another model is based on the use of landmarks from shadows cast by retinal blood vessels in the macula (Lopez-Gil et al. 2016).

7.4. Future work

Despite all the work done to elucidate whether even-order monochromatic aberrations help the eye to know in which direction to accommodate, the utility of these signed cues still remains unclear. Nonetheless the effect is likely subtle. Chapter 4 of the present thesis showed that accommodation could not be driven by the shape of blur produced by defocus together with some of these even-order

aberrations. However, there was no feedback from accommodation in the experiment, since the accommodative loop was opened with a small pinhole. An experiment, similar to the one described in Chapter 6, can be performed to study if these aberrations help the eye to decide which way to accommodate. There would be two blur-driven conditions: one similar to that in Chapter 6, and another condition where blur caused by certain even-order aberrations is added to the defocus target blur. Then, the two conditions would be compared against each other to see if accommodation is better when the blur from the even-order aberrations is present in the simulated target blur.

To determine with precision how many subjects use particular aberrations to accommodate better, greater sample sizes need to be tested in experiments similar to those already carried out (Chin et al. 2009a, 2009b; Bernal-Molina et al. 2017).

In Chapter 6 of the present thesis, subjects did accommodate in the blur-driven condition, although worse than in the vergence-driven condition. It would be interesting also to test if subjects can accommodate when the loop is closed in target contrast alone, not defocus blur. Perhaps eyes accommodate when the feedback loop is closed on target contrast alone, not defocus blur.

A most interesting experiment would be one in which light vergence could be changed without changing blur of the image on the retina. If the eye were able to accommodate in such an experiment, it would be certain proof that light vergence is the sufficient cue for driving accommodation. Nonetheless, this seems extremely hard to accomplish, since whenever there are changes in the vergence of the light, the target will suffer changes in blur accordingly. One approach that could be examined is pre-processing the target in such a way that is designed to counteract the blurring caused by the changes in light vergence, in a similar way as in Huang et al. (2014). The goal would be to pre-process the target so that the changes in light vergence introduced by the AO system would not cause changes in the blur of the target.

Appendix A. Assessment of the AO corrections

For the four experiments described in Chapter 5 and Chapter 6, it is critical that the AO system is able to correct the aberrations of the eye and induce the required levels of spherical defocus optimally during all trials and conditions with accuracy. To assess the precision of the AO corrections, the astigmatism and HOAs RMS error was computed for a 4-mm pupil during all the trials, and the median of the six trials among conditions calculated. The median absolute deviation was also calculated, since it is a robust measure of dispersion, more resilient to outliers than the standard deviation (Hoaglin et al. 1983). To assess the precision of the desired spherical defocus on the retina at each moment provided by the mirror, a sinusoidal function with a temporal frequency of 0.2 Hz was subtracted from the accommodative error measured with the wavefront sensor. Then, the median of this subtraction (vergence-driven condition), and the median of the accommodative errors measured with the sensor (blur-driven condition) were calculated for all trials. Additionally, the median absolute deviation was computed.

AO corrections in accommodation without feedback

Figure A1 shows the median astigmatism plus HOAs RMS throughout the six trials per subject and condition. The error bars represent the median absolute deviation. The correction of astigmatism and HOAs was optimal, as shown by the fact that the astigmatism and HOAs RMS was never greater than 0.1 μm. Looking at the trials individually, astigmatism and HOAs RMS were around or below 0.1 μm for all but two trials. For the other two, RMS error was between 0.1 and 0.2 μm.

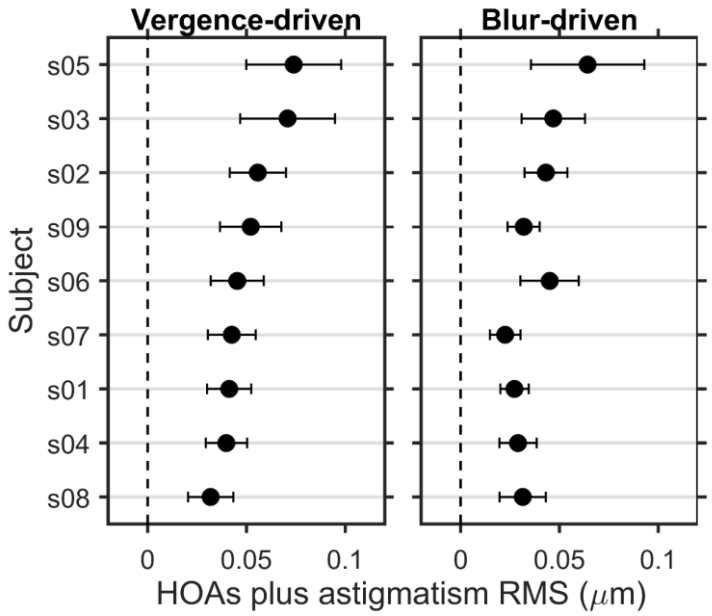

Figure A1. Median HOAs and astigmatism RMS during the six trials per subject and condition under study. Each panel represents a different condition. Subjects are arranged in descendent order of RMS obtained in the vergence-driven condition. Error bars represent the median absolute deviation.

Regarding the accuracy of providing the required level of defocus at the retina, Figure A2 shows the median of the error in the defocus induced by the deformable mirror throughout the six trials per subject and condition. The error bars represent the median absolute deviation. This error was the difference between the accommodative error measured by the Shack-Hartmann sensor and the level of defocus that needed to be provided at the retina at each moment, depending on the experimental condition. As it can be seen from Figure A2, the errors were quite small. The median values of the errors were always lower than 0.03 D, and the median absolute deviation was always below 0.09 D.

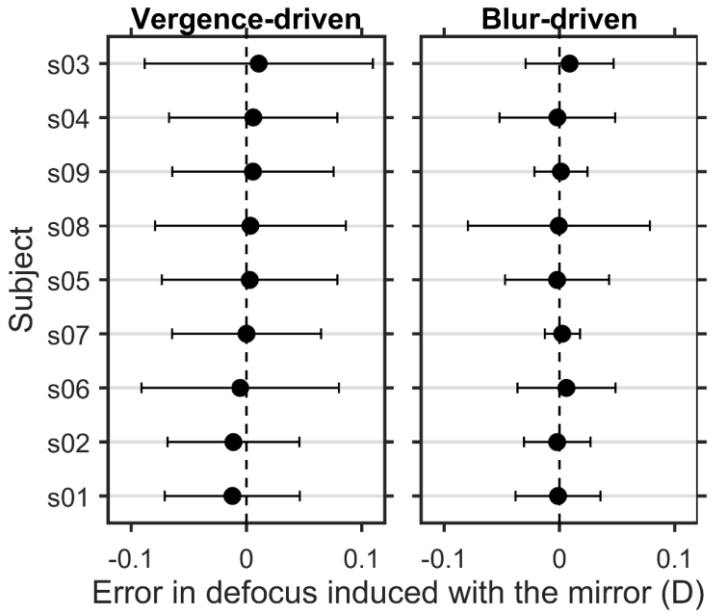

Figure A2. Median of the error in the defocus provided at the retina during the six trials per subject and condition under study. Each panel represents a different condition. Other details as in Figure A1.

Curd et al. (2013) showed that for pulse changes in vergence with a duration of 100 ms or less, the accommodation response was very small in magnitude or even absent. The subjects' responses to these fast pulses were about 0.2 D for both 1 and 2 D of accommodative demand. The errors introduced by the deformable mirror were more than 10 and 20 times smaller than the pulses described, and the correction lag was only 50 ms (frequency of measurements was 20 Hz). Thus, it is highly unlikely that these small errors introduced by the deformable mirror when trying to provide the required amount of defocus at the retina could elicit any response, neither could they provide an effective cue for accommodation.

AO corrections in accommodation with feedback

Figure A3 shows the median astigmatism and HOAs RMS for a 4-mm pupil throughout the six trials per subject and condition, both for the stationary and step-change stimuli sub-experiments. The error bars represent the median absolute deviation.

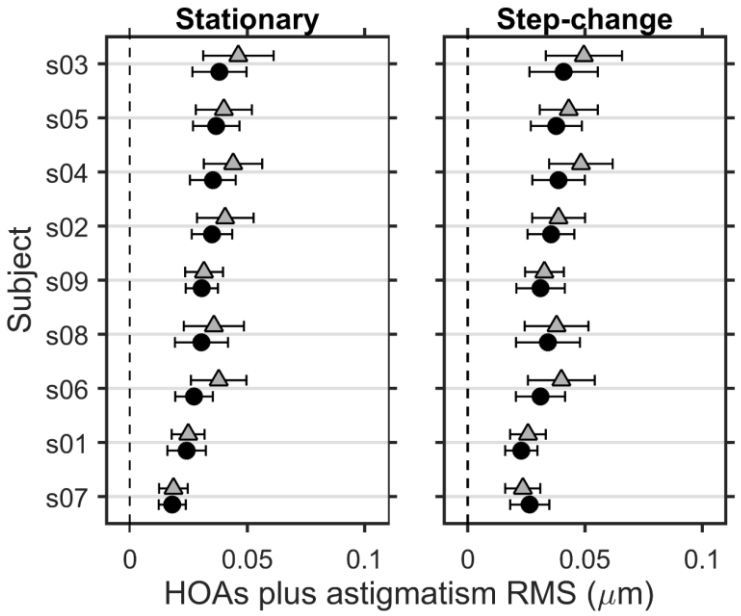

Figure A3. Median HOAs and astigmatism RMS during the six trials per subject and condition under study. Left panel shows the results for the stationary stimulus, whereas right panel shows the results for the step-change stimulus. Black circles show the results for the vergence-driven condition, whereas gray triangles show the results for the blur-driven condition. Subjects are arranged in descendent order of RMS obtained in the vergence-driven condition with the stationary stimulus. Error bars represent the median absolute deviation.

In these two experiments, the correction of aberration was quite precise, being the HOAs and astigmatism RMS lower than 0.07 μm in all trials. Figure A4 shows the HOAs and astigmatism RMS for the sinusoidal stimuli. In this experiment, the correction of aberrations was also very precise, only getting slightly worse at the maximum frequency of the sinusoidal (0.40 Hz). RMS was also greater than 0.1 μm in 2 out of 432 trials.

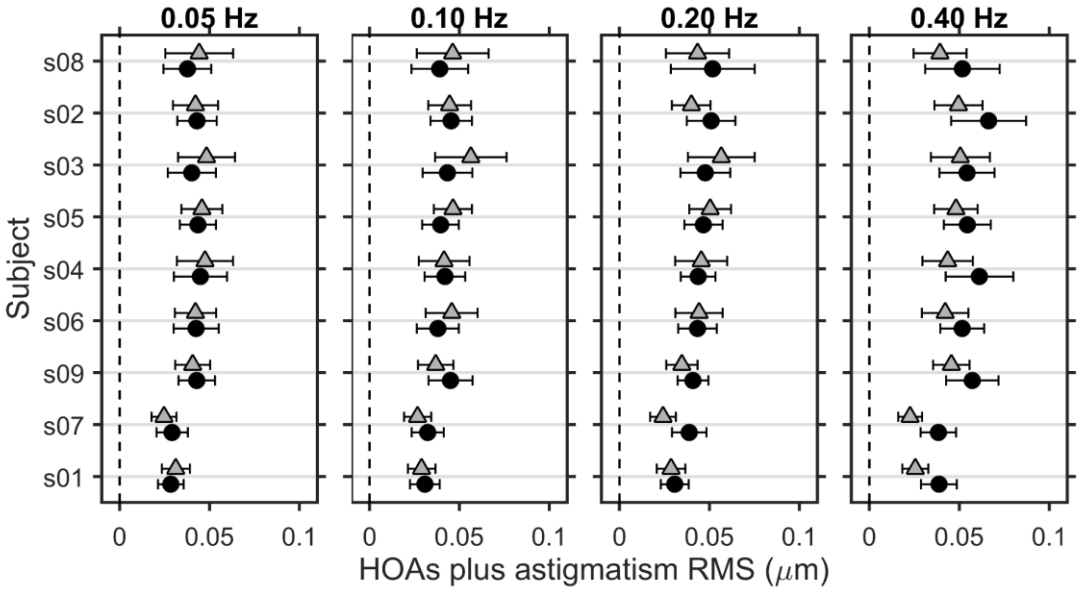

Figure A4. Median HOAs and astigmatism RMS during the six trials per subject and condition under study for the sinusoidal stimuli. Each panel shows the results for a different temporal frequency of the sinusoidal. From left to right: 0.05, 0.10, 0.20, and 0.40 Hz. Subjects are arranged in descendent order of RMS obtained in the vergence-driven condition, when the frequency was 0.20 Hz. Error bars represent the median absolute deviation. Other details as in Figure A3.

Another essential aspect was to ensure that the AO system provided the required level of defocus over time in each experimental condition. Figure A5 shows the median of the error in the defocus induced by the deformable mirror with respect to the desired one throughout the six trials per subject and condition. As can be seen, the error was very little for all subjects and conditions, being always smaller than 0.001 D for all trials. The median absolute deviation was always smaller than 0.05 D.

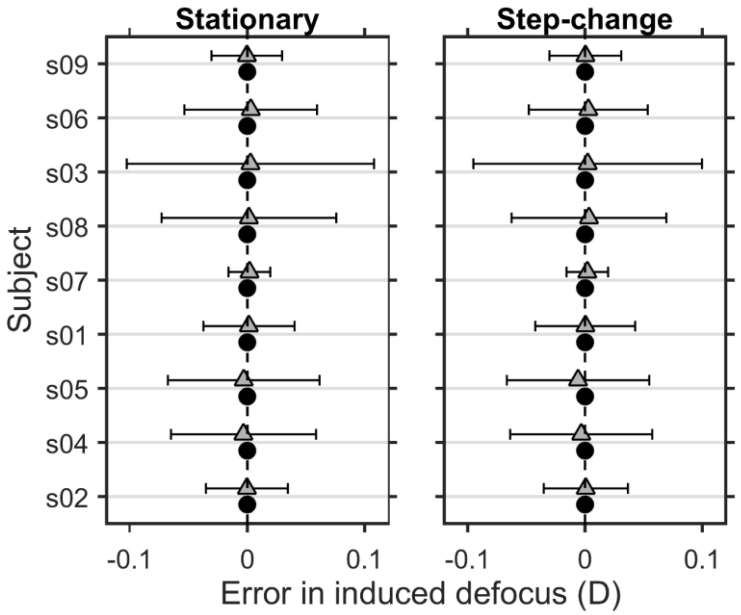

Figure A5. Median of the error in the defocus provided with respect to the one required during the six trials per subject and condition under study. Left panel shows the results for the stationary stimulus, whereas right panel shows the results for the step-change stimulus. Other details as in Figure A3.

Figure A6 shows the median of the error in the defocus induced by the deformable mirror with respect to the required one throughout the six trials per subject and condition, when the changes in the stimulus were sinusoidal. For the vergence-driven condition, the errors were also smaller than 0.001 D here. For the blur-driven condition, and for temporal frequencies up to and including 0.1 Hz, the behaviour is almost as good as the one showed when there were no changes (stationary stimulus), or when there were step-changes. For greater frequencies, the error was slightly greater, but never more than 0.01 D. The median absolute deviation was always lower than 0.05 D.

As explained in previously, the errors in defocus introduced by the AO system are not likely to elicit the accommodation response of the subjects or provide any effective cue for accommodation (Curd et al. 2013).

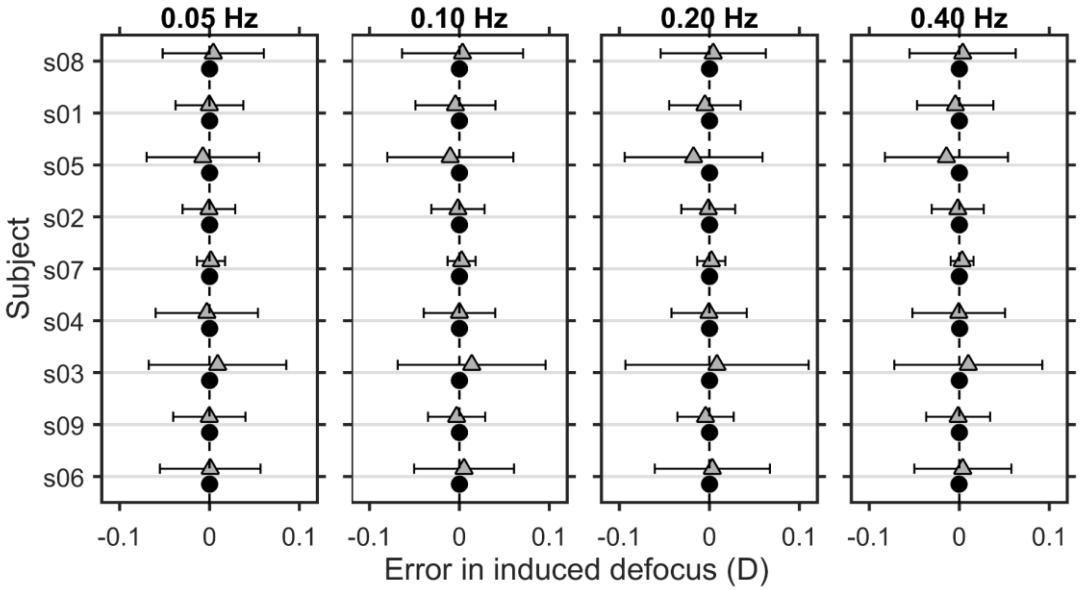

Figure A6. Median of the error in the defocus provided with respect to the one required during the six trials per subject and condition under study. Left panel shows the results for the stationary stimulus, whereas right panel shows the results for the step-change stimulus. Other details as in Figure A3.

Bibliography

Atchison, D. A., Charman, W. N. & Woods, R. L. (1997). Subjective depth-of-focus of the eye. *Optometry and Vision Science* **74**, 511–520.

Atchison, D. A., Collins, M. J., Wildsoet, C. F., Christensen, J. & Waterworth, M. D. (1995). Measurement of monochromatic ocular aberrations of human eyes as a function of accommodation by the Howland aberroscope technique. *Vision Research*, **35**, 313–323.

Babcock, H. W. (1953). The possibility of compensating astronomical seeing. *Publications of the Astronomical Society of the Pacific* **65**, 229–236.

Bedggood, P., Daaboul, M., Ashman, R., Smith, G. & Metha, A. (2008). Characteristics of the human isoplanatic patch and implications for adaptive optics retinal imaging. *Journal of Biomedical Optics* **13**, 024008.

Benard, Y., Lopez-Gil, N. & Legras, R. (2011). Optimizing the subjective depth-of-focus with combinations of fourth- and sixth-order spherical aberration. *Vision Research* **51**, 2471–2477.

Benjamin, W. J. (2006). Borish's Clinical Refraction. Philadelphia: W. B. Saunders Company.

Bernal-Molina, P., Marín-Franch, I., Del Águila-Carrasco, A. J., Esteve-Taboada, J. J., López-Gil, N., Kruger, P. B. & Montés-Micó, R. (2017). Human eyes do not need monochromatic aberrations for dynamic accommodation. *Ophthalmic and Physiological Optics*. In press.

Bernal-Molina, P., Montés-Micó, R., Legras, R. & López-Gil, N. (2014). Depth-of-field of the accommodating eye. *Optometry and Vision Science* **91**, 1208–1214.

Bracewell, R. N. (2000). The Fourier Transform and Its Applications. New York: McGraw Hill.

Cabello, J. (1945). Las causas de la miopía nocturna. *Anales de Física y Química* **41**, 439–448.

Campbell, F. W. (1957). The Depth of Field of the Human Eye. *Optica Acta* **4**, 157–164.

Campbell, F. W. & Westheimer, G. (1959). Factors influencing accommodation responses of the human eye. *Journal of the Optical Society of America* **49**, 568–571.

Charman, W. N. & Heron, G. (1988). Fluctuations in accommodation: a review. *Ophthalmic and Physiological Optics* **8**, 153–164.

Charman, W. N. & Heron, G. (2015). Microfluctuations in accommodation: an update on their characteristics and possible role. *Ophthalmic and Physiological Optics* **35**, 476–499.

Chen, L., Kruger, P. B., Hofer, H., Singer, B. & Williams, D. R. (2006). Accommodation with higher-order monochromatic aberrations corrected with adaptive optics. *Journal of the Optical Society of America A* **23**, 1–8.

Chen, Y., Jin, W., Zheng, Z., Zhang, C., Lin, H., Drobe, B., Bao, J. & Chen, H. (2017). Comparison of three monocular methods for measuring accommodative stimulus-response curves. *Clinical and Experimental Optometry* **100**, 155–161.

Cheng, H., Barnett, J. K., Vilupuru, A. S., Marsack, J. D., Kasthurirangan, S., Applegate, R. A. & Roorda, A. (2004). A population study on changes in wave aberrations with accomodation. *Journal of Vision* **4**, 272–280.

Chin, S. S., Hampson, K. M. & Mallen, E. A. H. (2009a). Effect of correction of ocular aberration dynamics on the accommodation response to a sinusoidally moving stimulus. *Optics Letters* **34**, 3274–3276.

Chin, S. S., Hampson, K. M. & Mallen, E. A. H. (2009b). Role of ocular aberrations in dynamic accommodation control. *Clinical and Experimental Optometry* **92**, 227–237.

Cowley, J. M. (1995). Diffraction Physics. Amsterdam: North Holland.

Curd, A. P., Hampson, K. M. & Mallen, E. A. H. (2013). Processing blur of conflicting stimuli during the latency and onset of accommodation. *Vision Research* **92**, 75–84.

Day, M., Gray, L. S., Seidel, D. & Strang, N. C. (2009). The relationship between object spatial profile and accommodation microfluctuations in emmetropes and myopes. *Journal of Vision* **9**, 1–13.

Del Águila-Carrasco, A. J., Marín-Franch, I., Bernal-Molina, P., Esteve-Taboada, J. J., Kruger, P. B., Montés-Micó, R. & López-Gil, N. (2017). Accommodation responds

to optical vergence and not defocus blur alone. *Investigative Ophthalmology and Visual Science* **58**, 1758–1763.

Delori, F. C., Webb, R. H. & Sliney, D. H. (2007). Maximum permissible exposures for ocular safety (ANSI 2000), with emphasis on ophthalmic devices. *Journal of the Optical Society of America A* **24**, 1250–1265.

Denieul, P. (1982). Effects of stimulus vergence on mean accommodation response, microfluctuations of accommodation and optical quality of the human eye. *Vision Research* **22**, 561–569.

Diether, S. & Wildsoet, C. F. (2005). Stimulus requirements for the decoding of myopic and hyperopic defocus under single and competing defocus conditions in the chicken. *Investigative Ophthalmology and Visual Science* **46**, 2242–2252.

Fernández, E. J. & Artal, P. (2005). Study on the effects of monochromatic aberrations in the accommodation response by using adaptive optics. *Journal of the Optical Society of America A* **22**, 1732–1738.

Fincham, E. F. (1951). The accommodation reflex and its stimulus. *The British Journal of Ophthalmology* **35**, 381–393.

Flitcroft, D. I. (1990). A neural and computational model for the chromatic control of accommodation. *Visual Neuroscience* **5**, 547–555.

Guo, L., Yang, J., Mai, J., Du, X., Guo, Y., Li, P., Yue, Y., Tang, D., Lu, C. & Zhang, W. H. (2016). Prevalence and associated factors of myopia among primary and middle school-aged students: a school-based study in Guangzhou. *Eye (London)* **30**, 796–804.

Hammond, D. S., Wallman, J. & Wildsoet, C. F. (2013). Dynamics of active emmetropisation in young chicks--influence of sign and magnitude of imposed defocus. *Ophthalmic and Physiological Optics* **33**, 215–226.

Hampson, K. M., Chin, S. S. & Mallen, E. A. (2009). Dual wavefront sensing channel monocular adaptive optics system for accommodation studies. *Optics Express* **17**, 18229–18240.

Hampson, K. M., Chin, S. S. & Mallen, E. A. H. (2010). Effect of temporal location of correction of monochromatic aberrations on the dynamic accommodation response. *Biomedical Optics Express* **1**, 879–894.

Heath, G. G. (1956). The influence of visual acuity on accommodative responses of the eye. *American Journal of Optometry and Archives of American Academy of Optometry* **33**, 513–524.

Hecht, E. (1987). Optics. Reading, MA: Addison-Wesley.

Hoaglin, D. C., Mosteller, F. & Tukey, J. W. (1983). Understanding robust and exploratory data analysis. New York: John Wiley & Sons.

Holden, B. A., Fricke, T. R., Wilson, D. A., Jong, M., Naidoo, K. S., Sankaridurg, P., Wong, T. Y., Naduvilath, T. J. & Resnikoff, S. (2016). Global Prevalence of Myopia and High Myopia and Temporal Trends from 2000 through 2050. *Ophthalmology* **123**, 1036–1042.

Huang, J., Barreto, A., Ren, P. & Adjouadi, M. (2014). Personalised and dynamic image precompensation for computer users with ocular aberrations. *Behaviour and Information Technology* **33**, 892–904.

Iskander, D. R., Collins, M. J., Morelande, M. R. & Zhu, M. (2004). Analyzing the dynamic wavefront aberrations in the human eye. *IEEE Transactions on Biomedical Engineering* **51**, 1969–1980.

Ittelson, W. H. & Ames, A. Jr. (1950). Accommodation, convergence, and their relation to apparent distance. *The Journal of Psychology* **30**, 43–62.

Jacobson, J. H., Romaine, H. H., Halberg, G. P. & Stephens, G. (1958). The electric activity of the eye during accommodation. *American Journal of Ophthalmology* **46**, 231–238.

Jaskulski, M., Marín-Franch, I., Bernal-Molina, P. & López-Gil, N. (2016). The effect of longitudinal chromatic aberration on the lag of accommodation and depth of field. *Ophthalmic and Physiological Optics* **36**, 657–663.

Johnson, C. A. (1976). Effects of luminance and stimulus distance on accommodation and visual resolution. *Journal of the Optical Society of America* **66**, 138–142.

Jorge, J., Braga, A. & Queirós, A. (2016). Changes in myopia prevalence among first-year university students in 12 years. *Optometry and Vision Science* **93**, 1262–1267.

Kasper, M., Fedrigo, E., Looze, D. P., Bonnet, H., Ivanescu, L. & Oberti, S. (2004). Fast calibration of high-order adaptive optics systems. *Journal of the Optical Society of America A* **21**, 1004–1008.

Kaufman, P. L. (1992). Accommodation and presbyopia: neuromuscular and biophysical aspects. In Adler's Physiology of the Eye: Clinical Application. St. Louis, Mo, USA: Mosby.

King, B. J., Sapoznik, K. A., Elsner, A. E., Gast, T. J., Papay, J. A., Clark, C. A. & Burns, S. A. (2017). SD-OCT and adaptive optics imaging of outer retinal tubulation. *Optometry and Vision Science* **94**, 411–422.

Kruger, P. B., López-Gil, N. & Stark, L. R. (2001). Accommodation and the Stiles–Crawford effect: theory and a case study. *Ophthalmic and Physiological Optics* **21**, 339–351.

Kruger, P. B., Mathews, S., Aggarwala, K. R. & Sanchez, N. (1993). Chromatic aberration and ocular focus: Fincham revisited. *Vision Research* **33**, 1397–1411.

Kruger, P. B., Mathews, S., Katz, M., Aggarwala, K. R. & Nowbotsing, S. (1997). Accommodation without feedback suggests directional signals specify ocular focus. *Vision Research* **37**, 2511–2526.

Kruger, P. B., Nowbotsing, S., Aggarwala, K. R. & Mathews, S. (1995). Small amounts of chromatic aberration influence dynamic accommodation. *Optometry and Vision Science* **72**, 656–666.

Kruger, P. B. & Pola, J. (1985). Changing target size is a stimulus for accommodation. *Journal of the Optical Society of America A* **2**, 1832–1835.

Kruger, P. B. & Pola, J. (1986). Stimuli for accommodation: blur, chromatic aberration and size. *Vision Research* **26**, 957–971.

Kruger, P. B. & Pola, J. (1987). Dioptric and non-dioptric stimuli for accommodation: target size alone and with blur and chromatic aberration. *Vision Research* **27**, 555–567.

Kruger, P. B., Stark, L. R. & Nguyen, H. N. (2004). Small foveal targets for studies of accommodation and the Stiles-Crawford effect. *Vision Research* **44**, 2757–2767.

Lakshminarayanan, V. & Fleck, A. (2011). Zernike polynomials: a guide. *Journal of Modern Optics* **58**, 545–561.

Lane, R. G. & Tallon, M. (1992). Wave-front reconstruction using a Shack–Hartmann sensor. *Applied Optics* **31**, 6902–6908.

Liang, J., Williams, D. R. & Miller, D. T. (1997). Supernormal vision and high-resolution retinal imaging through adaptive optics. *Journal of the Optical Society of America A* **14**, 2884–2892.

López-Gil, N., Fernández-Sánchez, V., Thibos, L. N. & Montés-Micó, R. (2009). Objective amplitude of accommodation computed from optical quality metrics applied to wavefront outcomes. *Journal of Optometry* **2**, 223–234.

Lopez-Gil, N., Jaskulski, M. T., Vargas-Martin, F. & Kruger, P. B. (2016). Retinal blood vessels may be used to detect the sign of defocus. *Investigative Ophthalmology and Visual Science* **57**, 3958–3958.

López-Gil, N., Martin, J., Liu, T., Bradley, A., Díaz-Muñoz, D. & Thibos, L. N. (2013). Retinal image quality during accommodation. *Ophthalmic and Physiological Optics* **33**, 497–507.

López-Gil, N., Rucker, F. J., Stark, L. R., Badar, M., Borgovan, T., Burke, S. & Kruger, P. B. (2007). Effect of third-order aberrations on dynamic accommodation. *Vision Research* **47**, 755–765.

Lundström, L. & Unsbo, P. (2007). Transformation of Zernike coefficients: scaled, translated, and rotated wavefronts with circular and elliptical pupils. *Journal of the Optical Society of America A* **24**, 569–577.

Madrid-Costa, D., Ruiz-Alcocer, J., Pérez-Vives, C., Ferrer-Blasco, T., López-Gil, N. & Montés-Micó, R. (2012). Visual simulation through different intraocular lenses using adaptive optics: effect of tilt and decentration. *Journal of Cataract and Refractive Surgery* **38**, 947–958.

Mahajan, V. N. (2007). Zernike polynomial and wavefront fitting. In Optical Shop Testing. New York: John Wiley & Sons.

Marcos, S., Werner, J. S., Burns, S. A., Merigan, W. H., Artal, P., Atchison, D. A., Hampson, K. M., Legras, R., Lundstrom, L., Yoon, G., Carroll, J., Choi, S. S., Doble, N., Dubis, A. M., Dubra, A., Elsner, A., Jonnal, R., Miller, D. T. , Paques, M., Smithson, H. E., Young, L. K., Zhang, Y., Campbell, M., Hunter, J., Metha, A., Palczewska, G., Schallek, J. & Sincich, L. C. (2017). Vision science and adaptive optics, the state of the field. *Vision Research* **132**, 3–33.

Marin-Franch, I., Bernal-Molina, P., Águila-Carrasco, A. J. D., Kruger, P. B., Esteve-Taboada, J.-J., Montés-Micó, R. & Lopez-Gil, N. (2016). Does dynamic accommodation respond to the shape of the blurred retinal image without changes in physical vergence? *Investigative Ophthalmology and Visual Science* **57**, 3952–3952.

Marín-Franch, I., Del Águila-Carrasco, A. J., Levecq, X. & López-Gil, N. (2017). Drifts in real-time partial wavefront correction and how to avoid them. *Applied Optics* **56**, 3989–3994.

McLin, L. N. & Schor, C. M. (1988). Voluntary effort as a stimulus to accommodation and vergence. Investigative *Ophthalmology and Visual Science* **29**, 1739–1746.

McLin Jr, L. N., Schor, C. M. & Kruger, P. B. (1988). Changing size (looming) as a stimulus to accommodation and vergence. *Vision Research* **28**, 883–898.

Metlapally, S., Tong, J. L., Tahir, H. J. & Schor CM. (2016). Potential role for microfluctuations as a temporal directional cue to accommodation. *Journal of Vision* 16, 1–11.

Miller, D. T. (2000). Retinal imaging and vision at the frontiers of adaptive optics. *Physics Today* **53**, 31–36.

Montés-Micó, R., Alió, J. L., Muñoz, G. & Charman, W. N. (2004). Temporal changes in optical quality of air–tear film interface at anterior cornea after blink. *Investigative Ophthalmology and Visual Science* **45**, 1752–1757.

Montés-Micó, R., López-Gil, N., Pérez-Vives, C., Bonaque, S. & Ferrer-Blasco, T. (2012). In vitro optical performance of nonrotational symmetric and refractive-diffractive aspheric multifocal intraocular lenses: impact of tilt and decentration. *Journal of Cataract and Refractive Surgery* **38**, 1657–1663.

Mordi, J. A. & Ciuffreda, K. J. (2004). *Dynamic aspects of accommodation: age and presbyopia. Vision Research* **44**, 591–601.

Morris, H. J., Blanco, L., Codona, J. L., Li, S. L., Choi, S. S. & Doble, N. (2015). Directionality of individual cone photoreceptors in the parafoveal region. *Vision Research* **117**, 67–80.

Mutti, D. O., Mitchell, G. L., Jones, L. A., Friedman, N. E., Frane, S. L., Lin, W. K., Moeschberger, M. L. & Zadnik, K. (2009). Accommodation, acuity, and their

relationship to emmetropization in infants. *Optometry and Vision Science* **86**, 666–676.

Ogle, K. N. & Schwartz, J. T. (1959). Depth of focus of the human eye. *Journal of the Optical Society of America* **49**, 273–280.

Otero, J. M. (1951). Influence of the state of accommodation on the visual performance of the human eye. *Journal of the Optical Society of America* **41**, 942–948.

Papadatou, E., Del Águila-Carrasco, A. J., Marín-Franch, I. & López-Gil, N. (2016). Temporal multiplexing with adaptive optics for simultaneous vision. *Biomedical Optics Express* **7**, 4102–4113.

Petrash, J. M. (2013). Aging and age-related diseases of the ocular lens and vitreous body. *Investigative Ophthalmology and Visual Science* **54**, ORSF54–ORSF59.

Phillips, S. & Stark, L. (1977). Blur: a sufficient accommodative stimulus. *Documenta* Ophthalmologica **43**, 65–89.

Platt, B. C. & Shack, R. (2001). History and principles of Shack-Hartmann wavefront sensing. *Journal of Refractive Surgery* **17**, S573–S577.

Porter, J., Queener, H., Lin, J., Thorn, K. & Awwal, A. A. S. (2006). Adaptive optics for vision science: Principles, practices, design and applications. Hoboken, New Jersey: John Wiley & Sons.

Qian, N. (1997). Binocular disparity and the perception of depth. *Neuron* **18**, 359–368.

Rocha, K. M., Vabre, L., Chateau, N. & Krueger, R. R. (2010). Enhanced visual acuity and image perception following correction of highly aberrated eyes using an adaptive optics visual simulator. *Journal of Refractive Surgery* **26**, 52–56.

Roddier, F. (1999). Adaptive optics in astronomy. New York: Cambridge University Press.

Roorda, A. (2011). Adaptive optics for studying visual function: a comprehensive review. *Journal of Vision* **11**, 1–21.

Scheiner, C. (1619). Oculus hoc est: Fundamental opticum. Innsbruck.

Schnapf, J. L., Kraft, T. W. & Baylor, D. A. (1987). Spectral sensitivity of human cone photoreceptors. *Nature* **325**, 439–441.

Schwiegerling, J. (2002). Scaling Zernike expansion coefficients to different pupil sizes. *Journal of the Optical Society of America A* **19**, 1937–1945.

Seet, B., Wong, T. Y., Tan, D. T. H., Saw, S. M., Balakrishnan, V., Lee, L. K. H. & Lim, A. S. M. (2001). Myopia in Singapore: taking a public health approach. *British Journal of Ophthalmology* **85**, 521–526.

Seidemann, A. & Schaeffel, F. (2002). Effects of longitudinal chromatic aberration on accommodation and emmetropization. *Vision Research* **42**, 2409–2417.

Smithline, L. M. (1974). Accommodative response to blur. *Journal of the Optical Society of America* **64**,1512–1516.

Southwell, W. H. (1980). Wave-front estimation from wave-front slope measurements. *Journal of the Optical Society of America* **70**, 998–1006.

Stark, L. R., Kruger, P. B., Rucker, F. J., Swanson, W. H., Schmidt, N., Hardy, C., Rutman, H., Borogvan, T., Burke, S., Badar, M. & Shah, R. (2009). Potential signal to accommodation from the Stiles–Crawford effect and ocular monochromatic aberrations. *Journal of Modern Optics* **56**, 2203–2216.

Stark, L. & Takahashi, Y. (1965). Absence of an odd-error signal mechanism in human accommodation. *IEEE Transactions on Biomedical Engineering* **12**, 138-146.

Takeda, T., Iida, T. & Fukui, Y. (1990). Dynamic eye accommodation evoked by apparent distances. *Optometry and Vision Science* **67**, 450–455.

Tarrant, J. & Roorda, A. (2006). The extent of the isoplanatic patch of the human eye. *Investigative Ophthalmology and Visual Science* **47**, 1195–1195.

Tarrant, J., Roorda, A. & Wildsoet, C. F. (2010). Determining the accommodative response from wavefront aberrations. *Journal of Vision* **10**, 1–16.

Thibos, L. N. (2000). Principles of Hartmann-Snack aberrometry. *Journal of Refractive Surgery* **16**, S563–S565.

Thibos, L. N., Applegate, R. A., Schwiegerling, J. T., Webb, R. & VSIA Standards Taskforce Members. (2002). Standards for reporting the optical aberrations of eyes. *Journal of Refractive Surgery* **18**, S652-S660.

Thibos, L. N., Hong, X., Bradley, A. & Applegate, R. A. (2004). Accuracy and precision of objective refraction from wavefront aberrations. *Journal of Vision* **4**, 329–351.

Thomas, S., Fusco, T., Tokovinin, A., Nicolle, M., Michau, V. & Rousset, G. (2006). Comparison of centroid computation algorithms in a Shack–Hartmann sensor. *Monthly Notices of the Royal Astronomical Society* **371**, 323–336.

Toraldo di Francia, G. (1949). Retina Cones as Dielectric Antennas. *Journal of the Optical Society of America* **39**, 324–324.

Troelstra, A., Zuber, B. L., Miller, D. & Stark, L. (1964). Accommodative tracking: a trial-and-error function. *Vision Research* **4**, 585–594.

Tucker, J. & Charman, W. N. (1975). The depth-of-focus of the human eye for Snellen letters. *American Journal of Optometry and Physiological Optics* **52**, 3–21.

Tyson, R. (2012). Principles of adaptive optics. Florida: Taylor and Francis Group.

Ukai, K. & Ichihashi, Y. (1991). Changes in ocular astigmatism over the whole range of accommodation. *Optometry and Vision Science* **68**, 813–818.

Vohnsen, B. (2014). Directional sensitivity of the retina: A layered scattering model of outer-segment photoreceptor pigments. *Biomedical Optics Express* **5**, 1569–1587.

von Helmholtz, H. (1866), Physiological optics. [Translation: D. L. MacAdam, Sources of Color Science, MIT Press, Cambridge, 1970].

Wheatstone, C. (1838). Contributions to the physiology of vision. Part the first. On some remarkable, and hitherto unobserved, phenomena of binocular vision. *Philosophical Transactions of the Royal Society of London* **128**, 371–394.

Whelan, P. M. & Hodgson, M. J. (1989). Essential Principles of Physics. Bristol: J.W. Arrowsmith Ltd.

Wildsoet, C. F. (1997). Active emmetropization — evidence for its existence and ramifications for clinical practice. *Ophthalmic and Physiological Optics* **17**, 279–290.

Williams, K. M., Bertelsen, G., Cumberland, P., Wolfram, C., Verhoeven, V. J. M., Anastasopoulos, E., Buitendijk, G. H., Cougnard-Grégoire, A., Creuzot-Garcher, C., Erke, M. G., Hogg, R., Höhn, R., Hysi, P., Khawaja, A. P., Korobelnik, J. F., Ried, J., Vingerling, J. R., Bron, A., Dartiques, J. F., Fletcher, A., Hofman, A., Kuijpers, R. W., Luben, R. N., Oxele, K., Topouzis, F., von Hanno, T., Mirshahi, A., Foster, P. J.,

van Dujin, C. M., Pfeiffer, N., Delcourt, C., Klaver, C. C., Rahi, J., Hammond, C. J.; European Eye Epidemiology (E(3)) Consortium. (2015). Increasing prevalence of myopia in Europe and the impact of education. *Ophthalmology* **122**, 1489–1497.

Wilson, B. J., Decker, K. E. & Roorda, A. (2002). Monochromatic aberrations provide an odd-error cue to focus direction. *Journal of the Optical Society of America A* **19**, 833–839.

Wyatt, H. J. (1995). The form of the human pupil. *Vision Research* **35**, 2021–2036.

Xu, R., Bradley, A., López Gil, N. & Thibos, L. N. (2015). Modelling the effects of secondary spherical aberration on refractive error, image quality and depth of focus. *Ophthalmic and Physiological Optics* **35**, 28–38.

Young, T. & Brocklesby, R. (1793). Observations on vision. *Philosophical Transactions of the Royal Society of London* **83**, 169–191.

Zernike, F. (1934). Diffraction theory of the knife-edge test and its improved form, the phase-contrast method. *Monthly Notices of the Royal Astronomical Society* **94**, 377–384.

Zhao, C. & Burge, J. H. (2007). Orthonormal vector polynomials in a unit circle, Part I: basis set derived from gradients of Zernike polynomials. *Optics Express* **15**, 18014–18024.

Zou, W. & Burns, S. A. (2009). High-accuracy wavefront control for retinal imaging with Adaptive-Influence-Matrix Adaptive Optics. *Optics Express* **17**, 20167–20177.

Publications and conference contributions

Journal publications

Esteve-Taboada JJ, Del Águila-Carrasco AJ, Bernal-Molina P, López-Gil N, Montés-Micó R, Kruger PB and Marín-Franch I (2017). Dynamic accommodation without feedback does not respond to isolated blur cues. Vision Research. *In press*.

Del Águila-Carrasco AJ, Marín-Franch I, Bernal-Molina P, Esteve-Taboada JJ, Kruger PB, Montés-Micó R and López-Gil N (2017). Accommodation responds to optical vergence and not defocus blur alone. Investigative Ophthalmology & Visual Science; 58: 1758-1763.

Marín-Franch I, Del Águila-Carrasco AJ, Bernal-Molina P, Esteve-Taboada JJ, López-Gil N, Montés-Micó R and Kruger PB (2017). There is more to accommodation of the eye tan simply minimizing retinal blur. Biomedical Optics Express. *Submitted*.

Marín-Franch I, Del Águila-Carrasco AJ, Levecq X and López-Gil N (2017). Drifts in real-time partial wavefront correction and how to avoid them. Applied Optics; 56: 3989-3994.

Conference contributions

Marin-Franch I, Bernal-Molina P, Del Águila-Carrasco AJ, Kruger PB, Esteve-Taboada JJ, Montés-Micó R and López-Gil N (2016). Does dynamic accommodation respond to the shape of the blurred retinal image without changes in physical vergence? The association for Research in Vision and Ophthalmology (ARVO) Annual Meeting. Seattle, Washington (USA).

López-Gil N, Marín-Franch I, Bernal-Molina P, Esteve-Taboada JJ, Montés-Micó R, Kruger PB and Del Águila-Carrasco AJ (2017). Does accommodation respond equally to artificially blurred as to real out-of-focus retinal images? The association for Research in Vision and Ophthalmology (ARVO) Annual Meeting. Baltimore, Maryland (USA).

Kruger PB, Marín-Franch I, Del Águila-Carrasco AJ, Bernal-Molina P, Esteve-Taboada J, Montés-Micó R and López-Gil N (2017). There is more to accommodation than simply maximizing retinal image contrast. The association for Research in Vision and Ophthalmology (ARVO) Annual Meeting. Baltimore, Maryland (USA).